The purpose of this thesis is to correlate the DFT results with the reported antifungal and or antibiotic activities. The optimized molecular geometry, bond lengths, bond angles and band gap were investigated. In this regard various heterocyclic compounds were used to find out their Quantum chemical parameters of the compounds viz. EA, IP, Electronegativity, hardness and softness showed strong correlation with the reported antifungal activity of studied compounds. Geometrical parameters have been compared with the available experimental results. The structure-activity relationship was also studied. The heterocyclic compounds studied in the era of the current thesis are benzoyl thiourea derivatives Linked with morpholine and piperidine, thiourea derivatives containing a thiazole moiety and allantofuranone and related compounds containing -lactone.

Dr. Rameshwar K. Dongare
Assistant Professor
Department of Chemistry
Ahmednagar College, Ahmednagar, Maharashtra, India 414 001

Dr. Radhakrishnan M. Tigote
Assistant Professor
Department of Chemistry, Dr. B. A. M. University sub-Campus,
Osmanabad, Maharashtra, India 413 501.

9 7 8 6 2 0 5 5 1 0 3 0 8

Rameshwar Dongare, Radhakrishnan Tigote

Rameshwar Dongare
Radhakrishnan Tigote

DFT BASED STUDY OF BIOLOGICALLY ACTIVE HETEROCYCLIC COMPOUNDS

LAP LAMBERT Academic Publishing

Rameshwar Dongare
Radhakrishnan Tigote

DFT BASED STUDY OF BIOLOGICALLY ACTIVE HETEROCYCLIC COMPOUNDS

Rameshwar Dongare
Radhakrishnan Tigote

DFT BASED STUDY OF BIOLOGICALLY ACTIVE HETEROCYCLIC COMPOUNDS

LAP LAMBERT Academic Publishing

Imprint

Cover image: www.ingimage.com

Publisher:
LAP LAMBERT Academic Publishing
is a trademark of
Dodo Books Indian Ocean Ltd. and OmniScriptum S.R.L Publishing group
Str. Armeneasca 28/1, office 1, Chisinau-2012, Republic of Moldova, Europe
Printed at: see last page
ISBN: 978-620-5-51030-8

Abstract

The purpose of this thesis is to correlate the DFT results with the reported antifungal and or antibiotic activities. The optimized molecular geometry, bond lengths, bond angles and band gap were investigated. In this regard various **heterocyclic compounds** were used to find out their quantum chemical parameters of the compounds viz. EA, IP, electronegativity, hardness (η) and softness (σ) showed strong correlation with the reported antifungal activity of studied compounds. Geometrical parameters have been compared with the available experimental results. The structure-activity relationship was also studied. The heterocyclic compounds studied in the era of the current thesis are benzoyl thiourea derivatives linked with morpholine and piperidine, thiourea derivatives containing a thiazole moiety, homoisoflavanone analogues and allantofuranone and related compounds containing γ-lactone.

The first chapter is about Introduction of quantum chemical methods. The second chapter describes DFT-based theoretical model for predicting loading and release of a pH-responsive sulfasalazine drug. The third chapter is about DFT studies and quantum chemical calculations of benzoyl thiourea derivatives linked with morpholine and piperidine for the evaluation of antifungal activity. Fourth chapter describes in detail the DFT calculations of thiourea derivatives containing a thiazole moiety for the evaluation of antifungal activity. While, the fifth chaper is about the DFT based investigations of antibiotic and antifungal activity of allantofuranone and aelated γ-lactone compounds. Whereas, the sixth chapter give details of the electronic structure and physico chemical property relationship for homoisoflavanone analogues. And in the last chapter the summary and future scope are compiled.

A full quantum-mechanical treatment would require the calculation of the system's many-nuclei, many-electron wave function; however, the relatively large mass of the nuclei means that for the vast majority of simulations their behaviour is

decoupled from the electrons and they may be treated as classical point-like particles (the Born–Oppenheimer approximation). In contrast to the nuclei, the low mass of electrons means that a full quantum-mechanical treatment is required to understand their behaviour, but the computational complexity of the many-body Schrödinger equation means that a solution is beyond current or foreseeable technologies for almost all material problems. However, DFT allows us to sidestep the computational difficulty by focusing on the electron density, instead of the many-body wave function. The underlying principle of DFT is that the total energy of the system is a unique functional of the electron density, hence it is unnecessary to compute the full many-body wave function of the system. However, the precise functional dependence of the energy on the density is not known. Kohn and Sham transformed this DFT problem of computing the ground state energy and particle density of an N-electron system to that of solving a set of independent-particle equations.

This work describes a theoretical model that combines classical pKa theory with quantum mechanical calculations to predict the extent of interaction between pH-dependent species over a full range of pH. To demonstrate the theoretical model, the drug loading and release of a pH-responsive drug delivery system consisting of sulfasalazine is loaded onto the positively charged trimethylammonium (TA)-functionalized mesoporous silica nanoparticle surface.

The interactions of drug molecules with the silica surface, in the absence and presence of FG, were calculated using the CASTEP calculations. For the silica surface with a positively charged FG, the interaction energy (E_{int}) is calculated using eq 1, whereas for the system without any FG, eq 2 is used.

$$E_{int} = E_{(\text{silica with FG+drug})} - E_{(\text{silica with FG})} - E_{(\text{drug})} \quad (1)$$

$$E_{int} = E_{(\text{silica + drug})} - E_{(\text{silica})} - E_{(\text{drug})} \quad (2)$$

The relative probability of combinations of a pair of molecules with two different protonation states is derived (S^0D^{-1}, $S^{-1}D^0$, S^0D^0, and $S^{-1}D^{-1}$), and density functional theory simulations of each combination are then used to calculate the pH-responsive binding energy. Overall, it is observed that the predicted model,

combined with periodic functional theory calculations on the TA-functionalized quartz surfaces, showed a strong agreement with experimental results that sulfasalazine was bound to MSN surfaces at low pH values but released at high pH values.

This section describes DFT studies and quantum chemical calculations of benzoyl thiourea derivatives of morpholine and piperidine (**BTP 1-3, BTM 4-6**) for the evaluation of antifungal activity. In general, good agreement between the calculated and experimental geometrical parameters have been observed. Overall, strong correlation is observed between biological activity and computed values of all the quantum chemical parameters viz. EA, IP, Electronegativity, hardness (η) and softness (σ). Lower values of Log P are indicative of stronger antifungal activity.

This section describes DFT / B3LYP study of thiourea derivatives containing a thiazole moiety (**1a-1d**).We were interested in exploring the frontier orbital energy and structure-activity relationship on the antifungal activities. It is reported that all the compounds exhibit significant antifungal activity, antifungal activity of **1c** is the strongest among the studied samples. Theoretical study brings out electronic characteristic responsible for antifungal activity. In general good agreement is observed between quantum chemical results and experimental observations. Overall, we observed strong correlation between biological activity and computed values of all the quantum chemical parameters viz. EA, IP, Electronegativity, hardness (η) and softness (σ). Lower values of Log P are indicative of stronger antifungal activity.

This work describes correlation between the DFT outcomes and the reported antibiotic and antifungal activity of Allantofuranone and related compounds. The structure of Allantofuranone and related compounds containing γ-lactone were optimized by Density Functional Theory (DFT) using B3LYP method with 6-31G (d,p) basis set. The optimized molecular geometry, bond lengths, bond angles and band gap were investigated. The outcomes of the DFT calculations were utilised to

formulate all the Quantum chemical parameters of the compounds viz. EA, IP, electronegativity, hardness (η) and softness (σ). Structural parameters have been compared with the available experimental results, to investigate the structure-activity relationship.The DFT calculations of compounds allantofuranone, xenofuranone A, xenofuranone B and WF 3681 revealed small HOMO-LUMO gap, lower value of LUMO, more lipophilic character and rich topography of Allantofuranone are prerequisite for antifungal activity. Here we highlight the electronic characteristics responsible for the strong biological activity, which separates Allantofuranone from other structurally similar compounds. Overall, we observed good correlation between biological activity and computed values of all the quantum chemical parameters.

The DFT study of seven 3-benzylidene-4-chromanone analogues were evaluated for their antifungal activity. All the compounds HIF 1-7 were optimized with B3LYP/ 6-31G (d,p) and various parameters were evaluated. IP, EA, hardness, softness and electronegativity correlates reasonably well with the antifungal activity. Log P has been found to have a clear association with antifungal activity. The compound HIF 3 is reported to be the most effective. The Log P value is seen to play important role in defining antifungal activity of molecules. HIF 3 is more lipophilic in nature, according to the Log P estimates. Stronger antifungal activity is indicated by higher Log P values. In the present work, the calculated values, i.e. geometric parameters, mulliken charges, frontier orbital analysis

We performed Quantum Chemical calculations to correlate the DFT results with the reported antifungal and or antibiotic activities. The optimized molecular geometry, bond lengths, bond angles and band gap were investigated. In this regard various **heterocyclic compounds** were used to find out their Quantum chemical parameters of the compounds viz. EA, IP, electronegativity, hardness (η) and softness (σ) showed strong correlation with the reported antifungal activity of studied compounds. Geometrical parameters have been compared with the available experimental results. The structure-activity relationship was also studied. The

heterocyclic compounds studied in the era of the current thesis are benzoyl thiourea derivatives linked with morpholine and piperidine, thiourea derivatives containing a thiazole moiety and allantofuranone and related compounds containing. Here we highlight the electronic characteristics responsible for the strong biological activity.

The proposed DFT model can be used for predicting the loading and release pH for the drugs and the surfaces with known pKa values, which will be very important / crucial for the **pH responsive drug delivery systems**. In the future, the DFT study and structure-activity relationship study may aid in the formulation of better antifungal and/or antibiotic heterocyclic compounds.

Acknowledgement

The first person I would like to thank is my guide **Dr. Radhakrishnan M. Tigote**, who has supported me throughout my thesis with his patience and knowledge whilst allowing me the room to work in my own way. He has been my teacher first and then guide. His understanding, encouragement and personal guidance have provided a good basis for the present thesis as well as life. He was always there to meet and discuss ideas, to proofread and mark up my papers and chapters and to help me think through my problems. His endurance and meticulous attention to the details has helped me to grow as research student and as a good person. Special thanks go to **Dr. Shaukatali N. Inamdar** who helped me a lot through discussions, correcting manuscript, proofreading and meticulous suggestions added considerably to my experience.

I want to express my deep thanks to Hon'ble, **Prof. D. K. Gaikwad**, Director, Dr. Babasaheb Ambedkar Marathwada University, Subcampus Osmanabad, I thank, **Dr. M. K. Patil**, Head, Department of Chemistry, Dr. B. A. M. University sub-Campus, Osmanabad and the former Head of Department, **Dr. K. P. Haval**. All the other faculty members were also always helpful and provided guidance whenever approached. I would like to mention the non-teaching staff from the Department of Chemistry for their assistance in every possible way.

I am thankful to **Prof. S. R. Gadre** and **Prof. S. P. Gejji** for their wisdom, invaluable advices, support and encouragement which have always been there for me whenever I need. Many thanks to my friends Dr. Milind, Dr. Mahadev, Dr. Ganesh, Dr. Jovan, Dr. Dinanath and Dr. Sameer. It is a pleasure to thank those who made this thesis possible. Thanks to my group members Ms Subiya Kazi, Ms.Rajkanya Bhore, Ms Reshma Bhosale, and Mr. Promod Dhokrat for their help during various stages of my work.

I sincerely admire the contribution of all my colleagues and friends, Dr. A. K. Kulkarni, Mr. S. B. Kasar, Mr. S. V. Rohokale, Mr. V. M. Kasab, Dr. S. R. Deshmukh, Dr. D. D. Gaikwad, Dr. V. A. Kawade, Mr. G. N. Ghumare, Ms. S. A.

Gunjal, Ms. S. G. Tikone, and all others who directly or indirectly helped, encouraged me and created a fun-filled environment for completion of this research work. I would like to express my sincere gratitude and regards to Principal Dr. R. J. Barnabas, Dr. A. V. Nagawade, (Head, Department of Chemistry, Ahmednagar College Ahmednagar) and Dr. V. V. Khanna, (former Head), for their support, inspiration, and guidance.

The most important one are my parents who deserve special mention for their inseparable support. I thank them for their encouragement, continuous support and faith in me. I think now, at the end of my Ph.D., is a good moment to thank them as well for all the time and effort they put into my education. This Ph. D. is the result of all these years. My regards to my younger brothers Sunil and Dnyaneshwar for their constant support and encouragement. Finally, and most importantly, I thank my wife, Smita for her love, support and care. Special mention of my sons Shardul and Arnav for keeping me joyful and cheerful.

Rameshwar K. Dongare

Dedicated to my beloved Parents

Index

List of Tables

List of Figures

Abbreviations

DFT	: Density functional theory
IP	: Ionization potential
EA	: Electron affinity
STO	: Slater-type atomic orbitals
GTO	: Gaussian-type atomic orbitals
CC	: Coupled cluster
GGA	: Generalized gradient approximations
LDA	: local density approximation
HOMO	: Highest occupied molecular orbital
LUMO	: Lowest unoccupied molecular orbital
BTP	: Benzoyl thiourea derivatives linked to piperidine
BTM	: Benzoyl thiourea derivatives linked to morpholine
MIC	: Minimum inhibitory concentration
SAR	: Structure-activity relationship
B3LYP	: Becke 3-parameter, Lee-Yang-Parr
GAMESS	: General atomic and molecular electronic structure system

CHAPTER 1:

Introduction to Quantum Chemical Methods

1.1 Atoms and Molecules

A system of atoms or molecules is represented by a dynamical picture in which negatively charged electrons move around positively charged nuclei. Within the systems, there are attraction and repulsive forces between the particles. The system's energy is determined by the attraction and repulsive interactions between the particles, as well as the kinetic energy generated by their motion. The question is, how do you calculate total electronic energy and the actual condition of the system? De Broglie proposed in 1923 that subatomic entities (nuclei and electrons) exhibit both wave and particle qualities at the same time. Furthermore, each electron in its own orbital is described as a standing wave. In 1925, Debye casually remarked that a wave equation should be used to describe matter because particles might be characterized as waves. Schrodinger presented the well-known time-independent wave equation,[1] which is given by Eq (1.1). He demonstrated that his theory is equivalent to matrix.

Heisenberg, Bonn, and Jordan developed mechanics (1925).

$$\hat{H}\Psi(1,\ldots,N) = E\Psi(1,\ldots,N) \tag{1.1}$$

The physical state of the system is completely represented by the wave function Ψ (1,..., N), which is dependent on the spatial and spin coordinates of all particles in the system. However, because to the Heisenberg uncertainty principle,[1] one cannot expect Ψ to provide definitive information on particle positions and thus the state of the system. Max Born[1] offered a probabilistic picture of the position of a particle (such as an electron). It was proposed that $|\Psi|^2$ dx represents the likelihood of detecting a particle in a tiny region dx in one dimension, with $|\Psi|^2$ representing the associated probability density. 'E' is the total electronic energy of the system in Eq. (1.1). Hamiltonian operator is an energy operator that takes into account all of the attractive and repulsive forces between the particles, as well as

the kinetic energy of each individual particle.[1, 2] For a N electron system, the molecular Hamiltonian is written as

$$\hat{H}_{total} = \hat{T}_n + \hat{T}_e + \hat{V}_{nn} + \hat{V}_{ne} + \hat{V}_{ee} \tag{1.2}$$

$$\hat{T}_n = -\sum_{A=1}^{M} \frac{1}{2M_A}\nabla_A^2; \quad \hat{T}_e = -\sum_{i=1}^{N} \frac{1}{2}\nabla_i^2; \quad \hat{V}_{nn} = +\sum_{A}^{M}\sum_{A<B}^{M} \frac{Z_A Z_B}{|\mathbf{R_A} - \mathbf{R_B}|};$$

$$\hat{V}_{ne} = -\sum_{A=1}^{M}\sum_{i=1}^{N} \frac{Z_A}{|\mathbf{r_i} - \mathbf{R_A}|} \quad \text{and} \quad \hat{V}_{ee} = +\sum_{i}^{N}\sum_{i<j}^{N} \frac{1}{|\mathbf{r_i} - \mathbf{r_j}|} \tag{1.3}$$

The kinetic energy of the nuclei and electrons are represented by $\hat{T}$n, $\hat{T}$e in the preceding equation. V_{nn}, V_{ne} and V_{ee} potential energies related to nuclear-nuclear, nuclear-electron, and electron-electron repulsion, respectively. The spatial coordinates of A^{th} nucleus and i^{th} electron are R_A and r_i, respectively. Because nuclei are substantially heavier than electrons, the Born-Oppenheimer approximation[1-3] allows one to imagine electrons moving in a field of stationary nuclei. As a result, the nuclei's kinetic energy could be neglected, and the internuclear repulsion could be assumed to be constant for a particular geometry. As a result, the total Hamiltonian of the system is given as inside the Born-Oppenheimer approximation as

$$\hat{H}_{total} = (\hat{T}_e + \hat{V}_{ne} + \hat{V}_{ee}) + \hat{V}_{nn} = \hat{H}_{electronic} + \hat{V}_{nn} \tag{1.4}$$

The total energy of a molecule for fixed nuclei is obtained by solving Eq. (1.1) with this Hamiltonian as the electronic energy E_{ele} ltis the nuclear-nuclear repulsion energy, V_{nn}

i.e.

$$E_{total} = \sum_{A=1}^{M}\sum_{A>B}^{M} \frac{Z_A Z_B}{|\mathbf{R_A} - \mathbf{R_B}|} + E_{ele} \tag{1.5}$$

It can be observed from Eqs. (l.2) and (l.5) that the total energy of the system forms the potential energy surface (PES) for nuclei motion.

Let's look at how a wave function for a single particle (called an orbital) is represented before getting into the details of the exact wave function. A complete description of an electron's state necessitates a spatial orbital Ψ (r) as well as a spin function α(ω) or β (ω) that describes its spin state ω = ±1/2. As a result, the resulting orbital, χ(x), is known as the spin orbital.[2] The spin orbitals are orthonormal to each other in general.

$\int d\mathbf{x}\ \chi_a^*(\mathbf{x})\ \chi_b(\mathbf{x}) = \delta_{ab}$; where, $\delta_{ab} = 1$ if $a = b$ and $\delta_{ab} = 0$ if $a \neq b$.

Because the electron is a fermion, the many-electron wave function representing a system of N identical electrons must be completely antisymmetric when the coordinates (both space and spin) of any two electrons in the system are interchanged. As a result, changing the coordinates of any two electrons should change the sign of the wave function. i.e.

$$\Psi(\mathbf{x_1}, \ldots, \mathbf{x_i}, \ldots \mathbf{x_j}, \ldots, \mathbf{x_N}) = -\Psi(\mathbf{x_1}, \ldots, \mathbf{x_j}, \ldots, \mathbf{x_i}, \ldots, \mathbf{x_N}) \qquad (1.6)$$

The Pauli exclusion principle[2] is stated in general terms with this constraint for many-electron wave functions.

Consider a system of non-interacting electrons with a Hamiltonian operator represented as the sum of one electron Hamiltonians, viz.

$$\hat{H} = \sum_{i=1}^{N} \hat{h}(i) \qquad (1.7)$$

Where h (i) is an operator for an electron's kinetic and nuclear attraction energy.

The spin orbitals are the appropriate eigenfunctions of h (i).

$$\hat{h}(i)\chi_a(\mathbf{x_i}) = \epsilon_a \chi_a(\mathbf{x_i}) \qquad (1.8)$$

An N-electron wave function is essentially the product of spin orbitals because $\hat{H}$ is the sum of one electron Hamiltonians.

$$\Psi^{HP}(\mathbf{x_1}, \mathbf{x_2}, \ldots, \mathbf{x_N}) = \chi_a(\mathbf{x_1})\chi_b(\mathbf{x_2}) \ldots \chi_k(\mathbf{x_N}) \qquad (1.9)$$

The Hartree product[2] is an eigenfunction of $\hat{H}$ with an eigenvalue E equal to the

sum of the orbital energies, ε_a, of the spin orbitals utilized in the creation of the wave function.

$$\hat{H}\Psi^{HP} = E\Psi^{HP} \tag{1.10}$$

$$E = \epsilon_a + \epsilon_b + \ldots + \epsilon_k \tag{1.11}$$

In the sense that the likelihood of finding any electron is independent of the probability of finding any other electron, the Hartree product is an uncorrelated or independent electron wave function. Another issue with the Hartree product wave function is that it violates the notion of anti-symmetry. However, using the spin orbitals as elements of a determinant, one can create a simple anti-symmetrized N-electron wave function as follows:

$$\Phi_0(\mathbf{x_1}, \mathbf{x_2}, \ldots, \mathbf{x_N}) = \frac{1}{\sqrt{N!}} \begin{vmatrix} \chi_1(\mathbf{x_1}) & \chi_2(\mathbf{x_1}) & \cdots & \chi_n(\mathbf{x_1}) \\ \chi_1(\mathbf{x_2}) & \chi_2(\mathbf{x_2}) & \cdots & \chi_n(\mathbf{x_N}) \\ \vdots & \vdots & & \vdots \\ \chi_1(\mathbf{x_N}) & \chi_2(\mathbf{x_N}) & \cdots & \chi_n(\mathbf{x_N}) \end{vmatrix} \tag{1.12}$$

A Slater determinant is a type of multi-electron wave function.[2, 4] A normalization constant is the factor $(N!)^{-1/2}$. This wave function describes N electrons in n spin orbitals without stating which electron is in which orbital. When the coordinates of two electrons are swapped, two rows of the determinant in Eq. (1.12) are swapped as well, changing the sign of the wave function and satisfying the anti-symmetry principle. The presence of the Coulomb and Fermi holes is an important aspect of the many-electron wave function. The Coulomb hole is named after the Coulombic repulsion between electrons, which makes it impossible to discover two electrons at the same location in space. The chance of binding two electrons with parallel spin at the same position in space is zero, which gives rise to the Fermi hole notion. The Fermi hole is taken care of by the Slater determinantal form of the wave function. The Coulomb hole state, on the other hand, is not properly ad- dressed. In other words, the motion of electrons with parallel spins is

correlated (probability is zero) within the single Slater determinantal description, while the motion of electrons with opposing spins is not. [2]

1.2 Hartree-Fock Theory

With the shape of a many electron wave-function and a many particle Hamiltonian, we're ready to go. Given a well-behaved trial wave function, Ψ_t, that obeys the applicable boundary conditions, the expectation value of the Hamiltonian, E_{app}, is larger than or equal to the corresponding exact ground state energy E_{gs}, according to the variation principle.

$$E_{gs} \leq E_{app} = \frac{\langle \Psi_t | \hat{H} | \Psi_t \rangle}{\langle \Psi_t \Psi_t \rangle} \tag{1.13}$$

and

$$\langle \Psi_t | \hat{H} | \Psi_t \rangle = \int \Psi_t^* \hat{H} \Psi_t d\tau \tag{1.14}$$

A single Slater determinantal wave function formed from the proper set of spin orbitals ($\chi_a|a = 1, 2,..., n$) is utilized in the Hartree-Fock (HF) approach.[5] Within the variational approach, the overall electronic energy of the system is minimized by altering spin orbitals. The ground state energy is known as HF energy, E_0, and the wave function is known as HF wave function, Ψ_0. The normalized N-electron Slater determinantal wave function's ground state energy is given

$$E_0 = \langle \Psi_0 | \hat{H} | \Psi_0 \rangle \tag{1.15}$$

i.e.

$$E_0 = \left\langle \Psi_0 \middle| \sum_{i=1}^{N} \hat{h}(i) + \sum_{i}^{N} \sum_{j>i}^{N} \frac{1}{r_{ij}} \middle| \Psi_0 \right\rangle \tag{1.16}$$

$1/r_{ij}$ denotes the electron-electron repulsion term, and $\hat{h}(i)$ is one electron operator specified in Eq. (1.7). The one electron term in the preceding equation can be expressed as by explicitly stating the Slater determinant and considering the

orthonormality of spin orbitals.

$$\left\langle \Psi_0|\hat{h}(1)|\Psi_0 \right\rangle = \sum_{a=1} \left\langle \chi_a(1)|\hat{h}(1)|\chi_a(1) \right\rangle = \sum_{a=1} \left\langle \chi_a|\hat{h}|\chi_a \right\rangle \qquad (1.17)$$

Eg. (1. 16)'s second term is more complicated, as it covers all N (N-1)/2 pairs of electrons. This is the fundamental stumbling block and bottleneck in HF theory. The second term is given as when the Slater determinant is expanded.

$$\left\langle \Psi_0|\sum_{i}^{N}\sum_{j>i}^{N}\frac{1}{r_{ij}}|\Psi_0 \right\rangle = \sum_{a,b} \langle \chi_a\chi_b|\chi_a\chi_b\rangle - \langle \chi_a\chi_b|\chi_b\chi_a\rangle = \sum_{a,b} \langle \chi_a\chi_b||\chi_a\chi_b\rangle \quad (1.18)$$

where,

$$\langle \chi_a\chi_b|\chi_c\chi_d\rangle = \int \chi_a^*(1)\chi_b^*(2)\frac{1}{r_{12}}\chi_c(1)\chi_d(2)d\mathbf{x_1}d\mathbf{x_2} \qquad (1.19)$$

As a result, Eq. (1.16) becomes the ground state energy of a closed shell system.

$$E_0 = \sum_{a=1} \left\langle \chi_a|\hat{h}|\chi_a \right\rangle + \frac{1}{2}\sum_{a,b} \langle \chi_a\chi_b||\chi_a\chi_b\rangle$$

In a condensed notation,

$$E_0 = \sum_{a=1} \left\langle a|\hat{h}|a \right\rangle + \frac{1}{2}\sum_{a,b} \langle ab||ab\rangle \qquad (1.20)$$

The goal of the HF theory now is to reduce this energy. The energy is minimized by varying the spin orbitals subject to orthogonality $\langle\chi_a|\chi_b\rangle = \delta_{ab}$ as, using Lagrange's method of indeterminate multipliers [19].

$$\delta\left\{ E - \sum_{a,b} \epsilon_{ba}\left\{\langle \chi_a|\chi_b\rangle - \delta_{ab}\right\}\right\} = 0 \qquad (1.21)$$

The Langrange multiplier, ε_{ab}, is used here. Using Eq (1.20)

$$\delta E = \sum_{a=1}\left\{\left\langle \delta a|\hat{h}|a\right\rangle + \left\langle a|\hat{h}|\delta a\right\rangle\right\}$$

$$+\frac{1}{2}\sum_{a.b}\left\{\langle \delta ab||ab\rangle + \langle a\delta b||ab\rangle + \langle ab||\delta ab\rangle + \langle ab||a\delta b\rangle\right\} \qquad (1.22)$$

We get the following by solving the previous equation and putting it in Eq (1.21).

$$\sum_{a=1} \int d\mathbf{x}_1 \delta\chi_a^*(1) \left[\hat{h}(1)\chi_a(1) + \sum_b \left(\hat{J}_b(1) - \hat{K}_b(1) \right) \chi_a(1) - \sum_b \epsilon_{ba}\chi_b(1) \right]$$
$$+ Complex\ Conjugate = 0 \qquad (1.23)$$

Because $\delta\chi_a(1)$ is arbitrary, the quantity in the square bracket for every a must be zero, and so,

$$\left[\hat{h}(1) + \sum_b \left(\hat{J}_b(1) - \hat{K}_b(1) \right) \right] \chi_a(1) = \sum_b \epsilon_{ba}\chi_b(1) \qquad (1.24)$$

$\hat{J}_b$ and $\hat{K}_b$ are the Coulomb and exchange operators, respectively, [2] and are defined as

$$\hat{J}_b(1)\chi_a(1) = \int d\mathbf{x}_2 \frac{\chi_b^*(2)\chi_b(2)}{r_{12}} \chi_a(1)$$
$$\hat{K}_b(1)\chi_a(1) = \int d\mathbf{x}_2 \frac{\chi_b^*(2)\chi_a(2)}{r_{12}} \chi_b(1) \qquad (1.25)$$

The Coulomb operator describes the Coulombic potential created by the orbital electron density $|\chi_b(2)|^2$ in a simple way. The exchange operator, on the other hand, is more complicated. It entails the transfer of electrons 1 and 2 to the right of $(r_{12})^{-1/2}$ in the foregoing equation. This word is an artifact of HF theory that originates from the usage of the Slater determinantal wave function. The Fock operator is the quantity in the square bracket of Eq. (1.24). As a result, the equation above can be simplified to the following form.

$$\hat{f}(1)|\chi_a(1)\rangle = \sum_b \epsilon_{ba}|\chi_b(1)\rangle \qquad (1.26)$$

This is referred to as a non-canonical (non-standard) HF equation. Using an appropriate unitary transformation, a conventional canonical HF equation of the form can be produced.

$$\hat{f}(1)|\chi_a(1)\rangle = \sum_a \epsilon_a|\chi_a(1)\rangle \qquad (1.27)$$

The *canonical Hartree-Fock equations*[2, 5] are used to describe these. The eigenvalues are the orbital energies provided by ε_a, and the associated orbitals are the classical HF orbitals. When the orbital energies are added together, the result

$$\sum_a \epsilon_a = \sum_a \left\langle \chi_a(1)|\hat{f}(1)|\chi_a(1)\right\rangle$$

$$\sum_a \epsilon_a = \sum_a \left\langle \chi_a(1)|\hat{h}(1)|\chi_a(1)\right\rangle + \sum_b \left\langle \chi_a(1)|\left(\hat{J}_b(1) - \hat{K}_b(1)\right)|\chi_a(1)\right\rangle \quad (1.28)$$

i.e.

$$\sum_a \epsilon_a = \sum_a \left\langle a|\hat{h}|a\right\rangle + \sum_b \langle ab||ab\rangle \quad (1.29)$$

It can be seen from Eqs. (1.20) and (1.29),

$$E_0 \neq \sum_a^N \epsilon_a \quad (1.30)$$

The total energy of the state function |Ψ0›| is not equal to the sum of orbital energies. Because the energy ε_a comprises Coulomb and exchange interactions between an electron in χ_a and electrons in all other occupied orbitals, coulomb and exchange interactions between an electron in χ_a and electrons in all other occupied orbitals are included in χ_b. The electron-electron repulsion term between the electrons in χ_a and χ_b is thus counted twice when ε_a and ε_b are added. The electron-electron repulsion is counted twice in the sum of orbital energy, resulting in the factor 1/2 in the total energy expression (Eq. (1.20)).

1.2.1 Koopmans' Theorem

A theory by Koopmans[2] indicates that the vertical ionization potential (IP) is only negative of the maximum occupied orbital energy, giving the orbital energies physical importance. Similarly, electron affinity (EA) is equal to the lowest unoccupied orbital energy minus one. Given an N-electron Hartree-Fock single determinant $|\,^N\Psi_0\,\rangle$ with occupied and virtual spin orbital energies ε_a and ε_r, respectively, the ionization potential to produce an electron single determinant $|\,^{N-1}\Psi_i\,\rangle$ with identical spin orbitals, obtained by removing an electron from spin orbital and the electron affinity to produce a electron single determinant $|\,^{N+1}\Psi^r\,\rangle$.

i.e.

$$IP = {}^{N-1}E_a - {}^{N}E_0 = -\epsilon_a \tag{1.31}$$

and

$$EA = {}^{N}E_0 - {}^{N+1}E^r = -\epsilon_r \tag{1.32}$$

Due to the cancelling of correlation energy (see Section 1.2.2 for details on correlation energy) with relaxation error, the vertical IPs are found to accord rather well with their experimental counterparts.[2] The EAs obtained in this manner, however, are not accurate.

1.2.2 The Roothaan-Hall Method

Roothaan and Hall[6] are responsible for a significant simplification of the standard HF equation, making the HF approach practical to execute. The spin-orbitals with opposite (spin-up and spin-down) spin functions are coupled together for closed-shell systems, and the problem can be reduced by just employing spatial orbitals after spin-integration. The process is known as the restricted Hartree-Fock (RHF) method, and it results in Roothaan Hall[6] equations. The open-shell RHF (ROHF) method can be used to solve numerous electron open-shell systems in which the majority of the electron are coupled up. On the other hand, this electron pairing simplification may not be considered, and the HF equations may be directly solved using spin-orbitals. The approach is known as the unconstrained Hartree-Fock (UHF) procedure, and it produces the Pople-Nesbet equations. [2] Roothaan,[6] who established the concept of basis functions to be used for describing geographical data, gave the HF closed shell equation a lot of practicality.

By properly integrating out the spin portion, orbitals can be obtained. The molecular orbitals are extended as a linear combination of atomic orbitals (AO's), which are written as a linear combination of the basis functions ϕu, resulting

$$\psi_i = \sum_{\mu=1}^{K} C_{\mu i}\phi_\mu \quad i = 1, 2, \ldots, K \tag{1.33}$$

A finite set of K basis functions is employed for practical computational reasons. Usually, the basic functions are centered on different atoms. The foundation functions will be described in further depth in the following Section. The difficulty of computing the HF molecular orbitals is reduced to the problem of calculating the set of expansion coefficients $C_{\mu i}$ when Eq. (1.33) is used. Matrix equations for $C_{\mu i}$ can be obtained by substituting the linear expansion into Eq (1.27). These equations are known as the Roothaan-Hall equations and are written

$$\sum_{\nu} F_{\mu\nu} C_{\nu i} = \epsilon_i \sum_{\nu} S_{\mu\nu} C_{\nu i} \quad i = 1, 2, \ldots, K \tag{1.34}$$

These equations can be written as FC = εSC, where F, C, and S are the Fock, coefficient, and overlap matrices, respectively, and the elements of these matrices are given as

$$F_{\mu\nu} = \int d^3 r_1 \, \phi_\mu^* \, \hat{f}(1) \, \phi_\nu \tag{1.35}$$

$$S_{\mu\nu} = \int d^3 r_1 \phi_\mu^* \, \phi_\nu \tag{1.36}$$

When the Fock operator is used explicitly, the Fock matrix element is

$$F_{\mu\nu} = H_{\mu\nu}^{core} + \sum_{\lambda\sigma} P_{\lambda\sigma} \left[\langle \mu\nu | \lambda\sigma \rangle - \frac{1}{2} \langle \mu\lambda | \nu\sigma \rangle \right] \tag{1.37}$$

where $H_{\mu\nu}^{core}$ is a matrix representation of one electron operator, $P_{\lambda\sigma}$ is the charge density bond order matrix, [2] and the quantities $\langle \mu\nu | \lambda\sigma \rangle$ are two electron-repulsion integrals Here,

$$H_{\mu\nu}^{core} = \int d^3 r_1 \, \phi_\mu^*(1) \hat{h}(1) \phi_\nu(1) \tag{1.38}$$

and for doubly occupied MOs

$$P_{\lambda\sigma} = 2 \sum_{i=1}^{occ} C_{\lambda i}^* C_{\sigma i} \tag{1.39}$$

As a result, the total electronic energy of a closed shell system is

$$E = \frac{1}{2}\sum_{\lambda\sigma}^{occ}\sum_{\mu\nu}^{occ} P_{\lambda\sigma}\left[H_{\mu\nu}^{core} + F_{\mu\nu}\right] \tag{1.40}$$

When this energy is combined with nuclear-nuclear repulsion energy, a total energy expression is obtained. Because the Fock matrix is dependent on the molecular orbital coefficients through the density matrix, the Roothaan-Hall equations are only formally linear. As a result, they must use an iterative approach to solve their problem. The technique is also known as the self-consistent-held (SCF) approach since the resulting molecular orbitals are iteratively produced from their own effective potential.

1.3 Basis Functions and Basis Sets

Individual molecule orbitals can be expressed as a linear combination of a limited set of *K* specified one-electron functions known as basis functions, as explained in the previous Section. Currently, there are two types of atomic basis functions in use. The Slater-type atomic orbitals are the first (STOs). The following is a general phrase for a STO focusing on R_A:

$$\phi_{l,m,n}^{STO}(\mathbf{r}) = N|\mathbf{r} - \mathbf{R_A}|^{(n-1)}e^{-\xi|\mathbf{r}-\mathbf{R_A}|}Y_{l,m}(\theta,\phi) \tag{1.41}$$

Here, N is the normalization constant, n is a principal quantum number, and (is the orbital exponent, which is an arbitrary positive value. The spherical harmonics, Y_{lm}, characterize the angular component of the orbital. STOs provide a decent representation of the radial distribution of atomic orbitals. In the presence of more than two atoms, however, integral evaluation over Slater type basis functions is extremely time consuming and inefficient. As a result, STOs are no longer commonly employed in molecular orbital computations. The Gaussian-type atomic orbitals are an alternate choice of basis functions presented by Boys.[7] (GTOs). The following is a general primitive GTO centered at R_A:

$$\phi_{l,m,n}^{GTO}(\mathbf{r}) = N x^l y^m z^n e^{-\xi|\mathbf{r}-\mathbf{R}_A|^2} \quad (1.42)$$

The s, p, d type basis functions are the primitive GTOs (PG) with $l + m + n = 0$, 1, 2, … respectively. Contractions are further linear combinations of these base functions. There are several different Gaussian basis functions, also known as basis sets that are commonly employed in quantum chemical computations, some of which are described below.

- A minimum basis set: Each of the occupied AOs is represented by a single basis function, i.e. one contraction per atomic orbital. To represent the STO type function, three PGs are integrated into one basis function in a STO-3G basis set.

- The double-zeta (DZ) basis set: each atomic orbital has two basis functions. Basis sets of triple zeta (TZ), quadrupole zeta (QZ), and other qualities can be built in the same way. Incorporating the effects of radial electron correlation demands the usage of DZ or superior basis set quality, in addition to enhanced flexibility at the HF-level.

- The split-valence (SV) basis set: For inner-shell AOs (one contraction per orbital), this basis set is minimum, while for valence AOs, it is double-zeta (two contractions per orbital).

- Polarization functions: To increase the flexibility of the AO-basis for atoms in a non-spherical environment, a set of functions corresponding to atomic orbitals is required, particularly during the creation of a chemical bond where electron polarization occurs. The symbols '*' and '**' denote the addition of polarization functions, implying the employment of a set of d and (d,p)-functions. The first and second row atoms (save the H-atom) receive d-functions, while the H-atom receives just p-functions.

- Diffuse functions: A set of functions used to describe the accumulation of

electron density away from nuclear centers, particularly in the case of anions and molecules with lone pairs of electrons. The diffuse functions are denoted by '+' and '++,' implying that the diffuse functions are added for H-atoms, heavy atoms, and H-atoms, respectively.

- Correlation-consistent basis sets: Dunning and collaborators [26] produced some of the most extensively used basis sets. Using extrapolation techniques, these are designed to approach the complete basis set (CBS) limit systematically. The basis sets for first- and second-row atoms are cc-pVnZ, where n=D, T (D=doub1e, T=triple, etc.). The 'cc-p' stands for 'correlation consistent polarized,' while the 'V' indicates that the basis sets are valence only.

STO-3G, 3-21G, 6-31G, 6-31G (d,p), 6-31 ++G(d,p), cc-pVnZ, and so on form a hierarchy of basis sets. Consider a methane molecule computation using a 6-31G basis set as an example. The H-atom is represented by four Gaussian primitives (PGs) and two contractions (3 and 1 respectively). The inner shell of a carbon atom has one contraction due to six PGs, while the valence shell has two contractions each for two 2s and three 2p (3 and I respectively). With 22 PGs, the total number of contractions for C-atom is 9. As a result, a methane level calculation of 6-31G contains 17 contractions and 38 PGs. This quantity is 23 contractions (44 PGs) in 6-31G (d) and 45 contractions (56 PGs) in 6-31G (d,p), respectively. Please see ref [2,7, 8] for further information on basis sets. The basis sets 6-311 ++G (2d, 2p), 6-31+G (d,p), and aug-cc-pVTZ have all been used in this thesis.

1.4 Electron Correlation and Correlated Methods

As previously stated, an electron moves in the average field generated by remaining electrons and the fixed nuclei in the HF theory. Coulomb's law, on the other hand, allows electrons to respond to each other instantly. Correlation energy is the difference between precise energy and HF energy. As previously stated, it

results from the HF method's ignoring of electron correlation, particularly Coulomb correlation. Another shortcoming of the spin-restricted closed-shell HF function is that it rarely leads to accurate molecular dissociation when nuclei are separated infinitely. For example, due to breakdown of the hydrogen molecule rather than dissociation into two neutral H atoms, a substantial inaccuracy of several eV's is obtained. Non-dynamical (static) correlation is the correlation energy coming from long-range correlation effects, such as molecule dissociation, and it can generally be dealt with using multiconfigurational SCF approaches (MCSCF). The electron correlation problem can be approached using a variety of theoretical approaches. The HF wave function, on the other hand, is commonly utilized as a foundation for associated theories, which are briefly explored in the following Sections.

1.5 Configuration Interaction

The oldest method for restoring dynamical correlation is the configuration interaction (CI) method.[9] For the construction of a correlated wave function, a collection of orthonormal orbitals produced as the eigenfunctions of the Fock operator within the HF theory is used. All feasible combinations of these orbitals can yield a complete set of antisymmetric wave functions for an N-electron system. The HF setup is, of course, one of these configurations. If all of the configurations are included, the exact wave function of the system will be produced. The precise wave function is represented as a linear combination of configuration state functions using this way.

$$\Psi = C_0\Phi_0 + \sum_R C_R\Phi_R \qquad (1.43)$$

C_R stands for variational parameters, and ϕ_R stands for reference configuration functions. The HF function ϕ_0 is usually the first term in the above equation. The expansion is known as single-reference CI or simply CI expansion when just the first term in the summation is used.[2] the expansion is known as multireference CI

(MRCI) expansion when there are several reference functions. The varied configuration states are achieved by simultaneously stimulating one, two, or more electrons from occupied HF ground state orbitals to virtual ones. The N occupied (occ) and (2k- N) virtual (*vir*) spin orbitals can be used to obtain $^{2k}C_N$ excited configurations, where k is the total number of basis functions. [2] The wave function is called Full CI (FCI) when all of these configurations are contained in it, and it is exact in the basis set limit. To minimize the overall energy of the system, the coefficients of configurations can be variationally optimized. In most cases, the entire wave function is written

$$\Psi = C_0\Phi_0 + \sum_{a}^{occ}\sum_{r}^{vir} C_a^r\Phi_a^r + \sum_{a<b}^{occ}\sum_{r<s}^{vir} C_{ab}^{rs}\Phi_{ab}^{rs} + \sum_{a<b<c}^{occ}\sum_{r<s<t}^{vir} C_{abc}^{rst}\Phi_{abc}^{rst} + \dots \qquad (1.44)$$

Φ_a^r, Φ_{ab}^{rs} and Φ_{abc}^{rst} are excited configurations that are single, doubly, triply, and so on (determinants). The FCI meets all of the requirements for a theoretical model. However, as the number of electrons and basis functions increases, FCI calculations become essentially hard to perform, even for tiny molecules with moderately big basis sets.

As a result, the stimulated determinants' expansion must be truncated. CI doubles is the wave function created by including only the HF and all doubly excited configurations (CID). This method[2] recovers a significant portion of the correlation energy. Other, highly excited configurations, such as Ct solos and doubles (CISD) and triples (CISDT), CISDT and quadrupoles (CISDTQ), and so on, can be included to improve accuracy.

The size-consistency and size-extensivity difficulties are caused by truncations of the CI expansion. The phrase size-consistency relates to the energy's additive separability during fragmentation. For example, if a molecule AB dissociates into its fragments A and B, the technique is size-consistent if the $E_{AB} = E_A + E_B$ and $\Psi_{AB} = \Psi_A\Psi_B$ are equal. If the wave functions are produced using the CISD approach, the Ψ_{AB} can include up to two electron excitations, while the

product $\Psi_A\Psi_B$ can contain up to four electron excitations, indicating CISD. In other words, any truncated CI will lack the size-consistency feature.

The scaling of the energy of the system with the number of electrons is connected to size-extensivity. The approach is considered to be size-extensive[2] if the total energy (and thus the correlation energy) of a system varies approximately linearly with the number of electrons, as in the HF image. Any truncated form of CI, in my opinion, cannot be regarded a valid theoretical model.

1.6 Coupled-Cluster Method

In recent years, the coupled cluster (CC) approach[10] has developed as a powerful tool for handling electron correlation for small to medium-sized molecules with excellent accuracy. The ground state wave function of an N-electron system is derived using the CC technique by acting on a reference wave function, commonly the Hartree-Fock configuration, with an exponential wave-operator.

$$|\Psi_0\rangle = e^{\hat{T}}|\Phi_0\rangle = (1 + \hat{T} + \frac{1}{2!}\hat{T}^2 + \frac{1}{3!}\hat{T}^3 + \ldots + \frac{1}{N!}\hat{T}^N)\Phi_0 \qquad (1.45)$$

The cluster operator $\hat{T}$ is made up of the one-electron excitation operator $\hat{T}_1$, two-electron excitation operator $\hat{T}_2$ and so on up to N-electron excitation operators.

operator $\hat{T}_N$,

$$\hat{T} = \hat{T}_1 + \hat{T}_2 + \hat{T}_3 + \ldots + \hat{T}_N \qquad (1.46)$$

The closed-shell HF wave function built of N occupied spin orbitals is the independent-particle reference function ϕ_0. The coupled-cluster singles and doubles (CCSD) approach[11-13] is defined by truncating the operator $\hat{T}$ following double excitations. The CCSD energy in a closed shell is given as,

$$E_{CCSD} = \left\langle \Phi_0|\hat{H}|\Phi_0 \right\rangle + \sum_{a,r} f_{ar} t_a^r + \sum_{a>b}\sum_{r>s} \langle ab||rs\rangle \, (t_{ab}^{rs} + t_a^r t_b^s - t_a^s t_b^r) \qquad (1.47)$$

The Fock matrix elements, cluster amplitude, and two- electron integrals are denoted by f_{ia}, t, and ‹ ij||ab ›, respectively. The amplitudes of the clusters are comparable to the expansion coefficients in CI. The method's only drawbacks are the non-linearity of the CC equation and its non-variational nature. The size-consistency and size-extensivity are ensured by the exponential character of the wave-operator and the connectedness of the terms. Although the CCSD approach is more comprehensive than the configuration interaction (CISD) method, it is frequently insufficiently accurate to determine molecular characteristics with high precision (within 1 percent of the full CI limit). In theory, the solution to this difficulty is to increase the number of terms in $\hat{T}$.

1.7 Møller-Plesset Perturbation Theory

Miller and Plesset's perturbative technique[14] is the most easy and popular method for accounting the correlation. The Hamiltonian operator of a molecule with N-electrons is separated into two pieces using this method: an unperturbed Hamiltonian $\hat{H}_0$ and a perturbation $\widehat{\lambda H}_1$ as.

$$\hat{H} = \hat{H}_0 + \lambda \hat{H}_1$$
$$\hat{H}_0 = \sum_i \hat{h}(i) + \hat{V}_{HF}$$
$$\hat{H}_1 = \sum_{i>j} \frac{1}{r_{ij}} - \hat{V}_{HF} \qquad (1.48)$$

The wave function and energy are also enlarged in the same way if the unperturbed wave function Ψ_0 is an eigenfunction of the unperturbed Hamiltonian $\hat{H}_0$ and eigenvalue as E_0

$$\Psi = \Psi_0 + \lambda\Psi_1 + \lambda^2\Psi_2 + \ldots + \lambda^n\Psi_n$$
$$E = E_0 + \lambda E_1 + \lambda^2 E_2 + \ldots + \lambda^n E_n \qquad (1.49)$$

We generate a hierarchy of equations by entering Eqs (1.48) and (1.49) into the Schrodinger equation and collecting terms of the same order in λ. The first three are

listed below:

$$\hat{H}_0\Psi_0 = E_0\Psi_0 \tag{1.50}$$

$$(\hat{H}_0 - E_0)\Psi_1 = (\hat{H}_1 - E_1)\Psi_0 \tag{1.51}$$

$$(\hat{H}_0 - E_0)\Psi_2 = (\hat{H}_1 - E_1)\Psi_1 + E_2\Psi_0 \tag{1.52}$$

The perturbed wave functions can be considered to be orthogonal to the zeroth-order function $\langle\Psi_0|\Psi_i\rangle = \delta_{ij}$ resulting in the so-called intermediate normalization of the total wave function $\langle\Psi|\Psi_0\rangle = 1$. The expressions for E are obtained using this normalization, the first three of which are:

$$E_0 = \left\langle \Psi_0|\hat{H}_0|\Psi_0 \right\rangle \tag{1.53}$$

$$E_1 = \left\langle \Psi_0|\hat{H}_1|\Psi_0 \right\rangle \tag{1.54}$$

$$E_2 = \left\langle \Psi_0|\hat{H}_1|\Psi_1 \right\rangle \tag{1.55}$$

In the expression for the second-order energy, the first-order wave-function occurs. It can be found by solving Eq (1.51). The unperturbed Hamiltonian $\hat{H}_0$ in the Miller-Plesset perturbation theory is chosen to be a sum of Fock-operators acting on each electron. The sum of the eigenvalues (orbital energies) for the occupied spin orbitals yields the zeroth-order energy right away. As a result, the HF energy is equal to the sum of the zeroth and first-order energy. We expand the first-order wave-function in determinants ϕ_μ to solve the first-order equation.

$$\Psi_1 = \sum_\mu C_\mu \Phi_\mu \tag{1.56}$$

All ϕ_μ, it is discovered, are $\hat{H}_0$ eigenfunctions with E_0 eigenvalues equal to the sum of the occupied spin-orbital energies. [2] The first order expansion coefficient is calculated using this expanded wave function.

$$C_\mu = -\frac{\left\langle \Phi_\mu|\hat{H}_1|\Psi_0 \right\rangle}{E_\mu - E_0} \tag{1.57}$$

The numerator contains the interaction between configuration ϕ_μ and the HF

reference function Ψ_0, as we can see. As a result, only those configurations for which this element is non-zero must be included in the first-order wave function expansion. We know they're the doubly excited configurations because of the Slater rules. The Brillouin theorem asserts that there is no interaction between the closed-shell HF wave function and singly excited configurations, hence singly excited configurations will not contribute. Thus,

$$\Psi_1 = \sum_{a>b} \sum_{r>s} C_{ab}^{rs} \Psi_{ab}^{rs} \tag{1.58}$$

a, b are occupied spin-orbitals, whereas r, s are virtual spin-orbitals. The coefficients in second-order Maller-Plesset perturbation theory are given by equation:

$$C_{ab}^{rs} = -\frac{\left\langle \Psi_0 | \hat{H} | \Psi_{ab}^{rs} \right\rangle}{\epsilon_r + \epsilon_s - \epsilon_a - \epsilon_b} \tag{1.59}$$

and the second order energy by

$$E_2 = -\sum_{a>b} \sum_{r>s} \frac{\left| \left\langle \Psi_0 | \hat{H} | \Psi_{ab}^{rs} \right\rangle \right|^2}{\epsilon_r + \epsilon_s - \epsilon_a - \epsilon_b} \tag{1.60}$$

The energy expression (1.49), which can be terminated in any order, has the property of size-extensivity, but it is not variational. The complexity and cost of computing the energy terms in this expansion grows fast as the order increases, i.e. normal calculations only employ up to second, third, or fourth order (MP2, MP3 or MP4).

1.8 Density Functional Theory

For the analysis of ground state energy and molecular characteristics, Density Functional Theory (DFT) is possibly the most commonly used and surely an appealing contemporary approach of computational quantum chemistry. Instead of

the traditional multiple particle wave function, the ground state electron density ρ(r) is used as the basic variable. The Hohenberg—Kohn (HK) theorem,[15] which states that "given a non-degenerate ground state of a cluster of electrons moving under the influence of an external potential V and their mutual repulsion, the electron density is a unique functional of V and vice versa," lay the groundwork for the DFT. i.e. the electronic vitality E is an electron density functional, E = E(ρ), and integrating to N for any trial density $\tilde{\rho}$(r) fulfils the following bound.

$$E[\tilde{\rho}] \geq E_{gs} \tag{1.61}$$

For the genuine energy functional, there is a variational principle. Such a trial density should adhere to requirements such as N- and V- representability [40]. By minimizing the energy functional, one can derive the ground state electron density ρ(r). However, the exact shape of the energy functional is unknown, and researchers have been looking for it for decades. Kohn-Sham (KS) proposed a very beneficial approach by rewriting the problem of estimating total electronic energy E as a function of electron density.[16] In DFT formalism, the KS scheme restores the traditional orbital image. The ground state energy is given as in this method.

$$E[\rho] = T_s[\rho] + J[\rho] + E_{xc}[\rho] \tag{1.62}$$

where $T_s(\rho)$, $J(\rho)$ and $E_{xc}(\rho)$ are constants, are the sum of the energy functionals for kinetic energy, electron-electron repulsion, and exchange-correlation energy. The electron density can be written

$$\rho(\mathbf{r}) = \sum_{a}^{N} |\chi_a|^2 \tag{1.63}$$

The following KS equations are produced by calculating the functional derivative of energy with respect to density and subjecting it to the orthonormality of KS orbitals (χ_i).[16]

$$[-\frac{1}{2}\nabla^2 + V_{eff}(\mathbf{r})]\chi_a(\mathbf{r}) = \epsilon_a \chi_a(\mathbf{r}) \tag{1.64}$$

The effective potential of Kohn-Sham is defined as follows:

On the right hand side, the first term represents the interaction of the electronic cloud with the nuclei (i.e., the external potential), the second term is the Coulombic potential due to electron repulsion, and the third term is the exchange-correlation potential calculated

$$V_{xc}(\mathbf{r}) = \frac{\delta E_{xc}[\rho]}{\delta \rho} \tag{1.66}$$

The total energy of the system is provided by after minor simplification.

$$E = \sum_{a}^{N} \epsilon_a - \frac{1}{2} \int \frac{\rho(\mathbf{r})\rho(\mathbf{r}')}{|\mathbf{r} - \mathbf{r}'|} d^3r \, d^3r' + E_{xc}[\rho] - \int V_{xc}(\mathbf{r})\rho(\mathbf{r}) d^3r \tag{1.67}$$

Here,

$$\sum_{a}^{N} \epsilon_a = \sum_{a}^{N} \left\langle \chi_a \left| -\frac{1}{2}\nabla^2 + V_{eff}(\mathbf{r}) \right| \chi_a \right\rangle \tag{1.68}$$

Eqs. (1.63), (1.64), and (1.65) must be solved in the same way each time. One starts with an estimated ρ(r), construts V_{eff} (r) and then finds a new ρ(r) from (1.63) and (1.64). Finally, using (1.67) and (1.68), we can calculate total energy.

Thus, KS equations are similar to HF equations in appearance, but KS- DFT differs from HF theory in its ability to completely capture electron-correlation effects. However, because the precise functional dependency of V_{xc},, on ρ(r) is unknown, certain estimates must be made.[17-22] The local density approximation (LDA) is the simplest possible approximation, consisting of replacing the exchange-correlation energy $E_{xc}(\rho)$ by

$$E_{xc}[\rho] = \int \epsilon_{xc}[\rho] \, \rho(\mathbf{r}) d^3r \tag{1.69}$$

Where $\varepsilon_{xc}(\rho)$ is the per-electron exchange-correlation energy of a homogeneous electron gas with density ρ(r).

$$V_{xc}[\rho] = \frac{\delta E_{xc}[\rho]}{\delta \rho} = \epsilon_{xc}[\rho] + \rho \frac{\delta \epsilon_{xc}[\rho]}{\delta \rho} \tag{1.70}$$

Slater presented the X_α- method before the KS-LDA method was published, in

which the correlation contribution to E_{xc} is ignored and the exchange contribution is regarded

$$E_{x\alpha} = -A\alpha \int \rho^{\frac{4}{3}}(\mathbf{r}) d^3r \qquad (1.71)$$

A is a well-chosen constant in this case. Indeed, if the correlation is neglected in LDA, the KS equation that results is the X_α equation with α= 2/3. In many circumstances, the LDA is reasonable, but introducing the electron density gradient resulted in a significant increase in accuracy.

$$E_{xc}[\rho] = \int d^3r\ \rho(\mathbf{r})\ \epsilon_{xc}(\rho(\mathbf{r}); \nabla\rho(\mathbf{r})) \qquad (1.72)$$

The unknown functional is approximated by an integral over a function that depends solely on the density and its gradient at a particular point in space, which is known as non-local approximation or generalized gradient approximations (GGA). There has recently been significant progress in the contribution of functionals, in addition to LDA and GGA. Various functional forms have been developed that allow the majority of the exchange-correlation energy to be recovered. The hybrid B3LYP exchange—correlation functional is used in this study.[19] This functional is given by

$$E_{xc}^{B3LYP} = (1-a)E_x^{LSDA} + aE_x^{HF} + b\Delta E_x^B + (1-c)E_c^{LSDA} + cE_c^{LYP} \qquad (1.73)$$

Where the constants a, b, and c have values of 0.20, 0.72, and 0.81, respectively. The acronyms E_x^{LSDA} and E_c^{LSDA} stand for local spin density approximation exchange and correlation energy, respectively, while E_x^{HF} stands for HF exchange. The phrases ΔE_x^B and $\Delta\ E_C^{LYP}$ stand for DFT exchange and correlation terms, respectively, thanks to Becke and Lee, Yang, and Parr. The difference between the total and accurate HF exchange is represented by the term AE B. Because of its broad applicability, the B3LYP functional has grown in popularity. For covalently bound systems, the method works well, and the results are equivalent to the exchange-correlation effects obtained using MP2-level. Hobza *et al*.[20] have pointed

out that the B3LP functional works effectively for H-bonded systems, despite failing to account for dispersion energy in stacking interactions. Also, very recently, Truhlar and Zhao[21, 22] developed new density functionals, namely MPWI B95, MPWB1K and found that these functionals yield good results for hydrogen bonding and weak interactions. In the present thesis, the B3LYP functionals have been used for some intramolecular hydrogen bonded systems and are critically compared.

Organic inhibitor's inhibitory action is mostly determined by its functional groups, steric effects, orbital character of donating electrons, electronic density of donor atoms, and other physicochemical and electronic features.[23, 24] Organic molecules that operate as inhibitors are known to be high in heteroatoms, such as sulphur, nitrogen, and oxygen. [25, 26]

The structures, dipole moments, vibration frequencies, nuclear magnetic resonance chemical shifts, optical properties, molecular electrostatic potentials, molecular mechanisms, and thermodynamic properties of heterocyclc compounds are all accurately analysed using density functional theory (DFT) methods.[27-30] Novel heterocyclic azo compounds were synthesised and described by combining diazonium salts with N-(4-methylpheneyl) maleimide and other sulfa compounds. The density function theory was calculated at the B3LYP level. The 6-311+G (d,p) higher basis set level was used to compute the HOMO-LUMO energies of the substances examined. At the same level of approach, Mulliken charge distributions of the examined substances were computed.[31]

To demonstrate the structural and geometrical parameters involved in the investigation, DFT and computational studies were performed on poly heterocyclic compounds containing triazolo derivatives. Molecular docking with the Tankyrase I enzyme as a target revealed that the heterocyclic compounds investigated act as ligands, connecting with the majority of active sites on Tankyrase I with interactions that are classified as H-bonding and VDW.[32] For Chromene derivates, molecule structure, spectroscopy and population studies, noncovalent interactions,

and electronic and nonlinear optical properties have all been investigated using DFT. Finally, Molecular docking studies determine its antiacetylcholinesterase action.[33] 2-Amino-5-trifluoromethyl-1,3,4-thiadiazole with Anticancer Properties: DFT Study of Electronic Properties, Spectroscopic Profile, and Biological Activity.[34-36]

Density functional theories were used to undertake theoretical calculations on geometry optimization, stability, reactivity, and molecular orbital description HOMO and LUMO of novel Schiff bases.[37, 38] To estimate chemical reactivity descriptors of pyridine derivatives containing selenium atoms, DFT calculations were performed in the gas phase using the B3LYP 6-311G (d,p) basis set. The outcomes of molecular docking and biological activity assessments have been illustrated using DFT data.[39] The energy gap can aid in understanding the reactivity behaviour and stability of 2-amino-3-cyano-4.6-diarylpyridine compounds, and DFT theory was utilised to explain the electronic characteristics of certain dyes.[40-42] Antioxidant and anticancer activity of selenium N-heterocyclic carbene compounds were evaluated using DFT.[43]

In conclusion, the DFT technique delivers reasonably accurate correlation energy estimations with minimal computing effort. The approach also has the advantage of using density as a basic variable rather than the traditional wave function. The underlying principle of DFT is that the total energy of the system is a unique functional of the electron density, hence it is unnecessary to compute the full many-body wave function of the system.

1.9 Semi-empirical Methods

The explicit assessment of two electron integrals, as well as other CPU time-intensive operations such as matrix diagonalization and the accompanying SCF technique, are a major barrier in ab initio computational quantum chemistry. This makes it difficult to apply ab initio approaches to massive molecular systems like polymers, protein folding, and molecular crystals, for example. These issues with

ab initio approaches could be solved by using *semi-empirical* methods, which are more approximate.[44]

Instead of computing the two electron integrals in ab initio treatment, some empirical parameters are employed, as the name suggests. The Huckel molecular orbital technique (HMO)[45] and the Pariser, Pople, and Parr (PPP)[46] methods are two such methods that have been extensively developed and employed for discovering the bonding and reactivity properties of organic molecules during the 1930s and 1960s.[47, 48]

Only π-electrons are explicitly considered in HMO, whereas the σ framework is ignored. The PPP approach was created to deal with spectroscopic features of molecules while keeping the HMO's r-electron bias. The zero differential overlap assumption is an important one in PPP (ZDO). The interaction of orbitals centered on distinct atoms is ignored in this example, and the electron repulsion integrals are simplified as follows:

$$\langle ij|kl\rangle = \langle ii|kk\rangle \, \delta_{ij}\delta_{kl} \qquad (1.74)$$

The Kronecker delta is represented by δ_{ij}. The PPP approach was popular in the 1960s and has proven to be effective for a variety of chemical problems.

The extended Huckel theory (EHT), which is applicable to both conjugated and non-conjugated molecules, considers only the valence electrons and incorporates geometry optimization (albeit limited) by minimizing the weighted sum of orbital energy, was the next phase of research. The Complete Neglect of Differential Overlap (CNDO)[49] and its enhanced form, the intermediate neglect of differential overlap (INDO),[50] provided even more improvement. Some electron repulsion integrals due to interaction of orbitals over the same atoms are ignored by the INDO model. Bond lengths and bond angles of conventional organic compounds are well represented by the CNDO and INDO models. They do, however, produce low dipole moments and binding energies. Bond energies are good when using the modified neglect of differential overlap (MNDO)[51] The AM1

(Austin model l)[51, 52] and PM3 (parametrized model 3)[52] on the other hand, are good for intermolecular hydrogen bonding in biological systems and have a lower heat of formation without sacrificing accuracy in molecular geometry and dipole moments. The specifics of these models can be found elsewhere. AMPAC and MOPAC are the most extensively used semi-empirical software.[53, 54]

The MOPAC-2000[55] includes the MOZYME module, which ensures that the approach may be applied to massive biomolecular systems. MOPAC-2007[56] can handle periodic boundaries in crystals, surfaces, and polymers, as well as the novel parameterization MOPAC-2016[57] for main group elements and transition metals utilizing experimental and ab initio data. This latest version additionally provides very accurate formation temps and molecule geometries.

The use of semi-empirical methods has the advantage of being able to handle huge molecule systems and calculate molecular characteristics in an acceptable amount of time. The nature of the approximate mode and the huge number of parameters involved are the only drawbacks of semi-empirical approaches. Semi-empirical approaches like AMI and PM3 models are solely employed in this thesis to generate the initial geometries of molecules, which are then subjected to rigorous ab initio calculations.

1.10 Molecular Dynamics Simulations

A purely classical and semi-classical method known as molecular dynamics (MD)[58] is used for large molecular systems to explore their equilibrium properties, transport phenomena, and transient behavior, in addition to ab initio and semi-empirical methods. For the mobility of the nuclei, the approach is based on Newtonian mechanics laws. This enables the tracking of particle paths in phase space as a function of time. Alder[59] used MD simulation to explore the transport features of a hard spherical gas, and Gibson and co-workers[60] used it to study the dynamics of radiation damage. Rahman[61] was the first to solve the problem of interacting atoms by using a more realistic Lennard-Jones potential. Other popular

MD variants include ab initio MD, Born-Oppenheimer MD, Car-Parrinelo MD, and so on. Rahman and Stillinger[62] published an earlier paper on MD simulation of liquid water. Since then, MD simulations have grown in popularity and have been used in a variety of complex systems. For example, Raugei *et al*.[63] studied the dynamics of water molecules in the Br^- solvation shell, and Bhide and Yashonath[64] studied the carbon nanotube. AMBER and GROMACS[64] are two popular MD simulation tools that are readily available.

1.11 References

1. Strich, A., Quantum chemistry, 4th ed. By Ira N. Levine, Prentice-Hall, Englewood Cliffs, NJ, 1991, X + 629 pp. Elementary quantum chemistry, 2nd ed. By Frank L. Pilar, McGraw-Hill International Editions, New York, 1990, XVI + 599 pp. *International Journal of Quantum Chemistry* **1992,** *43* (3), 439-441.
2. Szabó, A.; Ostlund, N. S., *Modern quantum chemistry : introduction to advanced electronic structure theory*. Mineola (N.Y.) : Dover publications: 1996.
3. Chen, J.; Houk, K. N., Molecular Modeling: Principles and Applications By Andrew R. Leach. Addison Wesley Longman Limited: Essex, England, 1996. 595 pp. ISBN 0-582-23933-8. *Journal of Chemical Information and Computer Sciences* **1998,** *38* (5), 939-939.
4. Slater, J. C., Note on Hartree's Method. *Physical Review* **1930,** *35* (2), 210-211.
5. Fock, V., Näherungsmethode zur Lösung des quantenmechanischen Mehrkörperproblems. *Zeitschrift für Physik* **1930,** *61* (1), 126-148.
6. Kolos, W., C. C, J. Roothaan. *Rev. Mod. Phys* **1960,** *32*, 205.
7. Boys, S. F.; Egerton, A. C., Electronic wave functions - I. A general method of calculation for the stationary states of any molecular system. *Proceedings of the Royal Society of London. Series A. Mathematical and Physical Sciences* **1950,** *200* (1063), 542-554.
8. Dunning Jr, T. H.; Hay, P. J., Modern theoretical chemistry. **1976**.
9. Shavitt, I., Graph theoretical concepts for the unitary group approach to the many-electron correlation problem. *International Journal of Quantum Chemistry* **1977,** *12* (S11), 131-148.
10. Bartlett, R. J., Many-Body Perturbation Theory and Coupled Cluster Theory for Electron Correlation in Molecules. *Annual Review of Physical Chemistry* **1981,** *32* (1), 359-401.

11. Purvis, G. D.; Bartlett, R. J., A full coupled- cluster singles and doubles model: The inclusion of disconnected triples. *The Journal of Chemical Physics* **1982,** *76* (4), 1910-1918.
12. Scuseria, G. E.; Janssen, C. L.; Schaefer, H. F., An efficient reformulation of the closed- shell coupled cluster single and double excitation (CCSD) equations. *The Journal of Chemical Physics* **1988,** *89* (12), 7382-7387.
13. Hampel, C.; Peterson, K. A.; Werner, H.-J., A comparison of the efficiency and accuracy of the quadratic configuration interaction (QCISD), coupled cluster (CCSD), and Brueckner coupled cluster (BCCD) methods. *Chemical Physics Letters* **1992,** *190* (1), 1-12.
14. Møller, C.; Plesset, M. S., Note on an Approximation Treatment for Many-Electron Systems. *Physical Review* **1934,** *46* (7), 618-622.
15. Hohenberg, P.; Kohn, W., Inhomogeneous Electron Gas. *Physical Review* **1964,** *136* (3B), B864-B871.
16. Kohn, W.; Sham, L. J., Self-Consistent Equations Including Exchange and Correlation Effects. *Physical Review* **1965,** *140* (4A), A1133-A1138.
17. Parr, R. G., Density functional theory of atoms and molecules. In *Horizons of quantum chemistry*, Springer: 1980; pp 5-15.
18. Brandas, E. J., *Propagating Insight: A Tribute to the Works of Yngve Ohrn*. Academic Press: 1999.
19. Lee, C.; Yang, W.; Parr, R. G., Development of the Colle-Salvetti correlation-energy formula into a functional of the electron density. *Physical Review B* **1988,** *37* (2), 785-789.
20. Černý, J.; Hobza, P., The X3LYP extended density functional accurately describes H-bonding but fails completely for stacking. *Physical Chemistry Chemical Physics* **2005,** *7* (8), 1624-1626.
21. Zhao, Y.; Pu, J.; Lynch, B. J.; Truhlar, D. G., Tests of second-generation and third-generation density functionals for thermochemical kinetics. *Physical Chemistry Chemical Physics* **2004,** *6* (4), 673-676.

22. Zhao, Y.; Truhlar, D. G., Benchmark Databases for Nonbonded Interactions and Their Use To Test Density Functional Theory. *Journal of Chemical Theory and Computation* **2005,** *1* (3), 415-432.
23. Imai, Y.; Nakajima, T.; Ueda, M., Preparation and properties of aromatic polypyrazoles from linear bis-β-diketones and aromatic dihydrazines. *Journal of Polymer Science: Polymer Chemistry Edition* **1981,** *19* (9), 2161-2165.
24. Kertit, S.; Es-Soufi, H.; Hammouti, B.; Benkaddour, M., 1-phenyl-5-mercapto-1, 2, 3, 4-tétrazole (PMT): un nouvel inhibiteur de corrosion de l'alliage Cu-Zn efficace à très faible concentration. *Journal de Chimie Physique et de Physico-Chimie Biologique* **1998,** *95* (9), 2070-2082.
25. Bouklah, M.; Hammouti, B.; Lagrenée, M.; Bentiss, F., Thermodynamic properties of 2,5-bis(4-methoxyphenyl)-1,3,4-oxadiazole as a corrosion inhibitor for mild steel in normal sulfuric acid medium. *Corrosion Science* **2006,** *48* (9), 2831-2842.
26. Bereket, G.; Öğretir, C.; Yurt, A., Quantum mechanical calculations on some 4-methyl-5-substituted imidazole derivatives as acidic corrosion inhibitor for zinc. *Journal of Molecular Structure: THEOCHEM* **2001,** *571* (1), 139-145.
27. Beytur, M.; Avinca, I., Molecular, Electronic, Nonlinear Optical and Spectroscopic Analysis of Heterocyclic 3-Substituted-4-(3-methyl-2-thienylmethyleneamino)-4,5-dihydro-1H-1,2,4-triazol-5-ones: Experiment and DFT Calculations. *Heterocyclic Communications* **2021,** *27* (1), 1-16.
28. Gümüş, S.; Türker, L., Substituent effect on the aromaticity of 1,3-azole systems. **2012,** *18* (1), 11-16.
29. Lienard, P.; Gavartin, J.; Boccardi, G.; Meunier, M., Predicting Drug Substances Autoxidation. *Pharmaceutical Research* **2015,** *32* (1), 300-310.
30. Azam, F.; Abodabos, H. S.; Taban, I. M.; Rfieda, A. R.; Mahmood, D.; Anwar, M. J.; Khan, S.; Sizochenko, N.; Poli, G.; Tuccinardi, T.; Ali, H. I., Rutin as promising drug for the treatment of Parkinson's disease: an assessment of MAO-B inhibitory potential by docking, molecular dynamics and DFT studies. *Molecular Simulation* **2019,** *45* (18), 1563-1571.

31. Almashal, F.; Jabar, A. M.; Dhumad, A. M., Synthesis, characterization and DFT computational studies of new heterocyclic azo compounds. *European Journal of Chemistry* **2018,** *9* (2), 84-88.
32. Abdelrehim, M. E.-s.; El-Sayed, S. D., A New Synthesis of Poly Heterocyclic Compounds Containing [1,2,4]triazolo and [1,2,3,4]tetrazolo Moieties and their DFT Study as Expected Anti-cancer Reagents. *Current Organic Synthesis* **2020,** *17* (3), 211-223.
33. Dlala, N. A.; Bouazizi, Y.; Ghalla, H.; Hamdi, N., DFT Calculations and Molecular Docking Studies on a Chromene Derivative. *Journal of Chemistry* **2021,** *2021*, 6674261.
34. Singh, I.; Al-Wahaibi, L. H.; Srivastava, R.; Prasad, O.; Pathak, S. K.; Kumar, S.; Parveen, S.; Banerjee, M.; El-Emam, A. A.; Sinha, L., DFT Study on the Electronic Properties, Spectroscopic Profile, and Biological Activity of 2-Amino-5-trifluoromethyl-1,3,4-thiadiazole with Anticancer Properties. *ACS Omega* **2020,** *5* (46), 30073-30087.
35. Domingo, L. R.; Ríos-Gutiérrez, M.; Pérez, P., Applications of the Conceptual Density Functional Theory Indices to Organic Chemistry Reactivity. *Molecules* **2016,** *21* (6).
36. Joshi, R.; Pandey, N.; Yadav, S. K.; Tilak, R.; Mishra, H.; Pokharia, S., Synthesis, spectroscopic characterization, DFT studies and antifungal activity of (E)-4-amino-5-[N'-(2-nitro-benzylidene)-hydrazino]-2,4-dihydro-[1,2,4]triazole-3-thione. *Journal of Molecular Structure* **2018,** *1164*, 386-403.
37. Salihović, M.; Pazalja, M.; Špirtović Halilović, S.; Veljović, E.; Mahmutović-Dizdarević, I.; Roca, S.; Novaković, I.; Trifunović, S., Synthesis, characterization, antimicrobial activity and DFT study of some novel Schiff bases. *Journal of Molecular Structure* **2021,** *1241*, 130670.
38. Rizk, S.; Awheda, I. M.; Smida, F. A., Synthesis and DFT Study of Newly Schiff Base and Fused Heterocyclic Compounds as Antibacterial Agent. *Journal Of Advances In Chemistry* **2019,** *16*, 5395-5403.

39. Abdellattif, M. H.; Abdel-Rahman, A. A. H.; Arief, M. M. H.; Mouneir, S. M.; Ali, A.; Hussien, M. A.; Okasha, R. M.; Afifi, T. H.; Hagar, M., Novel 2-Hydroselenonicotinonitriles and Selenopheno[2, 3-b]pyridines: Efficient Synthesis, Molecular Docking-DFT Modeling, and Antimicrobial Assessment. *Frontiers in Chemistry* **2021,** *9*.
40. Abdelrehim, M. E.-S., Synthesis of Some New Heterocyclic Azo Dyes Derived from 2-amino-3-cyano-4.6- diarylpyridines and Investigation of its Absorption Spectra and Stability using the DFT. *Current Organic Synthesis* **2021,** *18* (5), 506-516.
41. Abdelrehim, E.; El-Sayed, D., Geometric isomerism and DFT theoretical explanation of unexpected formation of N, N-disubstituted formamidines from 2-amino-3-cyano-4.6-diarylpyridines. **2020**.
42. Abdelrehim, E., Synthesis of Some New Heterocyclic Azo Dyes Derived from 2-amino-3-cyano-4.6-diarylpyridines and Investigation of its Absorption Spectra and Stability using the DFT. *Current Organic Synthesis* **2020**.
43. Yaqoob, M.; Gul, S.; Zubair, N. F.; Iqbal, J.; Iqbal, M. A., Theoretical calculation of selenium N-heterocyclic carbene compounds through DFT studies: Synthesis, characterization and biological potential. *Journal of Molecular Structure* **2020,** *1204*, 127462.
44. Cook, D. B.; Koch, W.; Stein, M., Handbook of Computational Quantum Chemistry. *Angewandte Chemie-German Edition* **1999,** *111* (7), 1059-1059.
45. Hubbs, C. L.; Hubbs, L. C., Apparent Parthenogenesis in Nature, in a Form of Fish of Hybrid Origin. *Science* **1932,** *76* (1983), 628-630.
46. Pariser, R.; Parr, R. G., A Semi- Empirical Theory of the Electronic Spectra and Electronic Structure of Complex Unsaturated Molecules. I. *The Journal of Chemical Physics* **1953,** *21* (3), 466-471.
47. Hoffmann, R., An Extended Hückel Theory. I. Hydrocarbons. *The Journal of Chemical Physics* **1963,** *39* (6), 1397-1412.

48. Hoffmann, R.; Lipscomb, W. N., Theory of Polyhedral Molecules. I. Physical Factorizations of the Secular Equation. *The Journal of Chemical Physics* **1962,** *36* (8), 2179-2189.
49. Pople, J. A.; Santry, D. P.; Segal, G. A., Approximate Self- Consistent Molecular Orbital Theory. I. Invariant Procedures. *The Journal of Chemical Physics* **1965,** *43* (10), S129-S135.
50. Maciel, G. E.; McIver, J. W.; Ostlund, N. S.; Pople, J. A., Approximate self-consistent molecular orbital theory of nuclear spin coupling. IV. Vicinal proton-proton coupling constants in substituted ethanes and ethylenes and related compounds. *Journal of the American Chemical Society* **1970,** *92* (15), 4497-4506.
51. Michael, J. S. D., Quantum Organic Chemistry. *Science* **1975,** *187* (4181), 1037-1044.
52. Dewar, M. J. S.; Zoebisch, E. G.; Healy, E. F.; Stewart, J. J. P., Development and use of quantum mechanical molecular models. 76. AM1: a new general purpose quantum mechanical molecular model. *Journal of the American Chemical Society* **1985,** *107* (13), 3902-3909.
53. Gilbert, T. M.; Check, C. E., AMPAC 8 with AGUI (AMPAC GUI) for Mac OSX SemiChem, Inc., P.O. Box 1649, Shawnee Mission, KS 66222. http://www.semichem.com. *Journal of the American Chemical Society* **2006,** *128* (18), 6265-6266.
54. Stewart, J. J. P., Optimization of parameters for semiempirical methods I. Method. *Journal of Computational Chemistry* **1989,** *10* (2), 209-220.
55. Früchtl, H. A.; Nobes, R. H.; Bliznyuk, A., Performance of mopac on parallel computers. *Journal of Molecular Structure: THEOCHEM* **2000,** *506* (1), 87-97.
56. Stewart, J. J. P., Optimization of parameters for semiempirical methods V: Modification of NDDO approximations and application to 70 elements. *Journal of Molecular Modeling* **2007,** *13* (12), 1173-1213.

57. Gieseking, R. L. M., A new release of MOPAC incorporating the INDO/S semiempirical model with CI excited states. *Journal of Computational Chemistry* **2021,** *42* (5), 365-378.
58. Allen, M. P.; Tildesley, D. J., *Computer simulation of liquids*. Oxford university press: 2017.
59. Alder, B. J.; Wainwright, T. E., Phase Transition for a Hard Sphere System. *The Journal of Chemical Physics* **1957,** *27* (5), 1208-1209.
60. Gibson, J. B.; Goland, A. N.; Milgram, M.; Vineyard, G. H., Dynamics of Radiation Damage. *Physical Review* **1960,** *120* (4), 1229-1253.
61. Rahman, A., Correlations in the Motion of Atoms in Liquid Argon. *Physical Review* **1964,** *136* (2A), A405-A411.
62. Bhide, S. Y.; Yashonath, S., n-Pentane and Isopentane in One-Dimensional Channels. *Journal of the American Chemical Society* **2003,** *125* (24), 7425-7434.
63. Case, D. A.; Cheatham Iii, T. E.; Darden, T.; Gohlke, H.; Luo, R.; Merz Jr, K. M.; Onufriev, A.; Simmerling, C.; Wang, B.; Woods, R. J., The Amber biomolecular simulation programs. *Journal of Computational Chemistry* **2005,** *26* (16), 1668-1688.
64. Hess, B.; Kutzner, C.; van der Spoel, D.; Lindahl, E., GROMACS 4: Algorithms for Highly Efficient, Load-Balanced, and Scalable Molecular Simulation. *Journal of Chemical Theory and Computation* **2008,** *4* (3), 435-447.

CHAPTER 2:

DFT-Based Theoretical Model for Predicting Loading and Release of a pH-Responsive Sulfasalazine Drug

2.1 Introduction

The drug and the drug delivery are most important, one cannot ignore the any one of these aspects for the best result. If the drug delivery system is not efficient, in such cases even the drug molecule fails in the clinical trial itself [1, 2]. It takes lot of time and money to discovery of new drug and get its clinical approval. To avoid these problems many drug carrier molecules were reportedly evolved using organic and inorganic molecules viz. liposomes, micelles, dendrimers, microspheres and nanoparticles. It's like using old drug with new coating or clothes to get the desired effects of the drug molecules. For a good drug delivery system, the prerequisites are low toxicity, biodegradability, biocompatibility, good cellular uptake, sustainable and targeted delivery. Diseases can be inhibited with minimum or no side effect, minimal dose and least frequency of doses by the use of effective drug delivery system [3, 4].

In the development of a better different drug delivery systems, the one of the ideal candidates is nanoparticles (NPs) which have specific features including enough small size to penetrate cell membranes, able to travel tiny arterioles and endothelial without causing clotting, binding and they also stabilizes the drugs [5-7]. The nanoparticles use for the entrapment of drugs are through use of liposomes, co-polymers, micelles, SiO_2, C and maghemite nanoparticles were already thoroughly studied and reported for the better drug delivery [8].

In recent time, use of meso-porous SiO_2 NPs (MSNs) (2-50 nm) as potential drug delivery system are widely explored due to their significant advantages viz. good biocompatibility, low apparent cytotoxicity, biodegradability, good excretion, ordered and uniform size, high surface areas, excellent stability, and effective and modifiable surface properties [9-14]. The major study was reported using the main two types i.e. MCM-41 and SBA-15 which provides good channels for the drug carriers affording silanol – containing surface. Though, silanol- group provides only weak H-bonding, there remains a need to design suitable functionalized mesoporous systems to introduce stronger host-guest interactions. Carefully functionalized (-NH_2 and -COOH groups) mesoporous SiO_2 NPs. These mesoporous SiO_2 NPs show better loading capacity than the most of the organic carriers viz. liposome, micelles and dendrimers as SiO_2 NPs possesses huge surface area (mostly greater than 1000 m^2

g^{-1}) and great pore volume. The mesoporous SiO_2 NPs are able to release drug as a response to internal conditions viz. pH and temperature [15-18].

Organ wise variations in the pH covers entire acidic and basic ranges e.g., stomach (pH 1.0 – 3.0), duodenum (pH 4.8 – 8.2), small intestine (pH 6.0 – 7.5), colon (7.0 – 7.5), rectum (pH 6.7 – 8.1) in plasma and ileum/jejunum (pH 7.4 – 8.0). For the development of pH-responsive drug delivery systems, these pH variations were well studied [19-25]. The specific intermolecular interactions administrated by difference in pH decides the physicochemical equilibrium established among the organ-drug molecule and drug delivery-drug molecule. Numerous pH-dependent interactions have been studied extensively primarily by experiments to explore the potential or best drug delivery materials. Economical and feasible screening to identify ideal drug delivery candidates is reported using the computational modelling [1, 12, 26-29]. New materials for drug delivery can be rationally designed through computations and subsequently tested by experiments and vice versa too to understand the basic mechanism of the drug delivery system. In this chapter, the work presents the CASTEP based computational studies of the experimental findings reported by Lee et. al. [30] to explore the pH-responsive loading and release of anti-inflammatory drug, **sulfasalazine**, on positively charge decorated silica surface. In the literature, Lee et. al. has shown that MSNs functionalised with tetraalkylammonium (TA) loads the drug sulfasalazine at acidic pH (2-5) due to positive charge and at basic pH (7.4) the drug is released due to deprotonation [30]. Inamdar et. al. studied the bottom-up nature of the interaction of drugs (sulfasalazine and alendronate) and modified silica surface at various pH [31, 32]. the authors firstly explained the computational methodology commonly used in this field. Then, the computational results were presented and discussed.

The major concluding remarks that were highlighted with a few perspectives for future studies made us select the method for our studies to utilised the same system with a different approach. The reports by Inamdar et. al. describes the computational work / DFT studies on the two major drug fragments of the sulfasalazine drug as N-(2-pyridyl) benzene sulfonamide (PBS) and salicylic acid (SA), while we used the similar strategy using the drug as whole without cutting it in small parts. In this chapter, detailed DFT studies on the whole drug sulfasalazine

loaded on MSN (TA functionalized SiO_2 NPs), as an ideal candidate for the pH responsive drug delivery system, is elaborated.

2.2 Materials and Methods

All the calculations have been done using CASTEP [33] module of MATERIALS STUDIO 2016. Density functional theory (DFT) within the generalized gradient approximation (GGA) using the functional of Perdew, Burke and Ernzerhof (PBE) [34] was applied to the exchange-correlation function [35]. Ultrasoft pseudopotentials in the Vanderbilt's formulation [36] along with medium plane wave cut-off energy of 489.8 eV was used throughout the calculations.

Geometry optimizations were performed using CASTEP with maximum SCF cycles set at 500 cycles. The TA functional group (FG) is attached to the silica surface on the middle Si atom in the second row replacing the hydroxyl group from the top, whereas for deprotonating the silica surface, H atom was removed from the hydroxyl group of the middle Si atom in the last row. For the calculations of the MSM mimic, we used the silica (1 0 1) surface as a model representing periodic silica. Drug molecule interaction with silica surface with the TA FG were used in the CASTEP calculation framework.

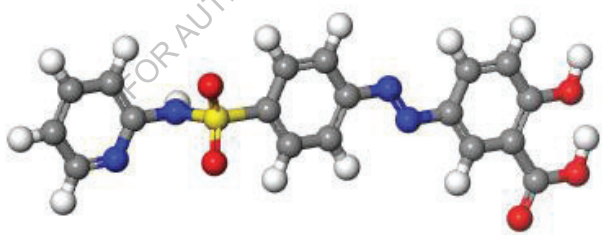

Figure 2.1: Molecular structure of Sulfasalazine drug

To test the model, the experimental results reported by Lee *et al.* [30] were utilised. Sulfasalazine is used to treat and prevent **bowel disease** called ulcerative colitis. It works inside the bowels by reducing the inflammation and the other symptoms of the disease. The structure of the **anti-inflammatory drug** molecule, sulfasalazine, is as shown in the **Figure 2.1** and it has reported to possesses two pKa values viz. 3.3 (carboxylic acid) and 6.24 (sulfonamide nitrogen) [37]. The acid−base reactions of the sulfasalazine drug at its two pKa values is as depicted in the **Figure 2.2 and 2.3**.

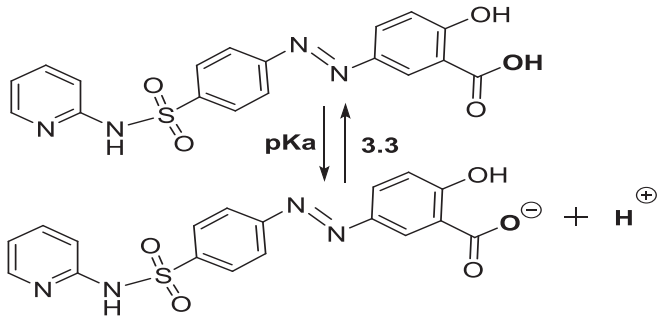

Figure 2.2: Acid−base reactions of the sulfasalazine drug at first pKa 3.3 (carboxylic acid)

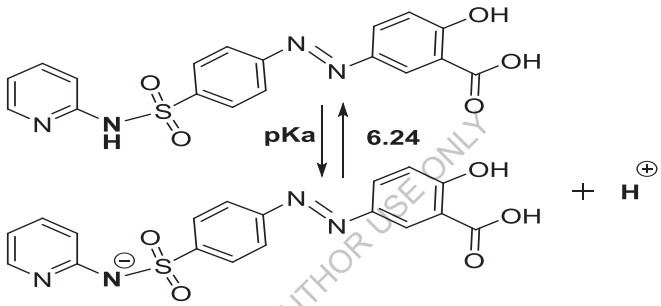

Figure 2.3: Acid−base reactions of the sulfasalazine drug at second pKa 6.24 (sulfonamide nitrogen)

2.3 Results and Discussion:

Lee *et al*. reported the synthesis of mesoporous SiO_2 NPs (MSN) with positively charged TA functional groups [30]. The report primarily focused on the loading and release of the anionic sulfasalazine drug molecules, which is used as an anti-inflammatory drug for bowel disease (IBD) which is related to intestinal disorders that cause prolonged inflammation of the digestive tract, onto the MSN–TA samples. The drug was reported getting loaded in acidic pH (2–5) while the drug was released in the basic (pH 7.4) buffer solution.

Based on the pKa values, drug molecules (D) exist mainly in two forms, neutral (0) and in deprotonated (-1) at various pH, i.e.the pKa of the drug leads to the formation the two species of the drug as neutral and deprotonated (**Figure 2.4**). We have used

the Silanol groups (SiOH) in the silica surface, the reported pKa values are 4.5 and 8.5 in the literature [38-40], and we used both these pKa values to study the pH responsive drug loading and releasing mechanism using DFT. In a similar way the silica surface (S) also exist in two states i.e. neutral (0) and in deprotonated (-1), i.e. for the silica surface also, the two pKa leads to the formation the two species of the silica as neutral and deprotonated (**Figure 2.5**) At any given pH, the fraction (F) can be calculated using rearranged Henderson-Hasselbalch equation [41] as shown in **equation 1**.

$$\textit{For deprotonated molecule:} \quad F_{-1} = \frac{1}{1+10^{pK_a-pH}}$$
$$\textit{and For neutral molecule:} \quad F_0 = 1 - \frac{1}{1+10^{pK_a-pH}} \qquad (1)$$

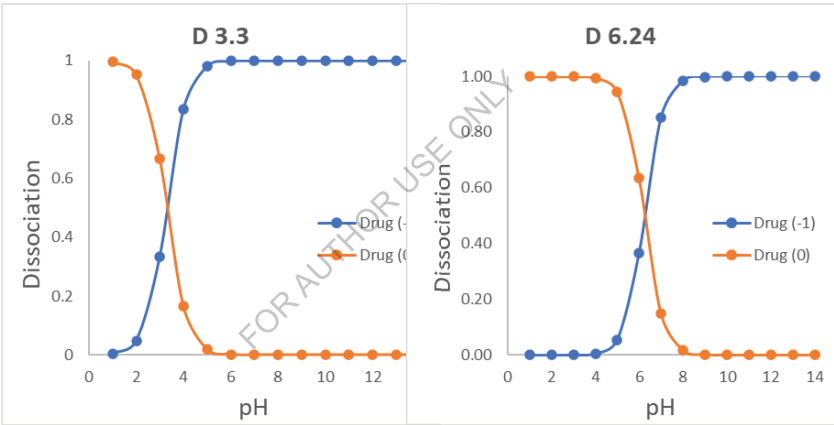

Figure 2.4: Illustration of dissociation of sulfasalazine drug with pH based on their pKa values. The Drug (-1) represents dissociated (deprotonated (-1)) and Drug (0) un-dissociated (neutral (0)) state of the molecules, respectively

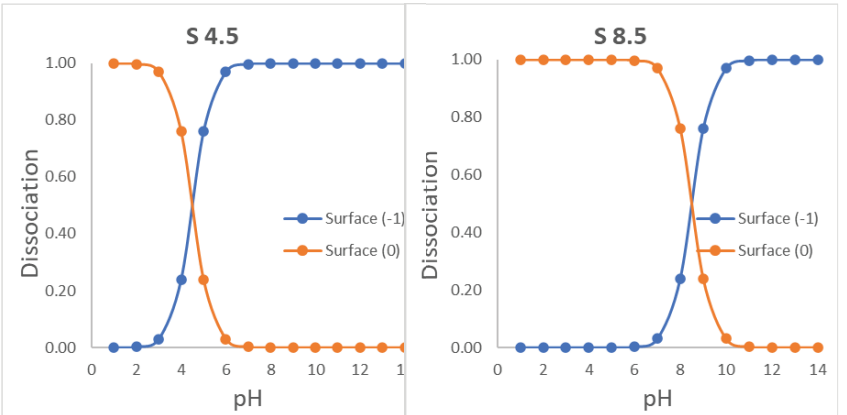

Figure 2.5: Illustration of dissociation of silica surface with pH based on their reported pKa values. The S (-1) represents dissociated (deprotonated (-1)) and Drug (0) un-dissociated (neutral (0)) state of the molecules, respectively

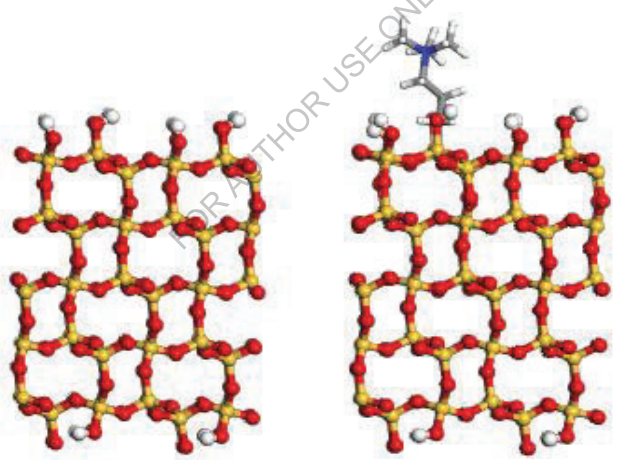

A) Neutral Silica surface without FG

B) Neutral Silica surface with FG

Figure 2.6: The silica surface without Functional group (A) and with TA functional group (B)

Thus two states of drug [D^0, D^{-1}] and surface [S^0, S^{-1}] gives four possible combinations viz. S^0 D^0, S^0 D^{-1}, S^{-1} D^0 and S^{-1} D^{-1}.

The optimised structures of the silica surface without Functional group and with TA functional group using the help of CASTEP calculations are depicted in the **Figure 2.6**. Drug binding affinity for the system with FG is termed as interaction energy (E_{int}) and is calculated using **eq. 2** [42] and the corresponding optimized structures are as shown in the **Figure 2.7**.

$$\boldsymbol{E_{int.}} = E_{(silica\ with\ FG\ +\ Drug)} - E_{(silica\ with\ FG)} - E_{(Drug)} \quad (2)$$

The CASTEP energy and the interaction energies were obtained as given in **Table 2.1**.

Drug Silica with FG, S0 D0 **Silica with FG, S0** **Drug, D0**

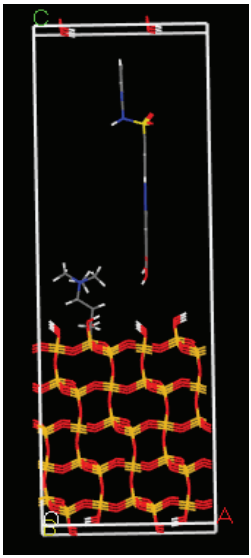

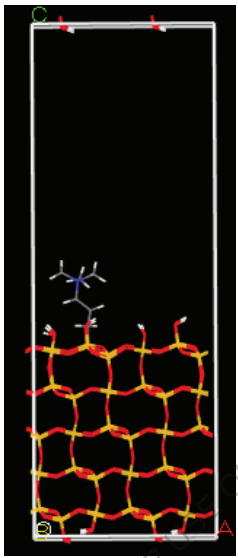

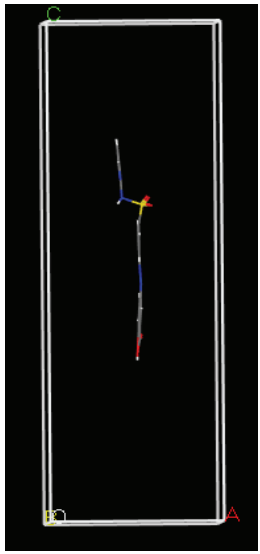

Optimized energy
-108156.36 eV

Optimized energy
-101491.8629 eV

Optimized energy
-6664.6813 eV

Figure 2.7: The interaction energy (E_{int}) calculated using the optimized CASTEP energy for each term in the equation 2 for the drug and TA functionalized silica surface

Table 2.1: CASTEP output energy after geometry optimization for the four combinations and the calculation of E_{int} in kcal/mol

System with FG	E_{Q+M}	E_Q	E_M	E_{int}, eV	E_{int} kcal/mol
Drug (0) + surface (0)	-108156.36	-101491.86	-6664.6813	0.18920	**4.3516**
Drug (0) + surface deproto (-1)	-108139.91	-101474.58	-6664.6813	-0.651800	**-14.9914**
Drug (-1) + surface deproto (-1)	-108123.74	-101474.58	-6651.5940	2.431900	**55.9337**
Drug deproto (-1) + surface (0)	-108142.53	-101491.86	-6651.5940	0.924100	**21.2543**

For the four combinations S^0 D^0, S^0 D^{-1}, S^{-1} D^0 and S^{-1} D^{-1}, the interaction energy was calculated and were added up after multiplying the fraction of combination gave rise to final binding energy at the given pH. The B.E. at the given pH was calculated by the sum of product of $E_{int.}$ and fraction present of the individual combination at that pH using **Equation 3**.

$$E_{B.E.} = E_{S(0)D(0)} \, x \, F_{S(0)} \, x \, F_{D(0)} + E_{S(0)D(-1)} \, x \, F_{S(0)} \, x \, F_{D(-1)} + E_{S(-1)D(0)} \, x \, F_{S(-1)} \, x \, F_{D(0)} + E_{S(-1)D(-1)} \, x \, F_{S(-1)} \, x \, F_{D(-1)} \quad (3)$$

Started with the whole drug sulfasalazine, its interaction energy was calculated by placing it on the silica surface with FG, various graphs obtained (based on the pKa values of drug and surface) for the drug loading and release onto TA functionalized silica surfaces are demonstrated in the bellow **Figures 2.8 - 2.11**.

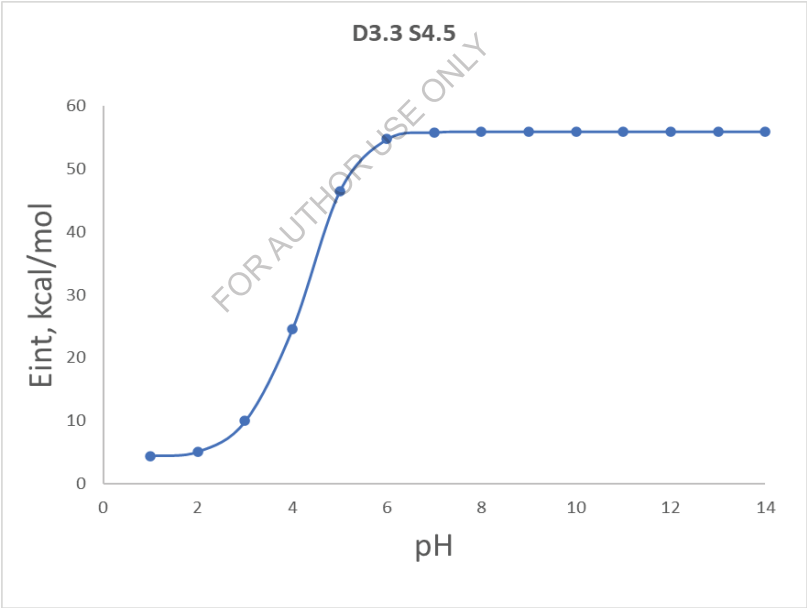

Figure 2.8: pH-Dependent binding energies (E_{int}) calculated for the sulfasalazine drug (using its first pKa value 3.3) with TA functionalized silica surface (using its first pKa value 4.5)

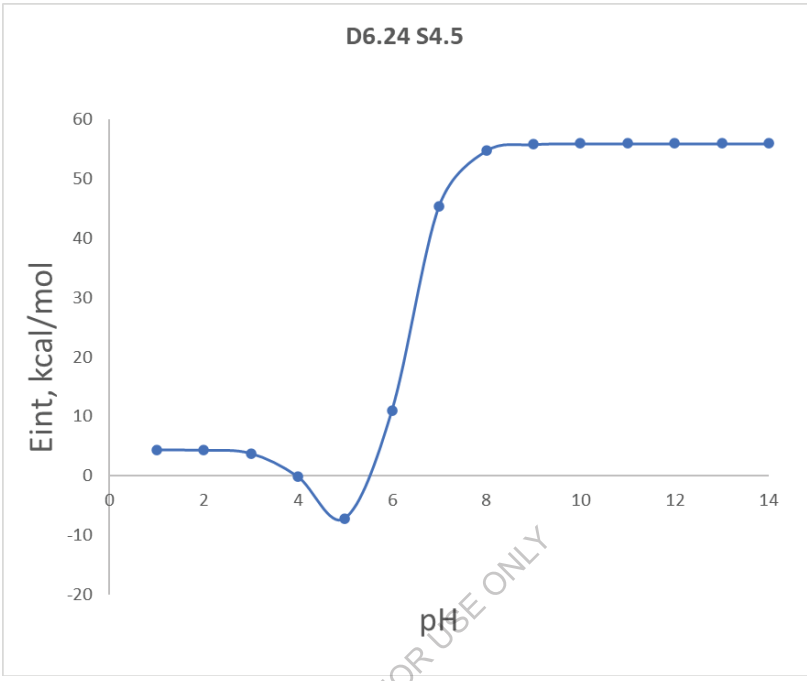

Figure 2.9: pH-Dependent binding energies (E_{int}) calculated for the sulfasalazine drug (using its second pKa value 6.24) with TA functionalized silica surface (using its first pKa value 4.5)

The more negative values for $E_{B.E}$ obtained from the calculation is suggestive of very strong binding (reflecting loading of the drug molecule on surface), while the higher positive $E_{B.E}$ values are suggestive of least or no interaction (representing release of drug molecule from the surface). The release is an outcome of strong electrostatic repulsion that generated between the silica surface and the negative drug molecules which can be seen in terms of very large positive B.E. indicating no interaction.

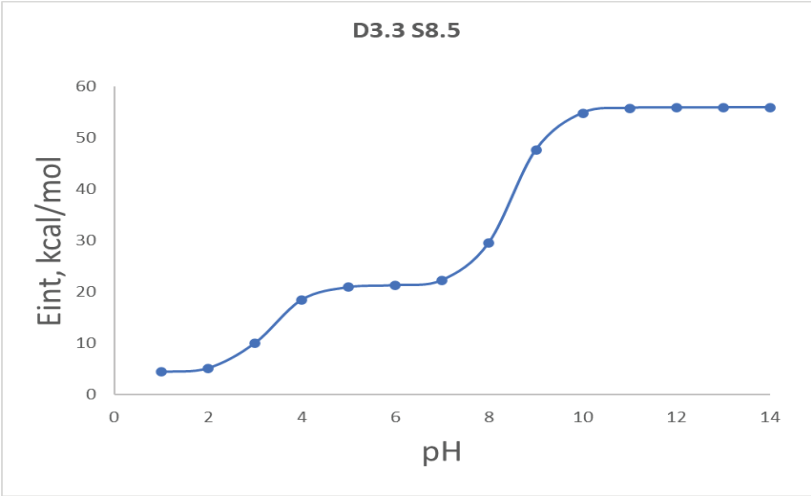

Figure 2.10: pH-Dependent binding energies (E_{int}) calculated for the sulfasalazine drug (using its first pKa value 3.3) with TA functionalized silica surface (using its second pKa value 8.5)

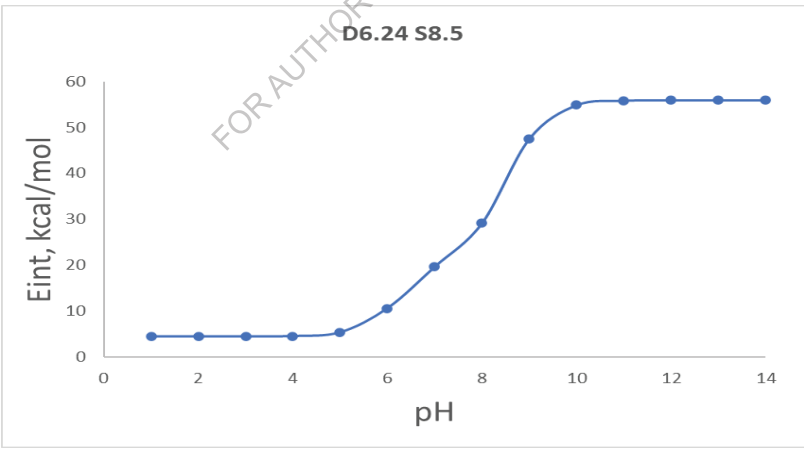

Figure 2.11: pH-Dependent binding energies (E_{int}) calculated for the sulfasalazine drug (using its second pKa value 6.24) with TA functionalized silica surface (using its second pKa value 8.5)

It should be noted that the E_{int} pH values at pH 1 are equal to the E_{int} of S^0D^0 and E_{int} pH values at pH 14 are equal to the E_{int} of $S^{-1}D^{-1}$. The drug loading and release mechanism observed based on the drug and surface pKa are as follows

Case I: Drug's first pKa 3.3 and Surface's first pKa 4.5

It can be clearly observed that the sulfasalazine drug is getting loaded on the silica surface at acidic pH of 1 to 2, it is in loaded condition even upto pH 5. The drug molecule is seen getting released after pH increases to 6 and higher to basic medium (**Figure 2.8**)

Case II: Drug's second pKa 6.24 and Surface's first pKa 4.5

For the higher pKa value of the drug, the situation is even more clear and promising for a good drug delivery system. It is observed that the drug is getting loaded at acidic pH of 1 to 3. It was getting strongly bounded/loaded on the silica surface in the pH range of 4 to 5. It can be seen loaded even at pH 6. The drug seems releasing in the basic medium from the pH 7 onwards (**Figure 2.9**).

Case III: Drug's first pKa 3.3 and Surface's second pKa 8.5

The loading and releasing seen slightly different when the Drug's first pKa 3.3 and Surface's second pKa 8.5 were considered. The drug is getting adsorbed/loaded at the acidic pH range from 1 to 3, while, it remains adsorbed/loaded on the silica surface from 4 to 7 pH. The drug is observed getting released in the basic medium of pH 8 and above (**Figure 2.10**).

Case IV: Drug's second pKa 6.24 and Surface's second pKa 8.5

When the Drug's second pKa 6.24 and Surface's second pKa 8.5 were considered, the mechanism seems promising too. The drug is getting adsorbed/loaded at the acidic pH range from 1 to 5, while, it remains adsorbed/loaded on the silica surface for pH 6 too. The drug is observed getting released in the basic medium of pH 7 onwards (**Figure 2.11**).

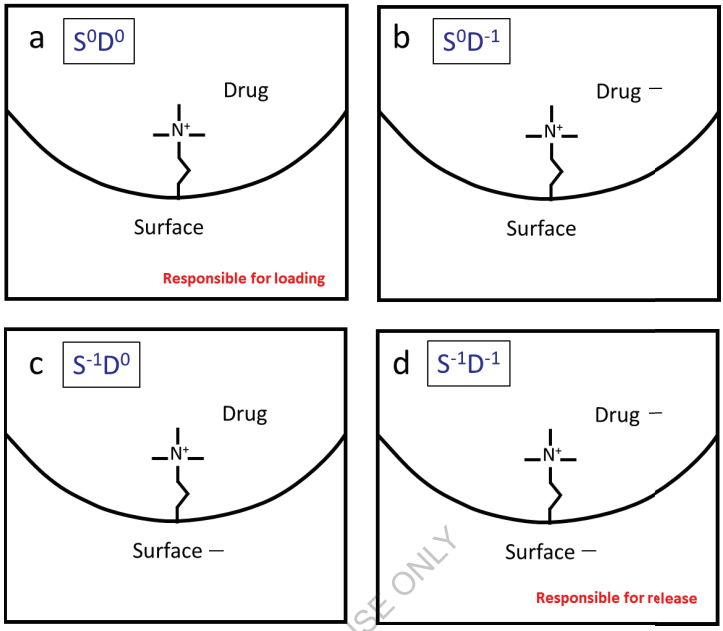

Scheme 2.1: Representation of the drug loading and release mechanism based on the four possible combinations arising from drug and surface pKa values. The combinations were identified as a) S^0D^0, b) S^0D^{-1}, c) $S^{-1}D^0$ and d) $S^{-1}D^{-1}$

Here we observed that among the four combinations, the combination S^0 D^0 is predominantly decides the drug loading in acidic stomach (pH 1.0 – 3.0), while the combination S^{-1} D^{-1} is responsible for the release of the drug in the basic intestine pH (6.0 – 7.5) as demonstrated in **Scheme 2.1**.

2.4 Conclusion:

DFT based CASTEP calculations were used successfully for the understanding the mechanism of the pH-dependent drug molecules loading and release based on the pKa values of drug and the silica surface. The B.E. of drug and surface in possible combinations S^0 D^0, S^0 D^{-1}, S^{-1} D^0, and S^{-1} D^{-1} were used to predict the pH of loading and release of sulfasalazine drug. It is reported that, the sulfasalazine drug molecule gets trapped in the MSN-TA nano-vehicle when passing through the stomach's acidic environment (pH 1.0 – 3.0), and getting released in intestine with slightly basic pH environment (6.0 – 7.5) [30]. The release is an outcome of strong electrostatic

repulsion that generated between the silica surface and the negative drug molecules which can be seen in terms of very large positive B.E. indicating no interaction. This is in support of the drug release mechanism proposed by the Lee *et al*. based on repulsion between the negative surface charge of the deprotonated silanol group and the anionic drug molecule [30]. The proposed model can be used for predicting the loading and release pH for the drugs and the surfaces with known pKa values, which will be very important / crucial for the pH responsive drug delivery systems.

2.5 References

1. Ramezanpour, M.; Leung, S. S.; Delgado-Magnero, K. H.; Bashe, B. Y.; Thewalt, J.; Tieleman, D. P., Computational and experimental approaches for investigating nanoparticle-based drug delivery systems. *Biochim Biophys Acta* **2016,** *1858* (7 Pt B), 1688-709.
2. Harvey, A. L., Natural products in drug discovery. *Drug Discovery Today* **2008,** *13* (19), 894-901.
3. Yang, K.; Luo, H.; Zeng, M.; Jiang, Y.; Li, J.; Fu, X., Intracellular pH-Triggered, Targeted Drug Delivery to Cancer Cells by Multifunctional Envelope-Type Mesoporous Silica Nanocontainers. *ACS Applied Materials and Interfaces* **2015,** *7* (31), 17399-17407.
4. Natarajan, J. V.; Nugraha, C.; Ng, X. W.; Venkatraman, S., Sustained-release from nanocarriers: a review. *Journal of Controlled Release* **2014,** *193*, 122-138.
5. Hubbell, J. A.; Chilkoti, A., Nanomaterials for Drug Delivery. *Science* **2012,** *337* (6092), 303.
6. Ma, K.; Sai, H.; Wiesner, U., Ultrasmall Sub-10 nm Near-Infrared Fluorescent Mesoporous Silica Nanoparticles. *Journal of the American Chemical Society* **2012,** *134* (32), 13180-13183.
7. Sahay, G.; Alakhova, D. Y.; Kabanov, A. V., Endocytosis of nanomedicines. *Journal of Controlled Release* **2010,** *145* (3), 182-195.
8. Alba, M.; Formentín, P.; Ferré-Borrull, J.; Pallarès, J.; Marsal, L. F., pH-responsive drug delivery system based on hollow silicon dioxide micropillars coated with polyelectrolyte multilayers. *Nanoscale Research Letters* **2014,** *9* (1), 411.
9. Datt, A.; El-Maazawi, I.; Larsen, S. C., Aspirin Loading and Release from MCM-41 Functionalized with Aminopropyl Groups via Co-condensation or Postsynthesis Modification Methods. *The Journal of Physical Chemistry C* **2012,** *116* (34), 18358-18366.
10. Slowing, I. I.; Trewyn, B. G.; Giri, S.; Lin, V. S. Y., Mesoporous Silica Nanoparticles for Drug Delivery and Biosensing Applications. *Advanced Functional Materials* **2007,** *17* (8), 1225-1236.
11. Jin, S.; Li, D.; Yang, P.; Guo, J.; Lu, J. Q.; Wang, C., Redox/pH stimuli-responsive biodegradable PEGylated P(MAA/BACy) nanohydrogels for

controlled releasing of anticancer drugs. *Colloids and Surfaces A: Physicochemical and Engineering Aspects* **2015,** *484*, 47-55.

12. Rimola, A.; Costa, D.; Sodupe, M.; Lambert, J. F.; Ugliengo, P., Silica surface features and their role in the adsorption of biomolecules: computational modeling and experiments. *Chem Rev* **2013,** *113* (6), 4216-313.
13. Vallet-Regi, M.; Rámila, A.; del Real, R. P.; Pérez-Pariente, J., A New Property of MCM-41: Drug Delivery System. *Chemistry of Materials* **2001,** *13* (2), 308-311.
14. Vallet-Regí, M.; Balas, F.; Arcos, D., Mesoporous Materials for Drug Delivery. *Angewandte Chemie International Edition* **2007,** *46* (40), 7548-7558.
15. Zhang, L.; Guo, R.; Yang, M.; Jiang, X.; Liu, B., Thermo and pH Dual-Responsive Nanoparticles for Anti-Cancer Drug Delivery. *Advanced Materials* **2007,** *19* (19), 2988-2992.
16. Zhu, C.; Zhang, X.; Wang, Q.; Zhang, R.; Wang, T., Thermo/pH dual responsive β-cyclodextrin magnetic microspheres for anti-cancer drug controlled release. *Journal of Controlled Release* **2015,** *213*, e21-e22.
17. Chen, L.; Feng, W.; Zhou, X.; Yin, Z.; He, C., Thermo-and pH dual-responsive mesoporous silica nanoparticles for controlled drug release. *Journal of Controlled Release* **2015,** *213*, e69-e70.
18. Baek, S.; Singh, R. K.; Kim, T.-H.; Seo, J.-w.; Shin, U. S.; Chrzanowski, W.; Kim, H.-W., Triple Hit with Drug Carriers: pH- and Temperature-Responsive Theranostics for Multimodal Chemo- and Photothermal Therapy and Diagnostic Applications. *ACS Applied Materials and Interfaces* **2016,** *8* (14), 8967-8979.
19. Lee, C.-S.; Na, K., Photochemically Triggered Cytosolic Drug Delivery Using pH-Responsive Hyaluronic Acid Nanoparticles for Light-Induced Cancer Therapy. *Biomacromolecules* **2014,** *15* (11), 4228-4238.
20. Hu, C.; Yu, L.; Zheng, Z.; Wang, J.; Liu, Y.; Jiang, Y.; Tong, G.; Zhou, Y.; Wang, X., Tannin as a gatekeeper of pH-responsive mesoporous silica nanoparticles for drug delivery. *RSC Advances* **2015,** *5* (104), 85436-85441.
21. Yoshida, T.; Lai, T. C.; Kwon, G. S.; Sako, K., pH- and ion-sensitive polymers for drug delivery. *Expert opinion on drug delivery* **2013,** *10* (11), 1497-1513.
22. Yuan, L.; Tang, Q.; Yang, D.; Zhang, J. Z.; Zhang, F.; Hu, J., Preparation of pH-Responsive Mesoporous Silica Nanoparticles and Their Application in

Controlled Drug Delivery. *The Journal of Physical Chemistry C* **2011,** *115* (20), 9926-9932.

23. Liu, J.-Q.; Li, X.-F.; Gu, C.-Y.; da Silva, J. C. S.; Barros, A. L.; Alves-Jr, S.; Li, B.-H.; Ren, F.; Batten, S. R.; Soares, T. A., A combined experimental and computational study of novel nanocage-based metal-organic frameworks for drug delivery. *Dalton Transactions* **2015,** *44* (44), 19370-19382.
24. DeMuth, P.; Hurley, M.; Wu, C.; Galanie, S.; Zachariah, M. R.; DeShong, P., Mesoscale porous silica as drug delivery vehicles: Synthesis, characterization, and pH-sensitive release profiles. *Microporous and Mesoporous Materials* **2011,** *141* (1-3), 128-134.
25. Heffernan, M. J.; Murthy, N., Polyketal Nanoparticles: A New pH-Sensitive Biodegradable Drug Delivery Vehicle. *Bioconjugate Chemistry* **2005,** *16* (6), 1340-1342.
26. Filipovic, N.; Saveljic, I.; Rac, V.; Graells, B. O.; Bijelic, G., Computational and experimental model of transdermal iontophorethic drug delivery system. *International Journal of Pharmaceutics* **2017**.
27. Bunker, A.; Magarkar, A.; Viitala, T., Rational design of liposomal drug delivery systems, a review: Combined experimental and computational studies of lipid membranes, liposomes and their PEGylation. *Biochimica et Biophysica Acta (BBA) - Biomembranes* **2016,** *1858* (10), 2334-2352.
28. Loverde, S. M., Computer simulation of polymer and biopolymer self-assembly for drug delivery. *Molecular Simulation* **2014,** *40* (10-11), 794-801.
29. Duncan, G. A.; Bevan, M. A., Computational design of nanoparticle drug delivery systems for selective targeting. *Nanoscale* **2015,** *7* (37), 15332-40.
30. Lee, C.-H.; Lo, L.-W.; Mou, C.-Y.; Yang, C.-S., Synthesis and Characterization of Positive-Charge Functionalized Mesoporous Silica Nanoparticles for Oral Drug Delivery of an Anti-Inflammatory Drug. *Advanced Functional Materials* **2008,** *18* (20), 3283-3292.
31. Shaukatali N. Inamdar; Khalid Ahmed; Nashiour Rohman; Skelton, A. A., Novel pKa/DFT-Based Theoretical Model for Predicting the Drug Loading and Release of a pH-Responsive Drug Delivery System. *J. Phys. Chem. C* **2018,** *122*, 12279-12290.
32. Khalid Ahmed; Shaukatali N. Inamdar; Nashiour Rohman; Skelton, A. A., Acidity constant and DFT-based modelling of pH-responsive alendronate

loading and releasing on propylamine modified silica surface. *Physical Chemistry Chemical Physics* **2021,** *23* (3), 2015-2024.

33. Clark Stewart, J.; Segall Matthew, D.; Pickard Chris, J.; Hasnip Phil, J.; Probert Matt, I. J.; Refson, K.; Payne Mike, C., First principles methods using CASTEP. In *Zeitschrift für Kristallographie - Crystalline Materials*, 2005; Vol. 220, p 567.
34. Perdew, J. P.; Burke, K.; Ernzerhof, M., Generalized Gradient Approximation Made Simple. *Physical review letters* **1996,** *77* (18), 3865-3868.
35. Meyer, B.; Rabaa, H.; Marx, D., Water adsorption on ZnO(10[1 with combining macron]0): from single molecules to partially dissociated monolayers. *Physical Chemistry Chemical Physics* **2006,** *8* (13), 1513-1520.
36. Vanderbilt, D., Soft self-consistent pseudopotentials in a generalized eigenvalue formalism. *Physical Review B* **1990,** *41* (11), 7892-7895.
37. Graham, G. G.; Pile, K. D., Sulfasalazine and Related Drugs. In *Encyclopedia of Inflammatory Diseases*, Parnham, M., Ed. Springer Basel: Basel, 2015; pp 1-5.
38. Ong, S.; Zhao, X.; Eisenthal, K. B., Polarization of water molecules at a charged interface: second harmonic studies of the silica/water interface. *Chemical Physics Letters* **1992,** *191* (3), 327-335.
39. Liu, X.; Cheng, J.; Lu, X.; Wang, R., Surface acidity of quartz: understanding the crystallographic control. *Phys Chem Chem Phys* **2014,** *16* (48), 26909-16.
40. Leung, K.; Nielsen, I. M. B.; Criscenti, L. J., Elucidating the Bimodal Acid−Base Behavior of the Water−Silica Interface from First Principles. *Journal of the American Chemical Society* **2009,** *131* (51), 18358-18365.
41. Aronson, J. N., The Henderson-Hasselbalch equation revisited. *Biochemical Education* **1983,** *11* (2), 68-68.
42. Fox, S. J.; Dziedzic, J.; Fox, T.; Tautermann, C. S.; Skylaris, C. K., Density functional theory calculations on entire proteins for free energies of binding: application to a model polar binding site. *Proteins* **2014,** *82* (12), 3335-46.

CHAPTER 3:

DFT Studies and Quantum Chemical Calculations of Benzoyl Thiourea Derivatives Linked with Morpholine and Piperidine for the Evaluation of Antifungal Activity

3.1 Introduction

The biological actions of pyridine, morpholine, and thiourea are diverse, including antibacterial and antifungal properties. [1-9] Diaryl thioureas have antifungal action against *Pyricularia oryzae* and *Drechslera oryzae*, different plant pathogens. [10] The signifcant pesticidal, fungicidal, antiviral, and plant growth regulating activity of acyl thioureas is well documented. [11]

Sulfur-linked 1,2,4-triazoles, on the other hand, are a promising group of sulphur compounds for use in lead chemical discovery, particularly the thione-substituted 1,2,4-triazole ring. Many bioactive sulphur-linked 1,2,4-triazoles have been found, including antibacterial, anticancer, anti-HIV, and fungicidal action, with certain pyridine derivatives preventing *Ralstonia solana*cearum, *Cercospora beticola sacc*., and *Colletotrichum orbiculare*.[12-15]

Fluorine introduced at a strategic point in a molecule is a powerful and diverse tool for the synthesis of organic compounds with biological activity potential by altering the steric and electronic properties. [16-22] Fluorine can increase the lipophilicity of organic compounds, increasing the rate of cell penetration and delivery of a drug to an active site. [23] Fluorinated thioureas are a new class of strong neuraminidase inhibitors for influenza viruses. [24] Yang *et al*. reported a theoretical calculation for benzoyl thiourea derivatives and their complexes with Cobalt to explain their antibacterial properties. [25] C. Li *et a*l. later reported on the antifungal properties of fluorine-containing thio-ureido complexes with Nickel (II). [26]

Here, we have used the ligands from these studies to evaluate the correlation between their activity and theoretical results. In this chapter, six compounds with benzoyl thiourea derivatives linked to piperidine (BTP 1, BTP 2 and BTP 3) and benzoyl thiourea derivatives linked to morpholine (BTM 4, BTM 5 and BTM 6) were optimized using DFT / B3LYP method. The structures of studied compounds are given in **Figure 3.1**. The effect of fluorine substitution, frontier orbital energy and structure-activity relationship on the antifungal activities was explored.

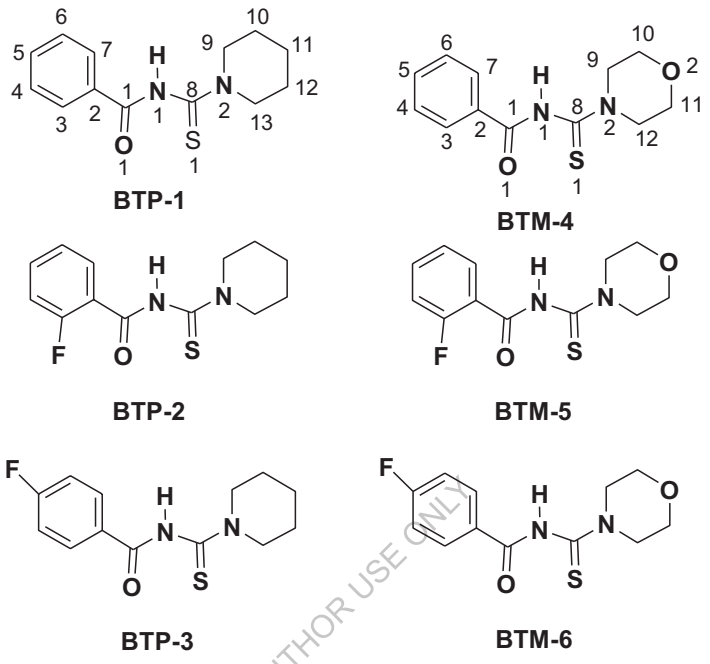

Figure 3.1: Structures of benzoyl thiourea piperidine derivatives (BTP 1-3) and benzoyl thiourea morpholine derivatives (BTM 4-6)

3.2 Results and Discussion

The obtained results are discussed as follows,

3.2.1 Comparison of DFT Structural Parameters with Experimental Values

The DFT calculations were carried out with B3LYP/6-31G (*d*,*p*) method in GAMESS package.[27] **Figure 3.2** depicts optimized structures of BTP 1-3 and BTM 4-6. The geometry parameter viz. Calculated bond distances, bond angles of compounds BTP 2, BTP 3 and BTM 6 are given **Table 3.1**. In general good agreement between the calculated and experimental bond lengths and bond angles[26] have been observed.

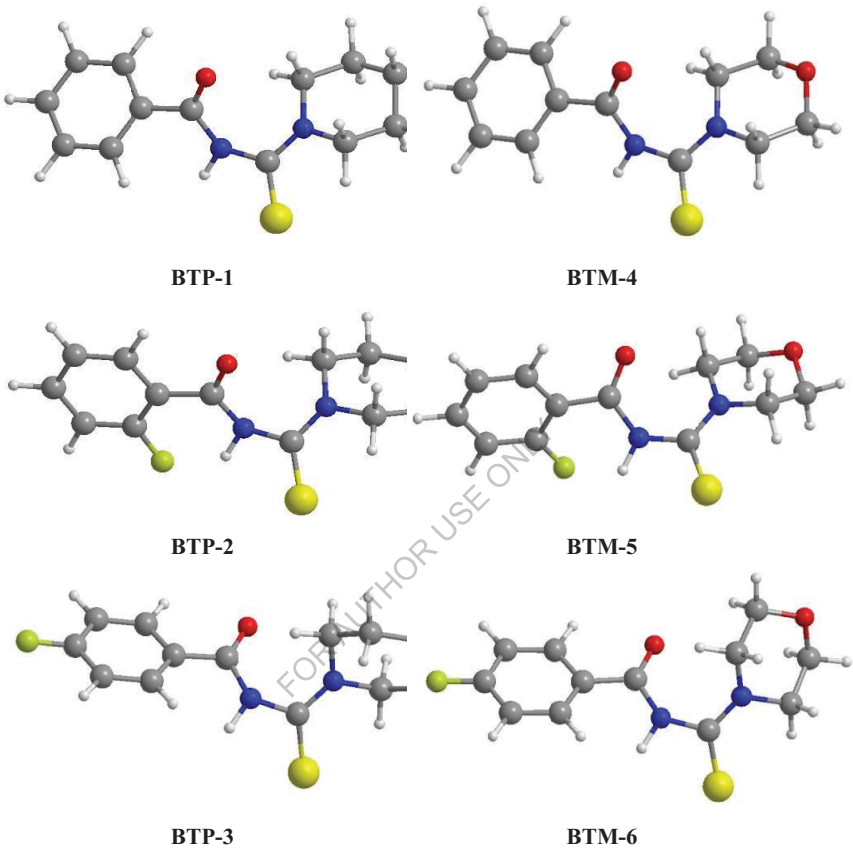

Figure 3.2: B3LYP/6-31G (*d*,*p*) optimized structures of BTP 1-3, BTM 4-6

Table 3.1: Comparative selected structure parameters of the compounds BTP 2, BTP 3 and BTM 6

Distances (Å)	**BTP 2**		**BTP 3**		**BTM 6**	
/ Angles (^{0})	**Expt.**	**DFT**	**Expt.**	**DFT**	**Expt.**	**DFT**
S1-C8	1.673	1.683	1.668	1.681	1.679	1.682
O1-C1	1.213	1.223	1.233	1.221	1.219	1.223
N1-C1	1.378	1.390	1.358	1.403	1.392	1.399
N1-C8	1.413	1.417	1.434	1.417	1.397	1.417
N2-C8	1.414	1.346	1.314	1.346	1.330	1.346
S1-C8-N1	125.634	125.954	127.287	126.164	124.036	125.642
S1-C8-N2	117.506	117.105	117.920	117.105	118.950	117.105

3.2.2 Frontier Orbital Energy Analysis

According to the frontier molecular orbital theory, HOMO and LUMO are the most important factors that affect the bioactivity. HOMO has the priority to provide electrons, while LUMO expresses ability of the compound to accept electrons.[28]

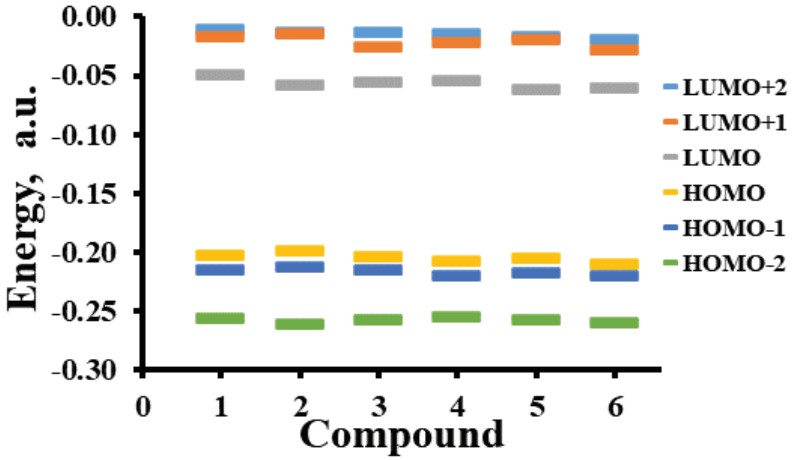

Figure 3.3: Energy levels of MO diagrams for compound BTP 1-3, BTM 4-6 calculated in their ground state in the gas phase structures

The energies of HOMO -2 to LUMO +2 orbitals for the compounds BTP 1-3 and BTM 4-6 are given in **Figure 3.3** and **Table 3.2**.

Table 3.2: Energy levels (a.u.) of MOs for compound BTP 1-3, BTM 4-6 calculated in their ground state in the gas phase

Compound	HOMO -2	HOMO -1	HOMO	LUMO	LUMO +1	LUMO +2
BTP 1	-0.2567	-0.2149	-0.2020	-0.0499	-0.0172	-0.0113
BTP 2	-0.2612	-0.2120	-0.1989	-0.0577	-0.0145	-0.0132
BTP 3	-0.2578	-0.2148	-0.2032	-0.0551	-0.0252	-0.0127
BTM 4	-0.2548	-0.2198	-0.2075	-0.0537	-0.0222	-0.0146
BTM 5	-0.2571	-0.2170	-0.2046	-0.0613	-0.0189	-0.0169
BTM 6	-0.2598	-0.2204	-0.2103	-0.0607	-0.0286	-0.0188

The quantum chemical parameters were calculated as described by Cakmak et. al.[29] According to the Janak's theorem, IP and EA can be obtained using HOMO and LUMO energies utilizing **Equation 1**.[30]

$$IP = -E_{HOMO}\ ,\ EA = -E_{LUMO} \qquad (1)$$

Hardness (η) is the distortion of chemical species or opposition to electron cloud polarization and can be calculated by **Equation 2.**[31] To understand the behaviour of chemical system the concepts of hardness and softness are used. The molecules with large energy gap are termed as hard while, the molecules with small energy gap are soft. Hence, hard molecules tend to be less polarizable than soft molecules.

$$\eta = (IP - EA) / 2 \qquad (2)$$

Reciprocal of global hardness gives softness (σ) of the molecules and is calculated using **Equation 3**.[32]

$$\sigma = 1 / \eta \qquad (3)$$

Electronegativity (χ) measures tendency of molecule towards electron attraction, which can be calculated by **Equation 4**.

$$\chi = -(E_{HOMO} + E_{LUMO})/ 2 \qquad (4)$$

Smaller ΔE implies higher chemical reactivity and lower kinetic stability for the investigated molecules.[29]

The quantum chemical parameters of compounds BTP 1-3 and BTM 4-6 were calculated using the above equations. Thus, obtained values of IP, EA, hardness, softness, and electronegativity associated with HOMO and LUMO energies[33-46] are formulated in **Table 3.3**. For the BTP compounds the sequence of the antifungal activity is BTP 1 < BTP 2 < BTP 3. This antifungal activity sequence is identical to the calculated sequence of electronegativity (χ). For the BTM compounds the sequence of antifungal activity is BTM 5 < BTP 6 < BTP 4. For these BTM compounds a direct correlation of antifungal activity is observed with E_{LUMO}, EA, hardness (η) and softness (σ).

Table 3.3: Quantum chemical parameters of compounds BTP 1-3 and BTM 4-6 calculated at B3LYP / 6-31G (d,p)

	E_{HOMO} (eV)	E_{LUMO} (eV)	IP	EA	η	σ	χ	MIC values*
BTP 1	-5.497	-1.358	5.497	1.358	2.069	0.483	3.427	31
BTP 2	-5.412	-1.570	5.412	1.570	1.921	0.521	3.491	27.5
BTP 3	-5.529	-1.499	5.529	1.499	2.015	0.496	3.514	20.5
BTM 4	-5.646	-1.461	5.646	1.461	2.093	0.478	3.554	2.5
BTM 5	-5.567	-1.668	5.567	1.668	1.950	0.513	3.618	31
BTM 6	-5.722	-1.652	5.722	1.652	2.035	0.491	3.687	8.0

* Antifungal activity against *Botrytis cinerea*[26]

3.2.3 Mulliken Atomic Charges

Table 3.4: Mulliken atomic charges for selected atoms using DFT

Atom	BTP 1	BTP 2	BTP 3	BTM 4	BTM 5	BTM 6
S1	-0.2868	-0.2793	-0.2830	-0.2790	-0.2711	-0.2722
F1	-	-0.2926	-0.2866	-	-0.2929	-0.2856
O1	-0.4958	-0.5016	-0.4918	-0.4938	-0.4998	-0.4983
O2	-	-	-	-0.4770	-0.4771	-0.4828
N1	-0.5505	-0.5756	-0.5599	-0.5508	-0.5730	-0.3846
N2	-0.3644	-0.3655	-0.3696	-0.3795	-0.3795	-0.5580
C1	0.54267	0.5787	0.5442	0.5409	0.5781	0.5505
C8	0.2831	0.2876	0.2907	0.2837	0.2850	0.2910

The calculated Mulliken atomic charges[47-61] for selected atoms are exhibited in **Table 3.4**. Two atoms C1, and C8 are the most positively charged ones, which can interact with the negative charged part of the receptor easily. The negative charges are mainly located on atoms N1, N2, S1, F1, and O1, so they can interact easily with the positive part of the receptor. C1 being most positive and N1 most negative therefore C1-N1 bond polarity plays a key role. Calculated C1-N1 bond distances of the compounds are 1.397, 1.390, 1.402, 1.399, 1.392 and 1.399. Longer the C1–N1 bond, more is the antifungal activity, BTP 3, BTM 4 and BTM 6 being more powerful.

3.3 Conclusion

The DFT study of benzoyl thiourea derivatives linked to morpholine and piperidine were evaluated for their antifungal activity. All the six compounds BTP 1-3 and BTM 4-6 were optimized with DFT and various parameters were evaluated. Mulliken charge analysis results were found consistent with the antifungal activity. The presence of morpholine group and fluorine at para position reported to be enhancing the antifungal activity, which is confirmed from the current DFT studies. In general, good agreement between the calculated and experimental bond lengths and bond angles have been observed. For the BTP compounds the antifungal activity sequence was found similar to that of calculated electronegativity. For the BTM compounds a direct correlation of antifungal activity is observed with E_{LUMO}, EA, hardness and softness.

3.4 References

1. Venkatachalam, T.; Sudbeck, E.; Uckun, F., Regiospecific synthesis, X-ray crystal structure and biological activities of 5-bromothiophenethyl thioureas. *Tetrahedron Letters* **2001,** *42* (38), 6629-6632.
2. Kim, B. Y.; Ahn, J. B.; Lee, H. W.; Kang, S. K.; Lee, J. H.; Shin, J. S.; Ahn, S. K.; Hong, C. I.; Yoon, S. S., Synthesis and biological activity of novel substituted pyridines and purines containing 2,4-thiazolidinedione. *European Journal of Medicinal Chemistry* **2004,** *39* (5), 433-447.
3. Kravchenko, D. V.; Kysil, V. M.; Tkachenko, S. E.; Maliarchouk, S.; Okun, I. M.; Ivachtchenko, A. V., Pyrrolo[3,4-c]quinoline-1,3-diones as potent caspase-3 inhibitors. Synthesis and SAR of 2-substituted 4-methyl-8-(morpholine-4-sulfonyl)-pyrrolo[3,4-c]quinoline-1,3-diones. *European Journal of Medicinal Chemistry* **2005,** *40* (12), 1377-1383.
4. Mohamed, M. S.; Kamel, M. M.; Kassem, E. M. M.; Abotaleb, N.; Abd El-moez, S. I.; Ahmed, M. F., Novel 6,8-dibromo-4(3H)quinazolinone derivatives of anti-bacterial and anti-fungal activities. *European Journal of Medicinal Chemistry* **2010,** *45* (8), 3311-3319.
5. Saeed, S.; Rashid, N.; Jones, P. G.; Ali, M.; Hussain, R., Synthesis, characterization and biological evaluation of some thiourea derivatives bearing benzothiazole moiety as potential antimicrobial and anticancer agents. *European Journal of Medicinal Chemistry* **2010,** *45* (4), 1323-1331.
6. Ventosa-Andrés, P.; Valdivielso, Á. M.; Pappos, I.; García-López, M. T.; Tsopanoglou, N. E.; Herranz, R., Design, synthesis and biological evaluation of new peptide-based ureas and thioureas as potential antagonists of the thrombin receptor PAR1. *European Journal of Medicinal Chemistry* **2012,** *58*, 98-111.
7. Yancheva, D.; Daskalova, L.; Cherneva, E.; Mikhova, B.; Djordjevic, A.; Smelcerovic, Z.; Smelcerovic, A., Synthesis, structure and antimicrobial activity of 6-(propan-2-yl)-3-methyl-morpholine-2,5-dione. *Journal of Molecular Structure* **2012,** *1016*, 147-154.
8. Krogul, A.; Cedrowski, J.; Wiktorska, K.; Oziminski, W. P.; Skupińska, J.; Litwinienko, G., Biological activity of Pd(II) complexes with mono- and

disubstituted pyridines--experimental and theoretical studies. *Bioorganic and medicinal chemistry letters* **2013,** *23* (9), 2765-2768.

9. Patel, N. B.; Purohit, A. C.; Rajani, D. P.; Moo-Puc, R.; Rivera, G., New 2-benzylsulfanyl-nicotinic acid based 1,3,4-oxadiazoles: Their synthesis and biological evaluation. *European Journal of Medicinal Chemistry* **2013,** *62*, 677-687.
10. Weiqun, Z.; Wen, Y.; Liqun, X.; Xianchen, C., N-Benzoyl-N′-dialkylthiourea derivatives and their Co(III) complexes: Structure, and antifungal. *Journal of Inorganic Biochemistry* **2005,** *99* (6), 1314-1319.
11. Duan, L.-P.; Xue, J.; Xu, L.-L.; Zhang, H.-B., Synthesis 1-Acyl-3-(2'-aminophenyl) thioureas as Anti-Intestinal Nematode Prodrugs. *Molecules* **2010,** *15* (10), 6941-6947.
12. Liu, X.-H.; Pan, L.; Ma, Y.; Weng, J.-Q.; Tan, C.-X.; Li, Y.-H.; Shi, Y.-X.; Li, B.-J.; Li, Z.-M.; Zhang, Y.-G., Design, Synthesis, Biological Activities, and 3D-QSAR of New N,N′-Diacylhydrazines Containing 2-(2,4-dichlorophenoxy)propane Moiety. *Chemical Biology and Drug Design* **2011,** *78* (4), 689-694.
13. Wu, J.; Kang, S.; Song, B.; Hu, D.; He, M.; Jin, L.; Yang, S., Synthesis and antibacterial activity against ralstonia solanacearum for novel hydrazone derivatives containing a pyridine moiety. *Chemistry Central Journal* **2012,** *6* (1), 28.
14. Kaldrikyan, M. A.; Melik-Oganjanyan, R. G.; Aresnyan, F. H., Synthesis and antitumor activity of 5-methylbenzofuryl-substituted 1,2,4-triazoles and triazoline-5-thiones. *Pharmaceutical Chemistry Journal* **2013,** *47* (4), 191-194.
15. Plech, T.; Wujec, M.; Kosikowska, U.; Malm, A., Synthesis and Antibacterial Activity of 4,5-disubstituted-1,2,4-triazole-3- thiones. *Letters in Drug Design and Discovery* **2013,** *10*, 917-922.
16. Smart, B. E., Fluorine substituent effects (on bioactivity). *Journal of Fluorine Chemistry* **2001,** *109* (1), 3-11.
17. Ismail, F. M. D., Important fluorinated drugs in experimental and clinical use. *Journal of Fluorine Chemistry* **2002,** *118* (1), 27-33.
18. Bonacorso, H. G.; Wentz, A. P.; Lourega, R. V.; Cechinel, C. A.; Moraes, T. S.; Coelho, H. S.; Zanatta, N.; Martins, M. A. P.; Höerner, M.; Alves, S. H., Trifluoromethyl-containing pyrazolinyl (p-tolyl) sulfones: The synthesis and

structure of promising antimicrobial agents. *Journal of Fluorine Chemistry* **2006,** *127* (8), 1066-1072.

19. Yonetoku, Y.; Kubota, H.; Okamoto, Y.; Ishikawa, J.; Takeuchi, M.; Ohta, M.; Tsukamoto, S.-i., Novel potent and selective calcium-release-activated calcium (CRAC) channel inhibitors. Part 2: Synthesis and inhibitory activity of aryl-3-trifluoromethylpyrazoles. *Bioorg Med Chem* **2006,** *14* (15), 5370-5383.
20. Filler, R.; Saha, R., Fluorine in medicinal chemistry: a century of progress and a 60-year retrospective of selected highlights. *Future Medicinal Chemistry* **2009,** *1* (5), 777-791.
21. Jagodzinska, M.; Huguenot, F.; Candiani, G.; Zanda, M., Assessing the Bioisosterism of the Trifluoromethyl Group with a Protease Probe. *ChemMedChem* **2009,** *4* (1), 49-51.
22. Szymanski, P.; Karpiński, A.; Mikiciuk-Olasik, E., Synthesis, biological activity and HPLC validation of 1,2,3,4-tetrahydroacridine derivatives as acetylcholinesterase inhibitors. *European Journal of Medicinal Chemistry* **2011,** *46* (8), 3250-3257.
23. Saeed, A.; Shaheen, U.; Hameed, A.; Naqvi, S. Z. H., Synthesis, characterization and antimicrobial activity of some new 1-(fluorobenzoyl)-3-(fluorophenyl)thioureas. *Journal of Fluorine Chemistry* **2009,** *130* (11), 1028-1034.
24. Ghorab, M. M.; Alsaid, M. S.; El-Gaby, M. S. A.; Elaasser, M. M.; Nissan, Y. M., Antimicrobial and anticancer activity of some novel fluorinated thiourea derivatives carrying sulfonamide moieties: synthesis, biological evaluation and molecular docking. *Chemistry Central Journal* **2017,** *11* (1), 32.
25. Yang, W.; Liu, H.; Li, M.; Wang, F.; Zhou, W.; Fan, J., Synthesis, structures and antibacterial activities of benzoylthiourea derivatives and their complexes with cobalt. *Journal of Inorganic Biochemistry* **2012,** *116*, 97-105.
26. Li, C.; Yang, W.; Liu, H.; Li, M.; Zhou, W.; Xie, J., Crystal structures and antifungal activities of fluorine-containing thioureido complexes with nickel(II). *Molecules (Basel, Switzerland)* **2013,** *18* (12), 15737-15749.
27. Schmidt, M. W.; Baldridge, K. K.; Boatz, J. A.; Elbert, S. T.; Gordon, M. S.; Jensen, J. H.; Koseki, S.; Matsunaga, N.; Nguyen, K. A.; Su, S.; Windus, T. L.; Dupuis, M.; Montgomery Jr, J. A., General atomic and molecular

electronic structure system. *Journal of Computational Chemistry* **1993,** *14* (11), 1347-1363.

28. Liu, X.-H.; Chen, P.-Q.; Wang, B.-L.; Li, Y.-H.; Wang, S.-H.; Li, Z.-M., Synthesis, bioactivity, theoretical and molecular docking study of 1-cyano-N-substituted-cyclopropanecarboxamide as ketol-acid reductoisomerase inhibitor. *Bioorganic and medicinal chemistry letters* **2007,** *17* (13), 3784-3788.
29. Cakmak, E.; Ozbakir Isin, D., A theoretical evaluation on free radical scavenging activity of 3-styrylchromone derivatives: the DFT study. *Journal of Molecular Modeling* **2020,** *26* (5), 98.
30. Janak, J. F., Proof that dE/dni = e in density-functional theory. *Physical Review B* **1978,** *18* (12), 7165-7168.
31. Parr, R. G.; Pearson, R. G., Absolute hardness: companion parameter to absolute electronegativity. *Journal of the American Chemical Society* **1983,** *105* (26), 7512-7516.
32. Pearson, R. G., Absolute electronegativity and hardness: application to inorganic chemistry. *Inorganic Chemistry* **1988,** *27* (4), 734-740.
33. Xu, Y.; Chu, Q.; Chen, D.; Fuentes, A., HOMO–LUMO Gaps and Molecular Structures of Polycyclic Aromatic Hydrocarbons in Soot Formation. *Frontiers in Mechanical Engineering* **2021,** *7*.
34. Joshi, B. D.; Thakur, G.; Chaudhary, M. K., Molecular Structure, Homo-Lumo and Vibrational Analysis Of Ergoline By Density Functional Theory. *Scientific World* **2021,** *14* (14), 21-30.
35. Joseph, S.; Thomas, S.; Mohan, J.; Kumar, A. S.; Jayasree, S. T.; Thomas, S.; Kalarikkal, N., Theoretical Study on Tuning Band Gap and Electronic Properties of Atomically Thin Nanostructured MoS2/Metal Cluster Heterostructures. *ACS Omega* **2021,** *6* (10), 6623-6628.
36. Mumit, M. A.; Pal, T. K.; Alam, M. A.; Islam, M. A.-A.-A.-A.; Paul, S.; Sheikh, M. C., DFT studies on vibrational and electronic spectra, HOMO-LUMO, MEP, HOMA, NBO and molecular docking analysis of benzyl-3-N-(2,4,5-trimethoxyphenylmethylene)hydrazinecarbodithioate. *Journal of molecular structure* **2020,** *1220*, 128715-128715.
37. De Lile, J. R.; Kang, S. G.; Son, Y.-A.; Lee, S. G., Do HOMO–LUMO Energy Levels and Band Gaps Provide Sufficient Understanding of Dye-

Sensitizer Activity Trends for Water Purification? *ACS Omega* **2020,** *5* (25), 15052-15062.

38. Townsend, P. A.; Grayson, M. N., Density Functional Theory Transition-State Modeling for the Prediction of Ames Mutagenicity in 1,4 Michael Acceptors. *Journal of Chemical Information and Modeling* **2019,** *59* (12), 5099-5103.
39. Matunová, P.; Jirásek, V.; Rezek, B., DFT calculations reveal pronounced HOMO–LUMO spatial separation in polypyrrole–nanodiamond systems. *Physical Chemistry Chemical Physics* **2019,** *21* (21), 11033-11042.
40. Choudhary, V.; Bhatt, A.; Dash, D.; Sharma, N., DFT calculations on molecular structures, HOMO–LUMO study, reactivity descriptors and spectral analyses of newly synthesized diorganotin(IV) 2-chloridophenylacetohydroxamate complexes. *Journal of Computational Chemistry* **2019,** *40* (27), 2354-2363.
41. Chen, D.; Wang, H., HOMO–LUMO Gaps of Homogeneous Polycyclic Aromatic Hydrocarbon Clusters. *The Journal of Physical Chemistry C* **2019,** *123* (45), 27785-27793.
42. Umar, Y.; Abdalla, S., DFT Study of the Molecular Structure, Conformational Preference, HOMO, LUMO, and Vibrational Analysis of 2-, and 3-Furoyl Chloride. *Journal of Solution Chemistry* **2017,** *46* (4), 741-758.
43. Pereira, F.; Xiao, K.; Latino, D. A. R. S.; Wu, C.; Zhang, Q.; Aires-de-Sousa, J., Machine Learning Methods to Predict Density Functional Theory B3LYP Energies of HOMO and LUMO Orbitals. *Journal of Chemical Information and Modeling* **2017,** *57* (1), 11-21.
44. Prabhaharan, M.; Prabakaran, A. R.; Gunasekaran, S.; Srinivasan, S., DFT studies on vibrational spectra, HOMO–LUMO, NBO and thermodynamic function analysis of cyanuric fluoride. *Spectrochimica Acta Part A: Molecular and Biomolecular Spectroscopy* **2015,** *136*, 494-503.
45. Barman, M. K.; Chatterjee, M.; Srivastava, B.; Mandal, B., Characterization and Density Functional Theory Optimization of a Simultaneous Binder (FSG-XO) of Two Different Species Exploiting HOMO–LUMO Levels: Photoelectronic and Analytical Applications. *Journal of Chemical and Engineering Data* **2015,** *60* (8), 2197-2208.
46. El-Mansy, M. A. M.; El-Nahass, M. M.; Khusayfan, N. M.; El-Menyawy, E. M., DFT approach for FT-IR spectra and HOMO–LUMO energy gap for N-(p-

dimethylaminobenzylidene)-p-nitroaniline (DBN). *Spectrochimica Acta Part A: Molecular and Biomolecular Spectroscopy* **2013,** *111*, 217-222.

47. Siddiqui, S. A., Molecular modeling and simulation for the design of dye sensitizers with mono- and di-substituted donor moieties. *Journal of Computational Electronics* **2022**.
48. Shinde, R., Ultrasound Assisted Synthesis, Molecular Structure,UV-Visible Assignments, MEP and Mulliken Charges Study of (E)-3-(4-chlorophenyl)-1-(4-methoxyphenyl) prop-2-en-1-one: Experimental and DFT Correlational. *Material Science Research India* **2021,** *18*, 86-96.
49. Dhonnar, S. L.; Sadgir, N. V.; Adole, V. A.; Jagdale, B. S., Molecular Structure, FT-IR Spectra, MEP and HOMO-LUMO Investigation of 2-(4-Fluorophenyl)-5-phenyl-1, 3,4-oxadiazole Using DFT Theory Calculations. *Advanced Journal of Chemistry-Section A* **2021,** *4* (3), 220-230.
50. Khosravi, M.; Murthy, V.; Mackinnon, I. D. R., Evaluation of DFT methods to calculate structure and partial atomic charges for zeolite N. *Computational Materials Science* **2020,** *171*, 109225.
51. Qian, H.; Deng, J.; Zhou, H.; Yang, X.; Chen, W., A DFT study on the adsorption of Ga-BNNT to SF6 decomposition products under partial discharge. *Results in Physics* **2019,** *14*, 102419.
52. Ertural, C.; Steinberg, S.; Dronskowski, R., Development of a robust tool to extract Mulliken and Löwdin charges from plane waves and its application to solid-state materials. *RSC Advances* **2019,** *9* (51), 29821-29830.
53. Toh, P. L.; Meepripruk, M.; Ang, L. S.; Sulaiman, S.; Mohamed-Ibrahim, M. I., First Principles Study on the Stability and Electronic Structures of 7,8-Dichloro-4-Oxo-4H-Chromene-3-Carbaldehyde. *Applied Mechanics and Materials* **2017,** *855*, 31-36.
54. Rogers, T. R.; Wang, F., Performing the Millikan experiment at the molecular scale: Determination of atomic Millikan-Thomson charges by computationally measuring atomic forces. *The Journal of chemical physics* **2017,** *147* (16), 161726-161726.
55. Pokharia, S.; Joshi, R.; Pokharia, M.; Yadav, S. K.; Mishra, H., A density functional theory insight into the structure and reactivity of diphenyltin(IV) derivative of glycylphenylalanine. *Main Group Metal Chemistry* **2016,** *39* (3-4), 77-86.

56. Govindasamy, P.; Gunasekaran, S.; S, S., Molecular geometry, conformational, vibrational spectroscopic, molecular orbital and Mulliken charge analysis of 2-acetoxybenzoic acid. *Spectrochimica Acta Part A: Molecular and Biomolecular Spectroscopy* **2014,** *130*, 329–336.
57. Azhagiri, S.; Jayakumar, S.; Gunasekaran, S.; Srinivasan, S., Molecular structure, Mulliken charge, frontier molecular orbital and first hyperpolarizability analysis on 2-nitroaniline and 4-methoxy-2-nitroaniline using density functional theory. *Spectrochimica Acta Part A: Molecular and Biomolecular Spectroscopy* **2014,** *124*, 199-202.
58. Reed, A. E.; Weinstock, R. B.; Weinhold, F., Natural population analysis. *The Journal of Chemical Physics* **1985,** *83* (2), 735-746.
59. Stone, A. J., Distributed multipole analysis, or how to describe a molecular charge distribution. *Chemical Physics Letters* **1981,** *83* (2), 233-239.
60. Mulliken, R. S., Electronic Population Analysis on LCAO–MO Molecular Wave Functions. I. *The Journal of Chemical Physics* **1955,** *23* (10), 1833-1840.
61. Löwdin, P. O., On the Non- Orthogonality Problem Connected with the Use of Atomic Wave Functions in the Theory of Molecules and Crystals. *The Journal of Chemical Physics* **1950,** *18* (3), 365-375.

CHAPTER 4:
DFT Calculations of Thiourea Derivatives Containing a Thiazole Moiety for the Evaluation of Antifungal Activity

4.1 Introduction

The thiazole moiety belongs to an important class of heterocycles containing N and S and when linked to a thiourea functional group forms the building block for pharmaceutical agents.[1] They display a wide variety of pharmaceutical activity, for instance bactericidal, anti-cancer[2], analgesic[3], fungicidal[4] and anti-hypertensive.[5] Thiouracils are similarly used as virucidal and anti-inflammatory agents.[6] Thiourea derivatives act as intermediates for the synthesis of variety of acyclic and heterocyclic compounds.[7, 8] Coumarins and thiazoles have a wide range of biological activity in medicine and pharmaceuticals, including antifungal properties.[9-12] Acyl thiourea and its derivatives exhibit antimicrobial, antibacterial, antifungal, antiviral, and plant-protection-regulating property.[13-19]

Log P is a most commonly used molecular descriptor in SAR analyses.[20-25] It is a quantitative descriptor of lipophilicity, one of the significant factors of pharmacokinetic properties. The lipophilicity modifies the penetration of bioactive molecules through the non-polar cell membranes. This property is usually determined by the partition coefficient, which is obtained from distribution studies of the compound between an immiscible polar and non-polar solvent pair. The inhibitory activity of a drug can be predicted by using Log P.

In this chapter, we report the study of four compounds (**1a** - **1d**) using DFT / B3LYP method. **Figure 4.1** depicts structures of the compounds used in the current study. We were interested in exploring the frontier orbital energy and structure-activity relationship on the antifungal activities. It is reported that all the compounds exhibit significant antifungal activity, antifungal activity of **1c** is the strongest among the studied samples.[26]

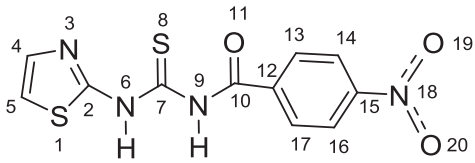

1a

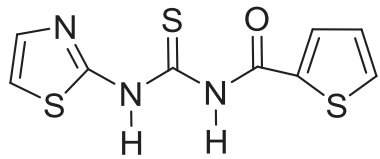

1b

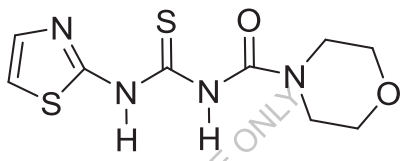

1c

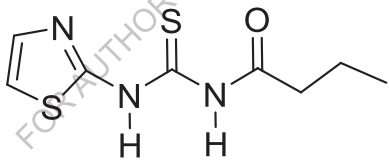

1d

Figure 4.1: Structures of the compounds under study, **1a - 1d**

4.2 Results and Discussion

4.2.1 Comparison of DFT Geometrical Parameters with Experimental Data.

The DFT calculations were carried out with B3LYP/6-31G (*d*,*p*) method in GAMESS package.[27] The geometrical parameters viz. Calculated bond distances and observed bond lengths of compound **1a** are given in **Table 4.1**. In general, good agreement between the calculated and experimental[26] bond lengths have been observed.

Table 4.1: Comparative selected structure parameters of the compound 1a

Distances (Å) / Angles (^{0})	**1a**	
	Expt	**DFT**
S(1)-C(2)	1.757	1.768
C(2)-N(3)	1.307	1.287
C(2)-N(6)	1.390	1.393
N(3)-C(4)	1.372	1.385
C(4)-C(5)	1.364	1.371
C(7)-S(8)	1.669	1.679
C(7)-N(9)	1.407	1.415
C(10)-O(11)	1.230	1.204
C(10)-C(12)	1.500	1.501
C(12)-C(13)	1.403	1.407
C(13)-C(14)	1.391	1.398
C(15)-C(16)	1.393	1.396
C(15)-N(18)	1.477	1.493
C(16)-C(17)	1.392	1.403
N(18)-O(19)	1.229	1.198
N(18)-O(20)	1.229	1.236
C(2)-S(1)-C(5)	87.717	88.748
S(1)-C(2)-N(3)	115.541	116.23
S(1)-C(2)-N(6)	126.156	128.451
N(3)-C(4)-C(5)	116.020	117.971
S(1)-C(5)-C(4)	110.387	109.319
C(2)-N(6)-C(7)	129.804	128.198
N(6)-C(7)-S(8)	127.298	123.853
N(6)-C(7)-N(9)	114.386	113.536
C(7)-N(9)-C(10)	129.358	129.322
C(7)-N(9)-H(24)	111.722	111.894

4.2.2 Frontier Orbital Energy Analysis

HOMO and LUMO of the compound are found to be essential factor that decides the bioactivity of the organic and other compounds. According to the frontier molecular orbital theory, HOMO has the priority to offer electrons, while LUMO can accept electrons first.[28] The energies of HOMO -2 to LUMO +2 orbitals are given **Table 4.2**. Molecular orbital diagram for the HOMOs and LUMOs are shown in **Figure 4.3**. Chem Bio 3D software was used to generate MO diagrams (extended Huckel theory). HOMOs of all the four compounds generally resides on the sulfonyl moiety and sulphur containing five membered ring and LUMOs of the compounds mainly resides on the carbonyl moiety.

Table 4.2: Energy levels (a.u.) of MOs for compounds **1a** – **1d** calculated in their ground state in the gas phase

Compound	HOMO-2	HOMO-1	HOMO	LUMO	LUMO+1	LUMO+2
1a	-0.2583	-0.2370	-0.2271	-0.1154	-0.0714	-0.0500
1b	-0.2293	-0.2224	-0.2198	-0.0532	-0.0156	-0.0148
1c	-0.2352	-0.2210	-0.2184	-0.0518	-0.0154	-0.0026
1d	-0.2568	-0.2272	-0.2259	-0.0642	-0.0181	-0.0171

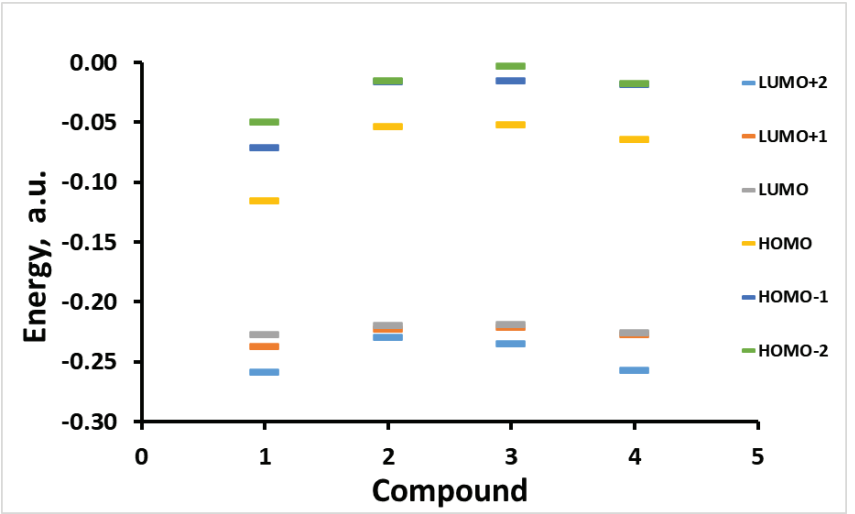

Figure 4.2: Energy levels of MO diagram for compounds **1a** - **1d** calculated in their ground state in the gas phase

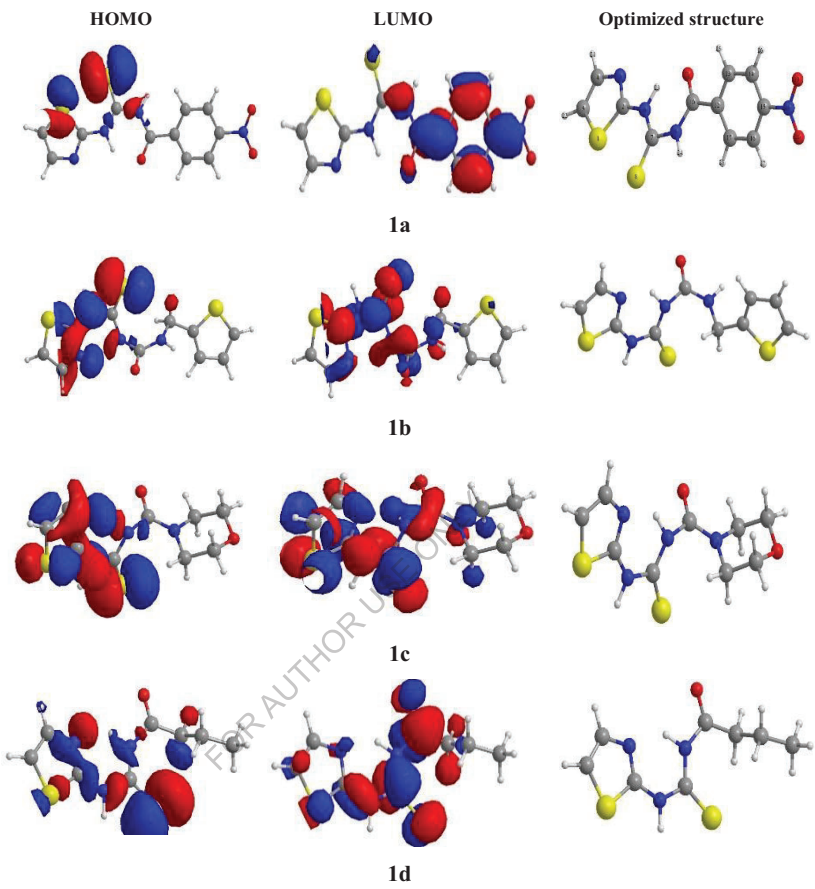

Figure 4.3: Molecular orbital diagram for the HOMOs, LUMOs and optimized structures of the four compounds **1a - 1d**.

The obtained values of IP, EA, hardness, softness, and electronegativity associated with HOMO and LUMO energies[29-42] are formulated in **Table 4.3**.

The quantum chemical parameters were calculated as described by Cakmak *et al*.[43] IP and EA can be determined using HOMO and LUMO energies were calculated according to the Janak's Theorem.[44]

$IP = -E_{HOMO}$, $EA = -E_{LUMO}$

Hardness (η) of the compound[45] can be described as distortion of chemical species or opposition to electron cloud polarization. Behaviour of the Chemical entity can be studied using the concepts of Hardness and softness. The molecule is considered soft if it has small energy gap while, the molecule is said to be hard, if has large energy gap. Thus, hard molecules are less polarizable than the soft molecules.

$\eta = (IP - EA)/ 2$

The inverse of global hardness provides softness of the molecules.[46,47]

$\sigma = 1/\eta$

Tendency of the molecules to attract the electrons is called as Electronegativity (χ) and is calculated using following equation.

$\chi = -(E_{HOMO} + E_{LUMO})/2$

Table 4.3: Quantum chemical parameters of compounds **1a - 1d** calculated at B3LYP / 6-31G (d,p)

	E_{HOMO} (eV)	E_{LUMO} (eV)	IP= $-E_{HOMO}$	EA= $-E_{LUMO}$	η= (I-A)/2	σ= 1/η	χ= (I+A)/2	Log P	MIC values*
1a	-6.180	-3.140	6.180	3.140	1.520	0.658	4.660	2.317	100
1b	-5.981	-1.448	5.981	1.448	2.267	0.441	3.714	2.302	50
1c	-5.943	-1.410	5.943	1.410	2.267	0.441	3.676	1.417	25
1d	-6.147	-1.747	6.147	1.747	2.200	0.455	3.947	2.559	100

* Antifungal activity against *C.glabrata*[26]

From **Table 4.3** it is also observed that higher the value of LUMO energy, more is the activity. This is in accordance with the literature which reported the strongest antifungal activity for **1c**. Furthermore, it is also observed that the antifungal activity correlates strongly with the computed values of all the quantum chemical parameters viz. EA, IP, Electronegativity, band gap, hardness (η) and softness (σ). From the Log P calculations it is observed that **1c** is less lipophilic in nature. Lower values of Log P are indicative of stronger antifungal activity.

4.3. Conclusion

The DFT calculations of thiourea derivatives containing a thiazole moiety (**1a** - **1d**) reveals electronic characteristics responsible for the strong biological activity. In general, good agreement between the calculated and experimental geometrical parameters have been observed. Overall, we observed strong correlation between biological activity and computed values of all the quantum chemical parameters viz. EA, IP, Electronegativity, hardness (η) and softness (σ). Lower values of Log P are indicative of stronger antifungal activity.

4.4. References

1. Eicher, T.; Hauptmann, S.; Speicher, A., *The chemistry of heterocycles: structures, reactions, synthesis, and applications*. John Wiley and Sons: 2013.
2. Suguira, K.; Schmid, A. F.; Schmid, M. M.; Brown, F. G., Effect ofcompounds on a spectrum of Rat tumors. *Cancer Chemother. Rep.* **1972,** *3* (1), 231-308.
3. Regnier, G.; Canevari, R.; Le Douarec, J.; Holstorp, S.; Daussy, J., Triphenylpropylpiperazine Derivatives as New Potent Analgetic Substances. *Journal of Medicinal Chemistry* **1972,** *15* (3), 295-301.
4. Pershin, G. N.; Shcherbakova, L. I.; Zykova, T. N.; Sokolova, V. N., Antibacterial activity of pyrimidine and pyrrolo-(3, 2-d)-pyrimidine derivatives. *Farmakologiia i toksikologiia* **1972,** *35* (4), 466-471.
5. Winter, C. A.; Risley, E. A.; Nuss, G. W. In *Carrageenin-induced Edema in Hind Paw of the Rat as an Assay for Antiinflammatory Drugs*, Proceedings of the Society for Experimental Biology and Medicine, 1962; pp 544-547.
6. Mojtahedi, M. M.; Saidi, M. R.; Shirzi, J. S.; Bolourtchian, M., Microwave promoted efficient synthesis of substituted uracils and thiouracils under solvent-free conditions. *Synthetic communications* **2002,** *32* (6), 851-855.
7. Ghorab, M. M.; El-Gaby, M. S. A.; Soliman, A. M.; Alsaid, M. S.; Abdel-Aziz, M. M.; Elaasser, M. M., Synthesis, docking study and biological evaluation of some new thiourea derivatives bearing benzenesulfonamide moiety. *Chemistry Central Journal* **2017,** *11* (1), 42.
8. Hashem, H. E.; Amr, A. E.-G. E.; Nossier, E. S.; Elsayed, E. A.; Azmy, E. M., Synthesis, Antimicrobial Activity and Molecular Docking of Novel Thiourea Derivatives Tagged with Thiadiazole, Imidazole and Triazine Moieties as Potential DNA Gyrase and Topoisomerase IV Inhibitors. *Molecules* **2020,** *25* (12), 2766.
9. Yang, G.; Shi, L.; Pan, Z.; Wu, L.; Fan, L.; Wang, C.; Xu, C.; Liang, J., The synthesis of coumarin thiazoles containing a trifluoromethyl group and their antifungal activities. *Arabian Journal of Chemistry* **2021,** *14* (1), 102880.
10. Elias, R.; Benhamou, R. I.; Jaber, Q. Z.; Dorot, O.; Zada, S. L.; Oved, K.; Pichinuk, E.; Fridman, M., Antifungal activity, mode of action variability, and

subcellular distribution of coumarin-based antifungal azoles. *European Journal of Medicinal Chemistry* **2019,** *179*, 779-790.

11. Yang, W.; Zhou, X.; Wu, Z., Design, Synthesis, Antifungal and Antibacterial Activities of N-phenyl and N-pyridinyl-5-(trifluoromethyl)-pyrazole-4-carboxamide Derivatives. *Journal of Heterocyclic Chemistry* **2018,** *55* (10), 2261-2269.
12. Zhukovskaya, O. N.; Spasov, A. A.; Kuz'menko, T. A.; Morkovnik, A. S.; Kucheryavenko, A. F.; Anisimova, V. A.; Salaznikova, O. A.; Gaidukova, K. A.; Kuznetsova, V. A.; Babkov, D. A.; Grechko, O. Y.; Eliseeva, N. V.; Rashchenko, A. I., Synthesis and Pharmacological Activity of Trifluoromethyl-Containing Imidazo[1,2-A]Benzimidazoles. *Pharmaceutical Chemistry Journal* **2018,** *52* (5), 385-391.
13. Ashfaq, M.; Tahir, M. N.; Muhammad, S.; Munawar, K. S.; Ali, A.; Bogdanov, G.; Alarfaji, S. S., Single-Crystal Investigation, Hirshfeld Surface Analysis, and DFT Study of Third-Order NLO Properties of Unsymmetrical Acyl Thiourea Derivatives. *ACS Omega* **2021,** *6* (46), 31211-31225.
14. Asghar, F.; Rana, S.; Fatima, S.; Badshah, A.; Lal, B.; Butler, I. S., Biologically active halo-substituted ferrocenyl thioureas: synthesis, spectroscopic characterization, and DFT calculations. *New Journal of Chemistry* **2018,** *42* (9), 7154-7165.
15. Mistry, B. M.; Shin, H.-S.; Pandurangan, M.; Patel, R. V., Synthesis of Acyl Thiourea Derivatives of 7-Trifluoromethyl-2-Pyridylquinazolin-4(3H)-one as Anticancer Agents. *Journal of Chemical Research* **2017,** *41* (10), 598-602.
16. Yun, T.; Qin, T.; Liu, Y.; Lai, L., Identification of acylthiourea derivatives as potent Plk1 PBD inhibitors. *European Journal of Medicinal Chemistry* **2016,** *124*, 229-236.
17. Contreras Aguilar, E.; Echeverría, G. A.; Piro, O. E.; Ulic, S. E.; Jios, J. L.; Tuttolomondo, M. E.; Molina, R. D. I.; Arena, M. E., Acyl thiourea derivatives: A study of crystallographic, bonding, biological and spectral properties. *Chemical Physics Letters* **2019,** *715*, 64-71.
18. Rauf, M. K.; Zaib, S.; Talib, A.; Ebihara, M.; Badshah, A.; Bolte, M.; Iqbal, J., Solution-phase microwave assisted parallel synthesis, biological evaluation and in silico docking studies of N,N′-disubstituted thioureas derived from 3-

chlorobenzoic acid. *Bioorganic and Medicinal Chemistry* **2016,** *24* (18), 4452-4463.

19. Kargar, H.; Fallah-Mehrjardi, M.; Ashfaq, M.; Munawar, K. S.; Tahir, M. N.; Behjatmanesh-Ardakani, R.; Amiri Rudbari, H.; Adabi Ardakani, A.; Sedighi-Khavidak, S., Zn(II) complexes containing O,N,N,O-donor Schiff base ligands: synthesis, crystal structures, spectral investigations, biological activities, theoretical calculations and substitution effect on structures. *Journal of Coordination Chemistry* **2021,** *74* (16), 2720-2740.
20. Leo, A.; Hansch, C.; Elkins, D., Partition coefficients and their uses. *Chemical Reviews* **1971,** *71* (6), 525-616.
21. Nasal, A.; Siluk, D.; Kaliszan, R., Chromatographic Retention Parameters in Medicinal Chemistry and Molecular Pharmacology. *Current Medicinal Chemistry* **2003,** *10*, 381-426.
22. Podunavac-Kuzmanović, S. O.; Cvetković, D. D.; Barna, D. J., Correlations between the lipophilicity and the inhibitory activity of different substituted benzimidazoles. *Chemical Industry and Chemical Engineering Quarterly/CICEQ* **2009,** *15* (3), 125-130.
23. Podunavac-Kuzmanović, S. O.; Velimirovic, S. D., Correlation between the lipophilicity and antifungal activity of some benzoxazole derivatives. *Acta Periodica Technologica* **2010,** *41*, 177-185.
24. Sławik, T.; Paw, B., Lipophilicity of Some N- and O- Substituted Alkanoic Acids of 1, 2- Benzisothiazol- 3 (2H)- one Determined by Reversed- Phase Thin Layer Chromatography. *Journal of liquid chromatography and related technologies* **2004,** *27* (6), 1043-1055.
25. Tiperciuc, B.; Sârbu, C., Prediction of the Chromatographic Retention (Lipophilicity) of Some New Methyl- Thiazole- Oxadiazoline Derivatives by Multivariate Regression Methods. *Journal of Liquid Chromatography and Related Technologies* **2006,** *29* (15), 2257-2270.
26. Saeed, S.; Rashid, N.; Jones, P. G.; Hussain, R.; Bhatti, M. H., Synthesis, spectroscopic characterization, crystal structure and antifungal activity of thiourea derivatives containing a thiazole moiety. *Central European Journal of Chemistry* **2010,** *8* (3), 550-558.
27. Schmidt, M. W.; Baldridge, K. K.; Boatz, J. A.; Elbert, S. T.; Gordon, M. S.; Jensen, J. H.; Koseki, S.; Matsunaga, N.; Nguyen, K. A.; Su, S.; Windus, T.

L.; Dupuis, M.; Montgomery Jr, J. A., General atomic and molecular electronic structure system. *Journal of Computational Chemistry* **1993,** *14* (11), 1347-1363.

28. Liu, X.-H.; Chen, P.-Q.; Wang, B.-L.; Li, Y.-H.; Wang, S.-H.; Li, Z.-M., Synthesis, bioactivity, theoretical and molecular docking study of 1-cyano-N-substituted-cyclopropanecarboxamide as ketol-acid reductoisomerase inhibitor. *Bioorganic and medicinal chemistry letters* **2007,** *17* (13), 3784-3788.
29. Xu, Y.; Chu, Q.; Chen, D.; Fuentes, A., HOMO–LUMO Gaps and Molecular Structures of Polycyclic Aromatic Hydrocarbons in Soot Formation. *Frontiers in Mechanical Engineering* **2021,** *7*.
30. Joshi, B. D.; Thakur, G.; Chaudhary, M. K., Molecular Structure, Homo-Lumo and Vibrational Analysis Of Ergoline By Density Functional Theory. *Scientific World* **2021,** *14* (14), 21-30.
31. Joseph, S.; Thomas, S.; Mohan, J.; Kumar, A. S.; Jayasree, S. T.; Thomas, S.; Kalarikkal, N., Theoretical Study on Tuning Band Gap and Electronic Properties of Atomically Thin Nanostructured MoS2/Metal Cluster Heterostructures. *ACS Omega* **2021,** *6* (10), 6623-6628.
32. Mumit, M. A.; Pal, T. K.; Alam, M. A.; Islam, M. A.-A.-A.-A.; Paul, S.; Sheikh, M. C., DFT studies on vibrational and electronic spectra, HOMO-LUMO, MEP, HOMA, NBO and molecular docking analysis of benzyl-3-N-(2,4,5-trimethoxyphenylmethylene)hydrazinecarbodithioate. *Journal of molecular structure* **2020,** *1220*, 128715-128715.
33. De Lile, J. R.; Kang, S. G.; Son, Y.-A.; Lee, S. G., Do HOMO–LUMO Energy Levels and Band Gaps Provide Sufficient Understanding of Dye-Sensitizer Activity Trends for Water Purification? *ACS Omega* **2020,** *5* (25), 15052-15062.
34. Townsend, P. A.; Grayson, M. N., Density Functional Theory Transition-State Modeling for the Prediction of Ames Mutagenicity in 1,4 Michael Acceptors. *Journal of Chemical Information and Modeling* **2019,** *59* (12), 5099-5103.
35. Matunová, P.; Jirásek, V.; Rezek, B., DFT calculations reveal pronounced HOMO–LUMO spatial separation in polypyrrole–nanodiamond systems. *Physical Chemistry Chemical Physics* **2019,** *21* (21), 11033-11042.
36. Choudhary, V.; Bhatt, A.; Dash, D.; Sharma, N., DFT calculations on molecular structures, HOMO–LUMO study, reactivity descriptors and spectral

analyses of newly synthesized diorganotin(IV) 2-chloridophenylacetohydroxamate complexes. *Journal of Computational Chemistry* **2019,** *40* (27), 2354-2363.

37. Chen, D.; Wang, H., HOMO–LUMO Gaps of Homogeneous Polycyclic Aromatic Hydrocarbon Clusters. *The Journal of Physical Chemistry C* **2019,** *123* (45), 27785-27793.
38. Umar, Y.; Abdalla, S., DFT Study of the Molecular Structure, Conformational Preference, HOMO, LUMO, and Vibrational Analysis of 2-, and 3-Furoyl Chloride. *Journal of Solution Chemistry* **2017,** *46* (4), 741-758.
39. Pereira, F.; Xiao, K.; Latino, D. A. R. S.; Wu, C.; Zhang, Q.; Aires-de-Sousa, J., Machine Learning Methods to Predict Density Functional Theory B3LYP Energies of HOMO and LUMO Orbitals. *Journal of Chemical Information and Modeling* **2017,** *57* (1), 11-21.
40. Prabhaharan, M.; Prabakaran, A. R.; Gunasekaran, S.; Srinivasan, S., DFT studies on vibrational spectra, HOMO–LUMO, NBO and thermodynamic function analysis of cyanuric fluoride. *Spectrochimica Acta Part A: Molecular and Biomolecular Spectroscopy* **2015,** *136*, 494-503.
41. Barman, M. K.; Chatterjee, M.; Srivastava, B.; Mandal, B., Characterization and Density Functional Theory Optimization of a Simultaneous Binder (FSG-XO) of Two Different Species Exploiting HOMO–LUMO Levels: Photoelectronic and Analytical Applications. *Journal of Chemical and Engineering Data* **2015,** *60* (8), 2197-2208.
42. El-Mansy, M. A. M.; El-Nahass, M. M.; Khusayfan, N. M.; El-Menyawy, E. M., DFT approach for FT-IR spectra and HOMO–LUMO energy gap for N-(p-dimethylaminobenzylidene)-p-nitroaniline (DBN). *Spectrochimica Acta Part A: Molecular and Biomolecular Spectroscopy* **2013,** *111*, 217-222.
43. Cakmak, E.; Ozbakir Isin, D., A theoretical evaluation on free radical scavenging activity of 3-styrylchromone derivatives: the DFT study. *Journal of Molecular Modeling* **2020,** *26* (5), 98.
44. Janak, J. F., Proof that dE/dni = e in density-functional theory. *Physical Review B* **1978,** *18* (12), 7165-7168.
45. Parr, R. G.; Pearson, R. G., Absolute hardness: companion parameter to absolute electronegativity. *Journal of the American Chemical Society* **1983,** *105* (26), 7512-7516.

46. Pearson, R. G., Absolute electronegativity and hardness: application to inorganic chemistry. *Inorganic Chemistry* **1988,** *27* (4), 734-740.
47. Dongare, R. K.; Inamdar, S. N.; Tigote, R. M., DFT Based Investigations of Antibiotic and Antifungal Activity of Allantofuranone and Related γ-Lactone Compounds. *Journal of Advanced Scientific Research* **2021,** *12* (2 (S1)), 336-339.

CHAPTER 5:

DFT Based Investigations of Antibiotic and Antifungal Activity of Allantofuranone and Related γ-Lactone Compounds

5.1 Introduction

Plant fungi adapt to their surroundings despite the fact that the chemical composition of the plant varies dramatically over the host's life cycle. The development of a highly evolved secondary metabolism by fungi to cope with both the plant defense system and competing with other parasites leads in a unique survival strategy. The plant pathogen Allantophomopsis lycopodina[1-4] has been linked to leaf lesions in lingonberries (Vaccinium vitis-idaea) and cranberry fruit rot (black rot).[5] Allantofuranone is found in the extract of Allantophomopsis lycopodina strain IBWF58B-05A, which has been reported to have significant and selective antibiotic and antifungal activity.[6] Allantofuranone is an uncommon -lactone molecule that has been shown to have beneficial biological properties. Dimeric γ-lactone**,** antimalarial radicicol, cytotoxic hamavellones A and B, antimycobacterial peniciller emophilane A and antifungal bacilysin are only a few examples of new and bioactive secondary metabolites found in soil-derived fungus.[7-15]

In this work, we present the study of four γ-lactone containing compounds (Allantofuranone, Xenofuranone A and B, WF 3681) using DFT / B3LYP method. **Figure 5.1** illustrates the chemical structures employed in the current study. Allantofuranone is known to have considerable antifungal activity, but other compounds, while structurally similar, have no antifungal action and have extremely low cytotoxicity.

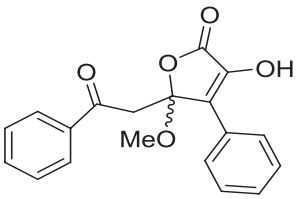

Allantofuranone **1**

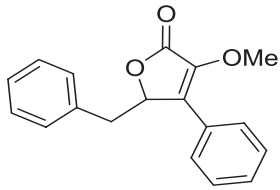

Xenofuranone A **2**

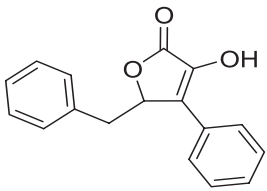

Xenofuranone B **3**

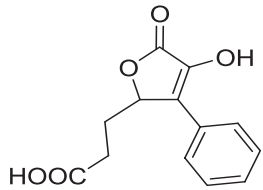

WF 3681 **4**

Figure 5.1: Structures of the Allantofuranone and related compounds

5.2 Results and Discussion

5.2.1 Comparison of DFT Structural Parameters with Experimental Data

The DFT calculations were done in GAMESS package[16] using the B3LYP/6-31G (d,p) method. **Table 5.1** shows the geometry parameter of compound Allantofuranone, which includes calculated bond distances and observed bond lengths. In general, there has been considerable agreement between computed and experimental bond lengths.[6]

Table 5.1: Comparative selected structure parameters of the compound Allantofuranone.

Distances (Å) / Angles (^{0})	Allantofuranone	
	Expt	DFT
O1-C13	1.400	1.403
O1-C14	1.447	1.430
O2-C10	1.228	1.221
O3-C16	1.354	1.353
O4-C23	1.354	1.342
O5-C16	1.218	1.211
C6-C8	1.478	1.464
C6-C13	1.525	1.533
C6-C23	1.341	1.348
C7-C8	1.399	1.410
C7-C12	1.399	1.394
C8-C17	1.400	1.411
C9-C10	1.503	1.500
C9-C18	1.398	1.403
C9-C22	1.397	1.404
C10-C11	1.513	1.527
C11-C13	1.526	1.533

5.2.2 Frontier Orbital Energy Analysis

The most essential factor that determines the bioactivity of organic and other substances is said to be HOMO and LUMO. The frontier molecular orbital theory states that HOMO prefers to provide electrons first, whereas LUMO prefers to take electrons first.[17] The energies of HOMO -2 to LUMO +2 orbitals are given **Table 5.2**. Molecular orbital diagram for the HOMOs and LUMOs are shown in **Figure 5.3**. Chem Bio 3D software was used to generate MO diagrams (extended Huckel theory). All four compounds have HOMOs on a five-membered ring moiety, and the three compounds Xenofuranone A, Xenofuranone B, and WF 3681 have LUMOs on five-membered ring moieties, whilst Allantofuranone has a LUMO on one of the benzoyl rings.

Table 5.2: Energy levels (a.u.) of MOs for compound Allantofuranone, Xenofuranone A and Xenofuranone B and WF 3681 calculated in their ground state in the gas phase.

Compound	HOMO-2	HOMO-1	HOMO	LUMO	LUMO+1	LUMO+2
Allantofuranone	-0.2546	-0.2513	-0.2161	-0.0579	-0.053	-0.0097
Xenofuranone A	-0.2430	-0.2402	-0.2295	-0.0419	-0.0173	-0.0047
Xenofuranone B	-0.2448	-0.2408	-0.2336	-0.0456	-0.0227	-0.0060
WF 3681	-0.2664	-0.2632	-0.2312	-0.0460	-0.0200	0.0002

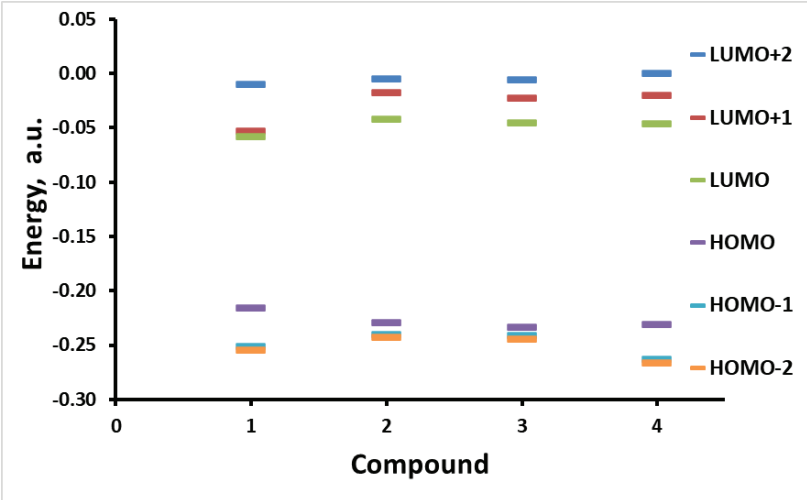

Figure 5.2: Energy levels of MO diagram for compounds Allantofuranone, Xenofuranone A and Xenofuranone B and WF 3681 calculated in their ground state in the gas phase.

HOMO	LUMO	Optimized structure
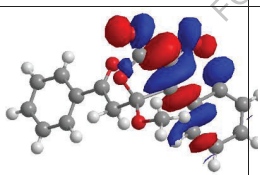	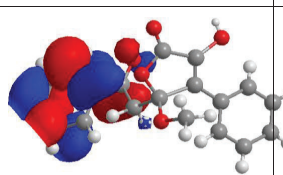	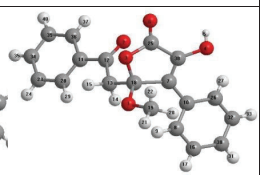
Allantofuranone		

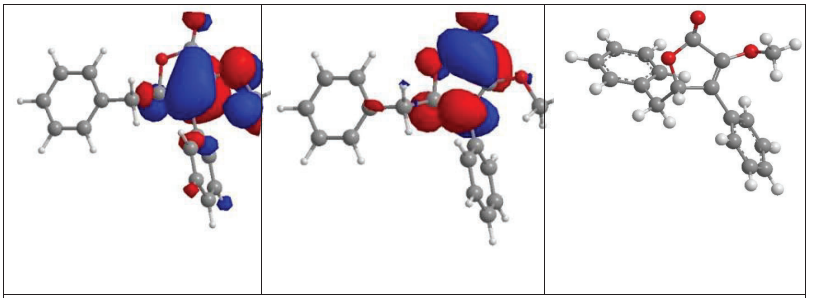

Xenofuranone A

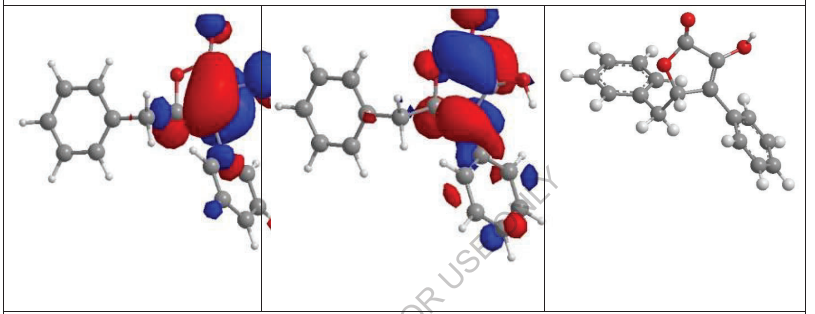

Xenofuranone B

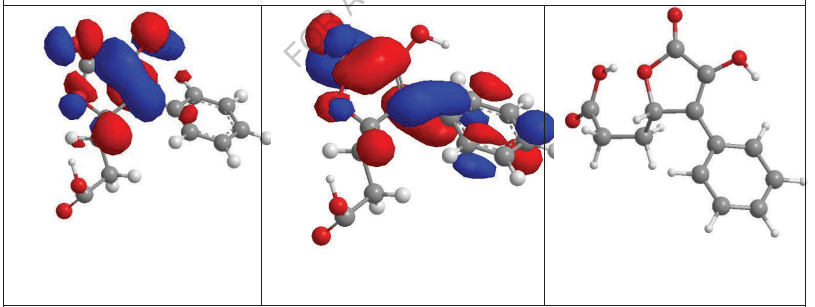

WF 3681

Figure 5.3: Molecular orbital diagram for the HOMOs, LUMOs and optimized structures of the four compounds Allantofuranone, Xenofuranone A, Xenofuranone B and WF 3681

Using the above equations, the quantum chemical parameters of four γ-lactone containing compounds were computed. The obtained values of IP, EA, hardness, softness, and electronegativity associated with HOMO and LUMO energies[18-31] are formulated in **Table 5.3**.

Cakmak *et al*.[32] describes how to calculate quantum chemical parameters. IP and EA can be obtained using HOMO and LUMO energies were calculated according to the Janak's Theorem[33].

$IP = -E_{HOMO}$, $EA = -E_{LUMO}$

Hardness (η) of the compound[34] expresses chemical species distortion or resistance to electron cloud polarisation. The ideas of hardness and softness were used to investigate the chemical entity's behaviour. If a molecule has a big energy gap, it is considered to be hard, and if it has a small energy gap, it is said to be soft. Soft molecules are therefore more polarizable than hard molecules.

$\eta = (IP-EA)/2$

The reciprocal of global hardness is used to calculate the softness of the molecules.[35]

$\sigma = 1/\eta$

Electronegativity (χ) is the ability of molecules to attract electrons, and it was computed using the equation below.

$\chi = -(E_{HOMO} + E_{LUMO})/2$

Table 5.3: Quantum chemical parameters of compounds Allantofuranone, Xenofuranone A and Xenofuranone B and WF 3681calculated at B3LYP/6-31G(d,p)

	E_{HOMO} (eV)	E_{LUMO} (eV)	ΔE (eV)	IP= $-E_{HOMO}$	EA= $-E_{LUMO}$	η= (I-A)/2	σ= 1/η	χ= (I+A)/2	Log P
Allantofuranone	-5.880	-1.576	4.30	5.880	1.576	2.152	0.465	3.728	3.695
Xenofuranone A	-6.245	-1.140	5.10	6.245	1.140	2.552	0.392	3.693	2.774
Xenofuranone B	-6.357	-1.241	5.12	6.357	1.241	2.558	0.391	3.799	2.412
WF 3681	-6.291	-1.252	5.04	6.291	1.252	2.520	0.397	3.771	1.101

It is clear from **Table 5.3** that the Allantofuranone has a smaller HOMO – LUMO energy gap when compared to other compounds. Furthermore, it has been found that the lower the LUMO energy value, the higher the activity. This is in line with the literature, which claims that Allantofuranone has the strongest antifungal action.

The activity is shown to be highly correlated with the estimated values of all quantum chemical parameters viz. EA, IP, Electronegativity, band gap, hardness (η) and softness (σ). Allantofuranone is more lipophilic in nature, according to the Log P estimates. Greater antifungal and antibacterial action is associated with higher Log P values.

5.3 Conclusion

The DFT calculations of the compounds Allantofuranone, Xenofuranone A, Xenofuranone B, and WF 3681 demonstrated that Allantofuranone has a small HOMO - LUMO gap, a lower LUMO value, a more lipophilic character, and a rich topography, all of which are required for antifungal action. The electronic properties that distinguish Allantofuranone from other structurally related compounds and are responsible for its remarkable biological action are highlighted. Overall, we found a significant correlation between biological activity and calculate values for all quantum chemical parameters, including EA, IP, electronegativity, band Gap, hardness (η) and softness (σ).

5.4 References

1. Rao, K. V.; Sadhukhan, A. K.; Veerender, M.; Ravikumar, V.; Mohan, E. V. S.; Dhanvantri, S. D.; Sitaramkumar, M.; Moses Babu, J.; Vyas, K.; Om Reddy, G., Butyrolactones from Aspergillus terreus. *Chemical and Pharmaceutical Bulletin* **2000,** *48* (4), 559-562.
2. Olatinwo, R. O.; Hanson, E. J.; Schilder, A. M. C., A First Assessment of the Cranberry Fruit Rot Complex in Michigan. *Plant Disease* **2003,** *87* (5), 550-556.
3. Putnam, M. L., Allantophomopsis lycopodina– a new aerial pathogen of lingonberry (Vaccinium vitis-idaea). *Plant Pathology* **2005,** *54* (2), 248-248.
4. Brachmann, A. O.; Forst, S.; Furgani, G. M.; Fodor, A.; Bode, H. B., Xenofuranones A and B: Phenylpyruvate Dimers from Xenorhabdus szentirmaii. *Journal of Natural Products* **2006,** *69* (12), 1830-1832.
5. Carris, L. M., Cranberry black rot fungi: Allantophomopsis cytisporea and Allantophomopsis lycopodina. *Canadian Journal of Botany* **1990,** *68* (10), 2283-2291.
6. Schüffler, A.; Kautz, D.; Liermann, J. C.; Opatz, T.; Anke, T., Allantofuranone, a new antifungal antibiotic from Allantophomopsis lycopodina IBWF58B-05A. *The Journal of Antibiotics* **2009,** *62* (3), 119-121.
7. Arunpanichlert, J.; Rukachaisirikul, V.; Chaiwarin, T.; Tantirungrotechai, Y.; Khamthong, N.; Phongpaichit, S.; Liamthong, S.; Sakayaroj, J., Dimeric γ-lactone derivatives from the soil-derived fungus Lasiodiplodia theobromae NSTRU-PN1.4. *Natural Product Research* **2020**, 1-11.
8. Isaka, K.; Suwa, Y.; Kimura, Y.; Yamagishi, T.; Sumino, T.; Tsuneda, S., Anaerobic ammonium oxidation (anammox) irreversibly inhibited by methanol. *Applied Microbiology and Biotechnology* **2008,** *81* (2), 379-385.
9. Sansinenea, E.; Ortiz, A., Secondary metabolites of soil Bacillus spp. *Biotechnology Letters* **2011,** *33* (8), 1523-1538.
10. Reino, J. L.; Guerrero, R. F.; Hernández-Galán, R.; Collado, I. G., Secondary metabolites from species of the biocontrol agent Trichoderma. *Phytochemistry Reviews* **2008,** *7* (1), 89-123.

11. Evidente, A.; Kornienko, A.; Cimmino, A.; Andolfi, A.; Lefranc, F.; Mathieu, V.; Kiss, R., Fungal metabolites with anticancer activity. *Natural Product Reports* **2014,** *31* (5), 617-627.
12. Ravi, B. N.; Perzanowski, H. P.; Ross, R. A.; Erdman, T. R.; Scheuer, P. J.; Finer, J.; Clardy, J., Recent research in marine natural products: the puupehenones. *Pure and Applied Chemistry* **1979,** *51* (9), 1893-1900.
13. Berti, F.; Forzato, C.; Nitti, P.; Pitacco, G.; Valentin, E., A study of the enantiopreference of lipase PS (Pseudomonas cepacia) towards diastereomeric dihydro-5-alkyl-4-hydroxymethyl-2(3H)-furanones. *Tetrahedron: Asymmetry* **2005,** *16* (6), 1091-1102.
14. Felluga, F.; Forzato, C.; Ghelfi, F.; Nitti, P.; Pitacco, G.; Pagnoni, U. M.; Roncaglia, F., Atom transfer radical cyclization (ATRC) applied to a chemoenzymatic synthesis of Quercus lactones. *Tetrahedron: Asymmetry* **2007,** *18* (4), 527-536.
15. Rukachaisirikul, V.; Arunpanichlert, J.; Sukpondma, Y.; Phongpaichit, S.; Sakayaroj, J., Metabolites from the endophytic fungi Botryosphaeria rhodina PSU-M35 and PSU-M114. *Tetrahedron* **2009,** *65* (51), 10590-10595.
16. Schmidt, M. W.; Baldridge, K. K.; Boatz, J. A.; Elbert, S. T.; Gordon, M. S.; Jensen, J. H.; Koseki, S.; Matsunaga, N.; Nguyen, K. A.; Su, S.; Windus, T. L.; Dupuis, M.; Montgomery Jr, J. A., General atomic and molecular electronic structure system. *Journal of Computational Chemistry* **1993,** *14* (11), 1347-1363.
17. Liu, X.-H.; Chen, P.-Q.; Wang, B.-L.; Li, Y.-H.; Wang, S.-H.; Li, Z.-M., Synthesis, bioactivity, theoretical and molecular docking study of 1-cyano-N-substituted-cyclopropanecarboxamide as ketol-acid reductoisomerase inhibitor. *Bioorganic and medicinal chemistry letters* **2007,** *17* (13), 3784-3788.
18. Xu, Y.; Chu, Q.; Chen, D.; Fuentes, A., HOMO–LUMO Gaps and Molecular Structures of Polycyclic Aromatic Hydrocarbons in Soot Formation. *Frontiers in Mechanical Engineering* **2021,** *7*.
19. Joshi, B. D.; Thakur, G.; Chaudhary, M. K., Molecular Structure, Homo-Lumo and Vibrational Analysis Of Ergoline By Density Functional Theory. *Scientific World* **2021,** *14* (14), 21-30.
20. Joseph, S.; Thomas, S.; Mohan, J.; Kumar, A. S.; Jayasree, S. T.; Thomas, S.; Kalarikkal, N., Theoretical Study on Tuning Band Gap and Electronic

Properties of Atomically Thin Nanostructured MoS2/Metal Cluster Heterostructures. *ACS Omega* **2021,** *6* (10), 6623-6628.

21. Mumit, M. A.; Pal, T. K.; Alam, M. A.; Islam, M. A.-A.-A.-A.; Paul, S.; Sheikh, M. C., DFT studies on vibrational and electronic spectra, HOMO-LUMO, MEP, HOMA, NBO and molecular docking analysis of benzyl-3-N-(2,4,5-trimethoxyphenylmethylene)hydrazinecarbodithioate. *Journal of molecular structure* **2020,** *1220*, 128715-128715.
22. De Lile, J. R.; Kang, S. G.; Son, Y.-A.; Lee, S. G., Do HOMO–LUMO Energy Levels and Band Gaps Provide Sufficient Understanding of Dye-Sensitizer Activity Trends for Water Purification? *ACS Omega* **2020,** *5* (25), 15052-15062.
23. Townsend, P. A.; Grayson, M. N., Density Functional Theory Transition-State Modeling for the Prediction of Ames Mutagenicity in 1,4 Michael Acceptors. *Journal of Chemical Information and Modeling* **2019,** *59* (12), 5099-5103.
24. Matunová, P.; Jirásek, V.; Rezek, B., DFT calculations reveal pronounced HOMO–LUMO spatial separation in polypyrrole–nanodiamond systems. *Physical Chemistry Chemical Physics* **2019,** *21* (21), 11033-11042.
25. Choudhary, V.; Bhatt, A.; Dash, D.; Sharma, N., DFT calculations on molecular structures, HOMO–LUMO study, reactivity descriptors and spectral analyses of newly synthesized diorganotin(IV) 2-chloridophenylacetohydroxamate complexes. *Journal of Computational Chemistry* **2019,** *40* (27), 2354-2363.
26. Chen, D.; Wang, H., HOMO–LUMO Gaps of Homogeneous Polycyclic Aromatic Hydrocarbon Clusters. *The Journal of Physical Chemistry C* **2019,** *123* (45), 27785-27793.
27. Umar, Y.; Abdalla, S., DFT Study of the Molecular Structure, Conformational Preference, HOMO, LUMO, and Vibrational Analysis of 2-, and 3-Furoyl Chloride. *Journal of Solution Chemistry* **2017,** *46* (4), 741-758.
28. Pereira, F.; Xiao, K.; Latino, D. A. R. S.; Wu, C.; Zhang, Q.; Aires-de-Sousa, J., Machine Learning Methods to Predict Density Functional Theory B3LYP Energies of HOMO and LUMO Orbitals. *Journal of Chemical Information and Modeling* **2017,** *57* (1), 11-21.
29. Prabhaharan, M.; Prabakaran, A. R.; Gunasekaran, S.; Srinivasan, S., DFT studies on vibrational spectra, HOMO–LUMO, NBO and thermodynamic

function analysis of cyanuric fluoride. *Spectrochimica Acta Part A: Molecular and Biomolecular Spectroscopy* **2015,** *136*, 494-503.

30. Barman, M. K.; Chatterjee, M.; Srivastava, B.; Mandal, B., Characterization and Density Functional Theory Optimization of a Simultaneous Binder (FSG-XO) of Two Different Species Exploiting HOMO–LUMO Levels: Photoelectronic and Analytical Applications. *Journal of Chemical and Engineering Data* **2015,** *60* (8), 2197-2208.
31. El-Mansy, M. A. M.; El-Nahass, M. M.; Khusayfan, N. M.; El-Menyawy, E. M., DFT approach for FT-IR spectra and HOMO–LUMO energy gap for N-(p-dimethylaminobenzylidene)-p-nitroaniline (DBN). *Spectrochimica Acta Part A: Molecular and Biomolecular Spectroscopy* **2013,** *111*, 217-222.
32. Cakmak, E.; Ozbakir Isin, D., A theoretical evaluation on free radical scavenging activity of 3-styrylchromone derivatives: the DFT study. *Journal of Molecular Modeling* **2020,** *26* (5), 98.
33. Janak, J. F., Proof that dE/dni = e in density-functional theory. *Physical Review B* **1978,** *18* (12), 7165-7168.
34. Parr, R. G.; Pearson, R. G., Absolute hardness: companion parameter to absolute electronegativity. *Journal of the American Chemical Society* **1983,** *105* (26), 7512-7516.
35. Pearson, R. G., Absolute electronegativity and hardness: application to inorganic chemistry. *Inorganic Chemistry* **1988,** *27* (4), 734-740.

CHAPTER 6:

Evaluation of Antifungal activity of Homoisoflavonone compounds using DFT

6.1 Introduction

Homoisoflavanones are oxygen-containing heterocyclic chemicals found in nature. The homoisoflavanones have a chromanone, chromone, or chromane ring in their sixteen-carbon skeleton. Anti-diabetic, anti-inflammatory, antibacterial, and anti-mutagenic bioactivities have all been found for homoisoflavonoids.[1] Antifungal action of isolated homoisoflavanones, 3-benzylidene-4-chromanones.[2-4] For the synthesis of homoisoflavanones, several experimental approaches have been devised.[5-10] However, there have been very few theoretical studies recorded. Isolated homoisoflavanones have also been reported to possess antifungal activity.[11-21] Isoflavanones and homoisoflavanones are structurally identical. 3-benzyl-3-hydroxy-4-chromanonesc, 3-benzylidene-4-chromanones, 3-benzyl-4-chromanones, and scillascillins are the four types of homoisoflavanones.[22] The antifungal activity of 3-benzylidene-4-chromanones has been discovered.

In SAR investigations, log P is the most commonly used molecular descriptor.[23-28] It's a numerical descriptor of lipophilicity, which is one of the most essential pharmacokinetic features. The lipophilicity of bioactive substances determines their ability to pass through non-polar cell membranes. The partition coefficient, which is acquired via distribution studies of the compound between an immiscible polar and non-polar solvent pair, is commonly used to determine this attribute. Log P can be used to indicate a drug's inhibitory activity.

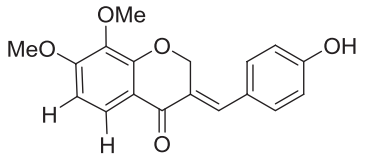

HIF 1

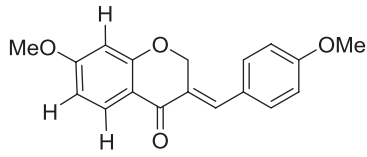

HIF 2

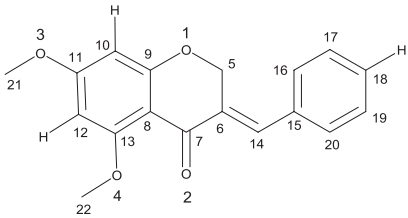

HIF 3

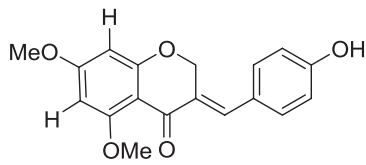

HIF 4

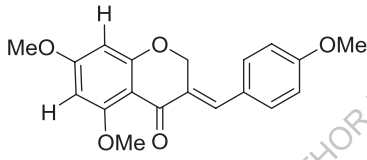

HIF 5

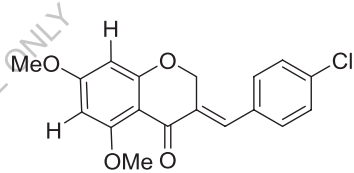

HIF 6

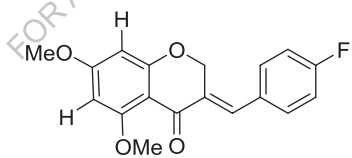

HIF 7

Figure 6.1: Structures of the Homoisoflavanones HIF 1-7

In this work, DFT studies on seven 3-benzylidene-4-chromanone analogues (Homoisoflavanones HIF 1-7) with varying substitution patterns are reported (**Figure 6.1**). Theoretical results are correlated with reported antifungal activities.[2] The results are useful to bring out common set of electronic characteristic responsible for bioactivity.

6.2. Results and Discussion

All the quantum chemical calculations were performed using DFT with B3LYP/6-31G (*d*,*p*) method using GAMESS pakage.[29] Initial geometries of the

homoisoflavanone analogues were generated using Chem Bio3D Ultra 14.0. Full geometry optimization was carried out without any geometrical constraints (**Figure 6.2**). The calculation of QSAR properties were performed by Chem Bio3D Ultra 14.0.

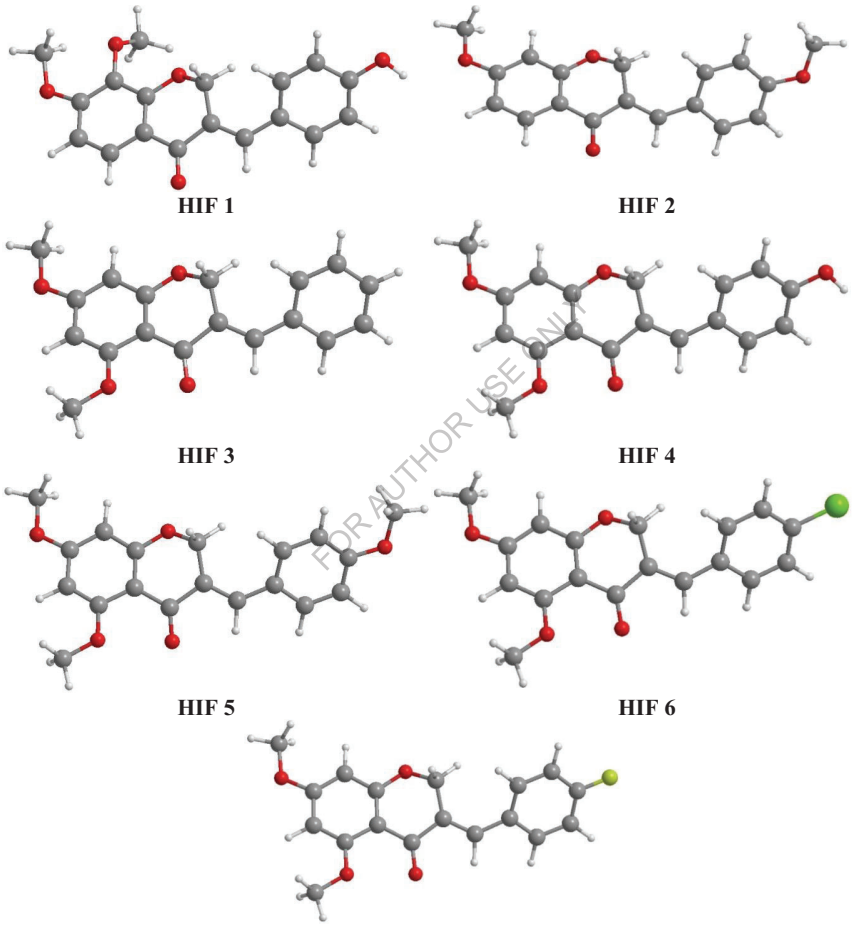

Figure 6.2: B3LYP/6-31G (*d*,*p*) optimized structures of the compounds HIF 1-7

6.2.1. Frontier Orbital Energy Analysis

The most critical features that impact bioactivity, according to the frontier molecular orbital theory, are HOMO and LUMO. The ability to donate electrons is expressed by HOMO, whereas the ability to take electrons is expressed by LUMO.[30] The energies of HOMO -2 to LUMO +2 orbitals are given **Table 6.1**. Molecular orbital diagram for the HOMOs and LUMOs are shown in **Figure 6.3**. The quantum chemical parameters were calculated as described by Cakmak et. al.[31] According to the Janak's theorem, IP and EA can be obtained using HOMO and LUMO energies utilizing **Equation 1**.[32]

$$IP = -E_{HOMO}\,, \qquad EA = -E_{LUMO} \quad (1)$$

Equation 2 can be used to calculate hardness (η), which is the distortion of chemical species or opposition to electron cloud polarisation.[33] The ideas of hardness and softness are utilised to understand the behaviour of chemical systems. Molecules having a big energy gap are called hard, while those with a small energy gap are called soft. As a result, rigid molecules have a lower polarizability than soft ones.

$$\eta = (IP - EA) / 2 \quad (2)$$

Reciprocal of global hardness gives softness (σ) of the molecules and is calculated using **Equation 3**.[34]

$$\sigma = {}^{1}/_{\eta} \quad (3)$$

Electronegativity is a metric that evaluates a molecule's proclivity for electron attraction and can be calculated using **Equation 4**.

$$\chi = -(E_{HOMO} + E_{LUMO})/\,2 \quad (4)$$

For the compounds under investigation, a lower ΔE indicates increased chemical reactivity and lower kinetic stability.[31]

The preceding equations were used to derive the quantum chemical characteristics of molecules HIF 1-7. **Table 6.2** shows the obtained values of IP, EA, hardness, softness, and electronegativity in relation to HOMO and LUMO energies[35-48]. There is a direct correlation between antifungal activity and Log P for these HIF compounds. Compound HIF 3 is reported to be most potent. HIF 3 is more lipophilic in nature, according to the Log P estimates. Stronger antifungal activity is indicated by higher Log P values. The

antifungal activity is quite well correlated with IP, EA, hardness (η), softness (σ) and electronegativity (χ).

Table 6.1: Energy levels (a.u.) of MOs for compound HIF 1-7 calculated in their ground state in the gas phase

Compound	HOMO -2	HOMO -1	HOMO	LUMO	LUMO +1	LUMO +2
HIF 1	-0.2212	-0.2170	-0.2107	-0.0638	-0.0126	-.0096
HIF 2	-0.2331	-0.2171	-0.2080	-0.0612	-0.0095	-0.0059
HIF 3	-0.2209	-0.2157	-0.2143	-0.0584	-0.0094	-0.0036
HIF 4	-0.2152	-0.2123	-0.2071	-0.0540	-0.0074	-0.0038
HIF 5	-0.2146	-0.2119	-0.2052	-0.0533	-0.0053	-0.0021
HIF 6	-0.2249	-0.2191	-0.2176	-0.0650	-0.0172	-0.0166
HIF 7	-0.2223	-0.2171	-0.2161	-0.0606	-0.0152	-0.0105

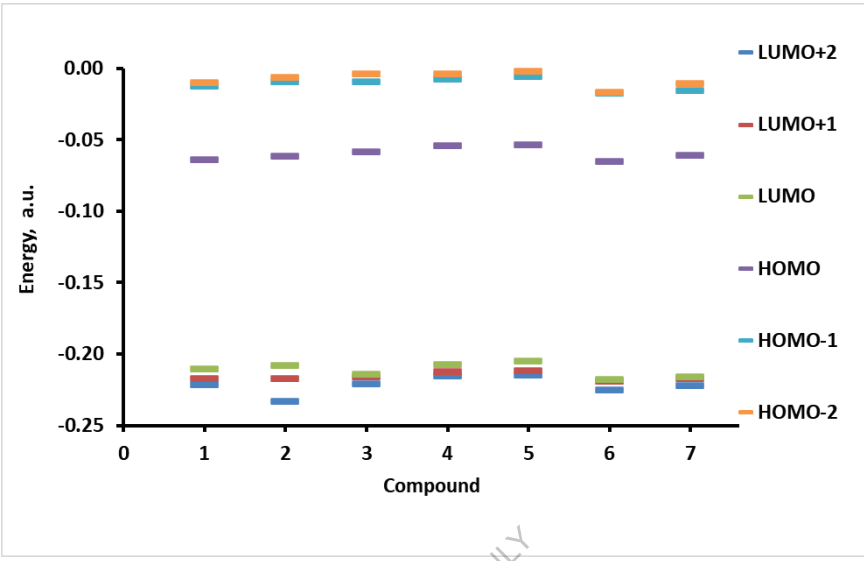

Figure 6.3: Energy levels of MO diagram for compounds HIF 1-7 calculated in their ground state in the gas phase.

Table 6.2: Quantum chemical parameters of compounds HIF 1-7 calculated at B3LYP / 6-31G (d,p)

Compd	E_{HOMO} (eV)	E_{LUMO} (eV)	IP= $-E_{HOMO}$	EA= $-E_{LUMO}$	η= (I-A)/2	σ= $1/\eta$	χ= (I+A)/2	Log P	MIC values*
HIF 1	-5.733	-1.736	5.733	1.736	1.999	0.500	3.735	0.7178	200
HIF 2	-5.660	-1.665	5.660	1.665	1.997	0.501	3.663	1.3602	42
HIF 3	-5.831	-1.589	5.831	1.589	2.121	0.471	3.710	1.5466	25
HIF 4	-5.635	-1.469	5.635	1.469	2.083	0.480	3.552	0.3174	300
HIF 5	-5.584	-1.450	5.584	1.450	2.067	0.484	3.517	0.6788	150
HIF 6	-5.921	-1.769	5.921	1.769	2.076	0.482	3.845	1.5438	70
HIF 7	-5.880	-1.649	5.880	1.649	2.116	0.473	3.765	1.0249	160

* Antifungal activity against *Candida albcans*[2]

6.2.2. Mulliken Atomic Charges

Table 6.3 shows the computed Mulliken atomic charges[49-63] for selected elements. The most positively charged atoms are C6 and C10, which can easily connect with the receptor's negative charged part. Because the negative charges are mostly found on the atoms O1, O2, and O3, they can easily connect with the receptor's positive part. C6 is the most positive, while O1 is the most negative.

Table 6.3: Mulliken atomic charges for selected atoms using DFT

Atom	HIF 1	HIF 2	HIF 3	HIF 4	HIF 5	HIF 6	HIF 7
O1	-0.546	-0.540	-0.537	-0.538	-0.538	-0.536	-0.537
O2	-0.508	-0.510	-0.489	-0.493	-0.492	-0.488	-0.489
O3	-0.529	-0.513	-0.517	-0.518	-0.518	-0.517	-0.517
C4	-0.006	-0.007	-0.012	-0.012	-0.012	-0.012	-0.013
C5	0.016	0.016	0.027	0.021	0.022	0.027	0.025
C6	0.369	0.371	0.383	0.383	0.382	0.383	0.383
C7	0.034	0.023	-0.018	-0.019	-0.018	-0.018	-0.017
C8	0.276	0.294	0.293	0.292	0.292	0.293	0.292
C9	0.245	-0.179	-0.186	-0.185	-0.185	-0.185	-0.185
C10	0.331	0.361	0.361	0.360	0.360	0.361	0.361
C11	-0.130	-0.121	-0.184	-0.185	-0.184	-0.184	-0.184
C12	-0.112	-0.112	0.327	0.326	0.326	0.328	0.327
C13	-0.151	-0.150	-0.155	-0.155	-0.155	-0.156	-0.155
C14	0.115	0.114	0.110	0.114	0.115	0.113	0.114
C15	-0.127	-0.134	-0.122	-0.127	-0.135	-0.119	-0.123
C16	-0.107	-0.139	-0.091	-0.107	-0.139	-0.076	-0.144
C17	0.333	0.355	-0.081	0.331	0.354	-0.093	0.356
C18	-0.134	-0.116	-0.088	-0.134	-0.116	-0.072	-0.140
C19	-0.122	-0.120	-0.113	-0.122	-0.121	-0.112	-0.117

6.3 Conclusion

The DFT study of seven 3-benzylidene-4-chromanone analogues were evaluated for their antifungal activity. All the compounds HIF 1-7 were optimized with B3LYP/ 6-31G (*d,p*) and various parameters were evaluated. IP, EA, hardness (η), softness (σ) and electronegativity (χ) correlates reasonably well with the antifungal activity. Log P has been found to have a clear association with antifungal activity. The compound HIF 3 is reported to be the most effective. HIF 3 is more lipophilic in nature, according to the Log P estimates. Stronger antifungal activity is indicated by higher Log P values.

6.4 References

1. Sparg, S. G.; van Staden, J.; Jäger, A. K., Pharmacological and phytochemical screening of two Hyacinthaceae species: Scilla natalensis and Ledebouria ovatifolia. *Journal of Ethnopharmacology* **2002,** *80* (1), 95-101.
2. Shaikh, M. M.; Kruger, H. G.; Smith, P.; Munro, O. Q.; Bodenstein, J.; du Toit, K., Crystal structure and potent antifungal activity of synthetic homoisoflavanone analogues. *Journal of Pharmacy Research* **2013,** *6* (1), 1-5.
3. Abegaz, B. M.; Kinfe, H. H., Naturally Occurring Homoisoflavonoids: Phytochemistry, Biological Activities, and Synthesis (Part II). *Natural Product Communications* **2019,** *14* (5), 1934578X19845813.
4. Rao, Y.; Fang, S.-H.; Tzeng, Y.-M., Anti-inflammatory activities of flavonoids isolated from Caesalpinia pulcherrima. *Journal of ethnopharmacology* **2005,** *100*, 249-53.
5. Shaikh, M.; Petzold, K.; Kruger, H. G.; du Toit, K., Synthesis and NMR elucidation of homoisoflavanone analogues. *Structural Chemistry* **2011,** *22* (1), 161-166.
6. Shaikh, M. M.; Maguire, G. E. M.; Kruger, H. G.; Toit, K. d., 3-Benzyl-5,7-dimethoxychroman-4-ol. *Acta Crystallographica Section E* **2011,** *67* (3), o703.
7. Das, B.; Thirupathi, P.; Ravikanth, B.; Aravind Kumar, R.; Sarma, A. V. S.; Basha, S. J., Isolation, Synthesis, and Bioactivity of Homoisoflavonoids from Caesalpinia pulcherrima. *Chemical and Pharmaceutical Bulletin* **2009,** *57* (10), 1139-1141.
8. Gopaul, K.; Koorbanally, N. A.; Shaikh, M.; Su, H.; Ramjugernath, D., 3-(3-Nitrobenzyl)-4H-chromen-4-one. *Acta Crystallographica Section E* **2013,** *69* (3), o364.
9. Lee, H.; Yuan, Y.; Rhee, I.; Corson, T. W.; Seo, S.-Y., Synthesis of Natural Homoisoflavonoids Having Either 5,7-Dihydroxy-6-methoxy or 7-Hydroxy-5,6-dimethoxy Groups. *Molecules* **2016,** *21* (8).
10. Heo, M.; Lee, B.; Sishtla, K.; Fei, X.; Lee, S.; Park, S.; Yuan, Y.; Lee, S.; Kwon, S.; Lee, J.; Kim, S.; Corson, T. W.; Seo, S.-Y., Enantioselective Synthesis of Homoisoflavanones by Asymmetric Transfer Hydrogenation and Their Biological Evaluation for Antiangiogenic Activity. *The Journal of Organic Chemistry* **2019,** *84* (16), 9995-10011.

11. Rao, V. M.; Damu, G. L. V.; Sudhakar, D.; Siddaiah, V.; Rao, C. V., New efficient synthesis and bioactivity of homoisoflavonoids. *Arkivoc* **2008,** *11*, 285-294.
12. Srinivas, K.; Rao, Y. K.; Mahender, I.; Das, B.; Krishna, K. R.; Kishore, K. H.; Murty, U., Flavanoids from Caesalpinia pulcherrima. *Phytochemistry* **2003,** *63* (7), 789-793.
13. Castelli, M. V.; López, S. N., Chapter 9 - Homoisoflavonoids: Occurrence, Biosynthesis, and Biological Activity. In *Studies in Natural Products Chemistry*, Atta ur, R., Ed. Elsevier: 2017; Vol. 54, pp 315-354.
14. Kumar, V.; Nayak, S., Homoisoflavonoids: isolation, chemical synthesis strategies and biological activities. *JPSCR Journal of Pharmaceutical Science and Clinical Research* **2020,** *12*, 1046-1055.
15. Sharma, S.; Patial, V.; Singh, D.; Sharma, U.; Kumar, D., Antimicrobial Homoisoflavonoids from the Rhizomes of Polygonatum verticillatum. *Chemistry and Biodiversity* **2018,** *15* (12), e1800430.
16. Namdar, R.; Makouie, N.; Nafisi, S., Study on the interaction of homoisoflavonoids with RNA. *Journal of Photochemistry and Photobiology B: Biology* **2013,** *128*, 100-106.
17. Gang, F.-L.; Zhu, F.; Yang, C.-F.; Li, X.-T.; Yang, H.; Sun, M.-X.; Wu, W.-J.; Zhang, J.-W., Antifungal, anti-inflamatory and neuritogenic activity of newly-isolated compounds from Disporopsis aspersa. *Natural Product Research* **2020,** *34* (11), 1521-1527.
18. Skrobiszewski, A.; GŁAdkowski, W.; Walczak, P.; GliszczyŃSka, A.; Maciejewska, G.; Klejdysz, T.; Nawrot, J. A. N.; WawrzeŃCzyk, C., Synthesis of β-aryl-γ-lactones and relationship: Structure – antifeedant and antifungal activity. *Journal of Chemical Sciences* **2015,** *127* (4), 687-699.
19. Kamboj, S.; Singh, R., Chromanone-A Prerogative Therapeutic Scaffold: An Overview. *Arabian Journal for Science and Engineering* **2021**.
20. Xu, X.; Cheng, K.; Cheng, W.; Zhou, T.; Jiang, M.; Xu, J., Isolation and chatacterization of homoisoflavonoids from Dracaena cochinchinensis and their osteogenic activities in mouse mesenchymal stem cells. *Journal of Pharmaceutical and Biomedical Analysis* **2016,** *129*, 466-472.
21. Zhu, F.; Yuan, C.; Gang, F.; Yang, C.; Wu, W.; Zhang, J., Bioassay-Guided Isolation of Antifungal Compounds from Disporopsis aspersa (Hua) Engl. ex

Diels against Pseudoperonospora cubensis and Phytophthora infestans. *Chemistry and Biodiversity* **2018,** *15* (7), e1800090.

22. Shaikh, M. M.; Kruger, H. G.; Bodenstein, J.; Smith, P.; du Toit, K., Anti-inflammatory activities of selected synthetic homoisoflavanones. *Natural Product Research* **2012,** *26* (16), 1473-1482.
23. Leo, A.; Hansch, C.; Elkins, D., Partition coefficients and their uses. *Chemical Reviews* **1971,** *71* (6), 525-616.
24. Nasal, A.; Siluk, D.; Kaliszan, R., Chromatographic Retention Parameters in Medicinal Chemistry and Molecular Pharmacology. *Current Medicinal Chemistry* **2003,** *10*, 381-426.
25. Sławik, T.; Paw, B., Lipophilicity of Some N- and O- Substituted Alkanoic Acids of 1, 2- Benzisothiazol- 3 (2H)- one Determined by Reversed- Phase Thin Layer Chromatography. *Journal of liquid chromatography and related technologies* **2004,** *27* (6), 1043-1055.
26. Tiperciuc, B.; Sârbu, C., Prediction of the Chromatographic Retention (Lipophilicity) of Some New Methyl- Thiazole- Oxadiazoline Derivatives by Multivariate Regression Methods. *Journal of Liquid Chromatography and Related Technologies* **2006,** *29* (15), 2257-2270.
27. Podunavac-Kuzmanović, S. O.; Cvetković, D. D.; Barna, D. J., Correlations between the lipophilicity and the inhibitory activity of different substituted benzimidazoles. *Chemical Industry and Chemical Engineering Quarterly/CICEQ* **2009,** *15* (3), 125-130.
28. Podunavac-Kuzmanović, S. O.; Velimirovic, S. D., Correlation between the lipophilicity and antifungal activity of some benzoxazole derivatives. *Acta Periodica Technologica* **2010,** *41*, 177-185.
29. Schmidt, M. W.; Baldridge, K. K.; Boatz, J. A.; Elbert, S. T.; Gordon, M. S.; Jensen, J. H.; Koseki, S.; Matsunaga, N.; Nguyen, K. A.; Su, S.; Windus, T. L.; Dupuis, M.; Montgomery Jr, J. A., General atomic and molecular electronic structure system. *Journal of Computational Chemistry* **1993,** *14* (11), 1347-1363.
30. Liu, X.-H.; Chen, P.-Q.; Wang, B.-L.; Li, Y.-H.; Wang, S.-H.; Li, Z.-M., Synthesis, bioactivity, theoretical and molecular docking study of 1-cyano-N-substituted-cyclopropanecarboxamide as ketol-acid reductoisomerase inhibitor. *Bioorganic and medicinal chemistry letters* **2007,** *17* (13), 3784-3788.

31. Cakmak, E.; Ozbakir Isin, D., A theoretical evaluation on free radical scavenging activity of 3-styrylchromone derivatives: the DFT study. *Journal of Molecular Modeling* **2020,** *26* (5), 98.
32. Janak, J. F., Proof that dE/dni = e in density-functional theory. *Physical Review B* **1978,** *18* (12), 7165-7168.
33. Parr, R. G.; Pearson, R. G., Absolute hardness: companion parameter to absolute electronegativity. *Journal of the American Chemical Society* **1983,** *105* (26), 7512-7516.
34. Pearson, R. G., Absolute electronegativity and hardness: application to inorganic chemistry. *Inorganic Chemistry* **1988,** *27* (4), 734-740.
35. Xu, Y.; Chu, Q.; Chen, D.; Fuentes, A., HOMO–LUMO Gaps and Molecular Structures of Polycyclic Aromatic Hydrocarbons in Soot Formation. *Frontiers in Mechanical Engineering* **2021,** *7*.
36. Joshi, B. D.; Thakur, G.; Chaudhary, M. K., Molecular Structure, Homo-Lumo and Vibrational Analysis Of Ergoline By Density Functional Theory. *Scientific World* **2021,** *14* (14), 21-30.
37. Joseph, S.; Thomas, S.; Mohan, J.; Kumar, A. S.; Jayasree, S. T.; Thomas, S.; Kalarikkal, N., Theoretical Study on Tuning Band Gap and Electronic Properties of Atomically Thin Nanostructured MoS2/Metal Cluster Heterostructures. *ACS Omega* **2021,** *6* (10), 6623-6628.
38. Mumit, M. A.; Pal, T. K.; Alam, M. A.; Islam, M. A.-A.-A.-A.; Paul, S.; Sheikh, M. C., DFT studies on vibrational and electronic spectra, HOMO-LUMO, MEP, HOMA, NBO and molecular docking analysis of benzyl-3-N-(2,4,5-trimethoxyphenylmethylene)hydrazinecarbodithioate. *Journal of molecular structure* **2020,** *1220*, 128715-128715.
39. De Lile, J. R.; Kang, S. G.; Son, Y.-A.; Lee, S. G., Do HOMO–LUMO Energy Levels and Band Gaps Provide Sufficient Understanding of Dye-Sensitizer Activity Trends for Water Purification? *ACS Omega* **2020,** *5* (25), 15052-15062.
40. Townsend, P. A.; Grayson, M. N., Density Functional Theory Transition-State Modeling for the Prediction of Ames Mutagenicity in 1,4 Michael Acceptors. *Journal of Chemical Information and Modeling* **2019,** *59* (12), 5099-5103.

41. Matunová, P.; Jirásek, V.; Rezek, B., DFT calculations reveal pronounced HOMO–LUMO spatial separation in polypyrrole–nanodiamond systems. *Physical Chemistry Chemical Physics* **2019,** *21* (21), 11033-11042.
42. Choudhary, V.; Bhatt, A.; Dash, D.; Sharma, N., DFT calculations on molecular structures, HOMO–LUMO study, reactivity descriptors and spectral analyses of newly synthesized diorganotin (IV) 2-chloridophenylacetohydroxamate complexes. *Journal of Computational Chemistry* **2019,** *40* (27), 2354-2363.
43. Chen, D.; Wang, H., HOMO–LUMO Gaps of Homogeneous Polycyclic Aromatic Hydrocarbon Clusters. *The Journal of Physical Chemistry C* **2019,** *123* (45), 27785-27793.
44. Umar, Y.; Abdalla, S., DFT Study of the Molecular Structure, Conformational Preference, HOMO, LUMO, and Vibrational Analysis of 2-, and 3-Furoyl Chloride. *Journal of Solution Chemistry* **2017,** *46* (4), 741-758.
45. Pereira, F.; Xiao, K.; Latino, D. A. R. S.; Wu, C.; Zhang, Q.; Aires-de-Sousa, J., Machine Learning Methods to Predict Density Functional Theory B3LYP Energies of HOMO and LUMO Orbitals. *Journal of Chemical Information and Modeling* **2017,** *57* (1), 11-21.
46. Prabhaharan, M.; Prabakaran, A. R.; Gunasekaran, S.; Srinivasan, S., DFT studies on vibrational spectra, HOMO–LUMO, NBO and thermodynamic function analysis of cyanuric fluoride. *Spectrochimica Acta Part A: Molecular and Biomolecular Spectroscopy* **2015,** *136*, 494-503.
47. Barman, M. K.; Chatterjee, M.; Srivastava, B.; Mandal, B., Characterization and Density Functional Theory Optimization of a Simultaneous Binder (FSG-XO) of Two Different Species Exploiting HOMO–LUMO Levels: Photoelectronic and Analytical Applications. *Journal of Chemical and Engineering Data* **2015,** *60* (8), 2197-2208.
48. El-Mansy, M. A. M.; El-Nahass, M. M.; Khusayfan, N. M.; El-Menyawy, E. M., DFT approach for FT-IR spectra and HOMO–LUMO energy gap for N-(p-dimethylaminobenzylidene)-p-nitroaniline (DBN). *Spectrochimica Acta Part A: Molecular and Biomolecular Spectroscopy* **2013,** *111*, 217-222.
49. Siddiqui, S. A., Molecular modeling and simulation for the design of dye sensitizers with mono- and di-substituted donor moieties. *Journal of Computational Electronics* **2022**.

50. Shinde, R., Ultrasound Assisted Synthesis, Molecular Structure,UV-Visible Assignments, MEP and Mulliken Charges Study of (E)-3-(4-chlorophenyl)-1-(4-methoxyphenyl) prop-2-en-1-one: Experimental and DFT Correlational. *Material Science Research India* **2021,** *18*, 86-96.
51. Dhonnar, S. L.; Sadgir, N. V.; Adole, V. A.; Jagdale, B. S., Molecular Structure, FT-IR Spectra, MEP and HOMO-LUMO Investigation of 2-(4-Fluorophenyl)-5-phenyl-1, 3,4-oxadiazole Using DFT Theory Calculations. *Advanced Journal of Chemistry-Section A* **2021,** *4* (3), 220-230.
52. Khosravi, M.; Murthy, V.; Mackinnon, I. D. R., Evaluation of DFT methods to calculate structure and partial atomic charges for zeolite N. *Computational Materials Science* **2020,** *171*, 109225.
53. Qian, H.; Deng, J.; Zhou, H.; Yang, X.; Chen, W., A DFT study on the adsorption of Ga-BNNT to SF6 decomposition products under partial discharge. *Results in Physics* **2019,** *14*, 102419.
54. Ertural, C.; Steinberg, S.; Dronskowski, R., Development of a robust tool to extract Mulliken and Löwdin charges from plane waves and its application to solid-state materials. *RSC Advances* **2019,** *9* (51), 29821-29830.
55. Toh, P. L.; Meepripruk, M.; Ang, L. S.; Sulaiman, S.; Mohamed-Ibrahim, M. I., First Principles Study on the Stability and Electronic Structures of 7,8-Dichloro-4-Oxo-4H-Chromene-3-Carbaldehyde. *Applied Mechanics and Materials* **2017,** *855*, 31-36.
56. Rogers, T. R.; Wang, F., Performing the Millikan experiment at the molecular scale: Determination of atomic Millikan-Thomson charges by computationally measuring atomic forces. *The Journal of chemical physics* **2017,** *147* (16), 161726-161726.
57. Pokharia, S.; Joshi, R.; Pokharia, M.; Yadav, S. K.; Mishra, H., A density functional theory insight into the structure and reactivity of diphenyltin(IV) derivative of glycylphenylalanine. *Main Group Metal Chemistry* **2016,** *39* (3-4), 77-86.
58. Govindasamy, P.; Gunasekaran, S.; S, S., Molecular geometry, conformational, vibrational spectroscopic, molecular orbital and Mulliken charge analysis of 2-acetoxybenzoic acid. *Spectrochimica Acta Part A: Molecular and Biomolecular Spectroscopy* **2014,** *130*, 329–336.

59. Azhagiri, S.; Jayakumar, S.; Gunasekaran, S.; Srinivasan, S., Molecular structure, Mulliken charge, frontier molecular orbital and first hyperpolarizability analysis on 2-nitroaniline and 4-methoxy-2-nitroaniline using density functional theory. *Spectrochimica Acta Part A: Molecular and Biomolecular Spectroscopy* **2014,** *124*, 199-202.
60. Reed, A. E.; Weinstock, R. B.; Weinhold, F., Natural population analysis. *The Journal of Chemical Physics* **1985,** *83* (2), 735-746.
61. Stone, A. J., Distributed multipole analysis, or how to describe a molecular charge distribution. *Chemical Physics Letters* **1981,** *83* (2), 233-239.
62. Mulliken, R. S., Electronic Population Analysis on LCAO–MO Molecular Wave Functions. I. *The Journal of Chemical Physics* **1955,** *23* (10), 1833-1840.
63. Löwdin, P. O., On the Non- Orthogonality Problem Connected with the Use of Atomic Wave Functions in the Theory of Molecules and Crystals. *The Journal of Chemical Physics* **1950,** *18* (3), 365-375.

CHAPTER 7:

Summary and Future Scope

Summary

DFT based CASTEP calculations were used successfully for the understanding the mechanism of the pH-dependent drug molecules loading and release based on the pKa values of drug and the silica surface. The B.E. of drug and surface in possible combinations S^0 D^0, S^0 D^{-1}, S^{-1} D^0, and S^{-1} D^{-1} were used to predict the pH of loading and release of sulfasalazine drug. It is reported that, the sulfasalazine drug molecule gets trapped in the MSN-TA nano-vehicle when passing through the stomach's acidic environment (pH 1.0 – 3.0), and getting released in intestine with slightly basic pH environment (6.0 – 7.5). The release is an outcome of strong electrostatic repulsion that generated between the silica surface and the negative drug molecules which can be seen in terms of very large positive B.E. indicating no interaction.

The DFT study of benzoyl thiourea derivatives linked to morpholine and piperidine were evaluated for their antifungal activity. Mulliken charge analysis results were found consistent with the antifungal activity. The presence of morpholine group and fluorine at para position reported to be enhancing the antifungal activity, which is confirmed from the current DFT studies. In general, good agreement between the calculated and experimental bond lengths and bond angles have been observed. For the BTP compounds the antifungal activity sequence was found similar to that of calculated electronegativity. For the BTM compounds a direct correlation of antifungal activity is observed with E_{LUMO}, EA, hardness and softness.

The DFT calculations of thiourea derivatives containing a thiazole moiety reveals electronic characteristics responsible for the strong biological activity. In general, good agreement between the calculated and experimental geometrical parameters have been observed. Overall, we observed strong correlation between biological activity and computed values of all the quantum chemical parameters Lower values of Log P are indicative of stronger antifungal activity.

The DFT calculations of the compounds Allantofuranone, Xenofuranone A, Xenofuranone B, and WF 3681 demonstrated that Allantofuranone has a small HOMO-LUMO gap, a lower LUMO value, a more lipophilic character, and a rich topography, all of which are prerequisite for antifungal action. The electronic properties that distinguish Allantofuranone from other structurally related compounds and are responsible for its remarkable biological action are highlighted.

Overall, we found a significant correlation between biological activity and calculate values for all quantum chemical parameters, including EA, IP, electronegativity, band Gap, hardness (η) and softness (σ).

The DFT study of seven 3-benzylidene-4-chromanone analogues were evaluated for their antifungal activity. All the compounds were optimized with B3LYP/ 6-31G (*d*,*p*) and various parameters were evaluated. IP, EA, hardness (η), softness (σ) and electronegativity (χ) correlates reasonably well with the antifungal activity. Log P has been found to have a clear association with antifungal activity. The compound HIF3 is reported to be the most effective. HIF 3 is more lipophilic in nature, according to the Log P estimates. Stronger antifungal activity is indicated by higher Log P values.

Future Scope

The proposed DFT model can be used for predicting the loading and release pH for the drugs and the surfaces with known pKa values, which will be very important / crucial for the **pH responsive drug delivery systems**.

In the future, the DFT study and structure-activity relationship study may aid in the formulation of better antifungal and/or antibiotic heterocyclic compounds.

Publications:

1. DFT based investigations of antibiotic and antifungal activity of allantofuranone and related γ-lactone compounds, ***Rameshwar K. Dongare****, Shaukatali N. Inamdar, Radhakrishnan M. Tigote*, **Journal of Advanced Scientific Research**, June **2021**, 12 (2S1), 336-339.
2. DFT Studies and Quantum Chemical Calculations of Benzoyl Thiourea Derivatives Linked with Morpholine and Piperidine for the Evaluation of Antifungal Activity, ***Rameshwar K. Dongare,*** *Shaukatali N. Inamdar and Radhakrishnan M. Tigote*, **Current Physical Chemistry**, Accepted **January 2022.** DOI: 10.2174/1877946812666220111141742
3. DFT calculations of thiourea derivatives containing a thiazole moiety for the evaluation of antifungal activity, ***Rameshwar K. Dongare****, Shaukatali N. Inamdar, Radhakrishnan M. Tigote*, **Journal of Advanced Scientific Research**, Accepted December **2021.**
4. Evaluation of Antifungal activity of Homoisoflavonone compounds using DFT, ***Rameshwar K. Dongare****, Shaukatali N. Inamdar, Radhakrishnan M. Tigote*, Manuscript under preparation.